

**Atmospheric Effects of Irrigation in
Monsoon Climate:
The Indian Subcontinent**

Obbe Arjan Tuinenburg

Thesis committee

Promotor

Prof. dr. P. Kabat

Director/CEO, International Institute for Applied Systems Analysis, Laxenburg, Austria
Professor of Earth System Science, Wageningen University

Co-promotor

Dr. R.W.A. Hutjes

Associate professor, Earth System Science Group
Wageningen University

Other members

Prof. dr. P.A. Dirmeyer, George Mason University, Fairfax, Virginia, USA

Prof. dr. A.A.M. Holtslag, Wageningen University

Prof. dr. B.J.J.M. van den Hurk, Utrecht University

Prof. dr. H.H.G. Savenije, Delft University of Technology

This research was conducted under the auspices of the SENSE Research School

**Atmospheric Effects of Irrigation in
Monsoon Climate:
The Indian Subcontinent**

Obbe Arjan Tuinenburg

Thesis

submitted in fulfilment of the requirements for the degree of doctor
at Wageningen University

by the authority of the Rector Magnificus

Prof. dr. M.J. Kropff,

in the presence of the

Thesis Committee appointed by the Academic Board

to be defended in public

on Monday 15 April 2013

at 4 p.m. in the Aula.

Obbe Arjan Tuinenburg
Atmospheric Effects of Irrigation in Monsoon Climate:
The Indian Subcontinent
179 pages

Thesis, Wageningen University, Wageningen, NL (2013)
With references, with summaries in Dutch and English

ISBN 978-94-6173-499-2

Contents

1	General Introduction	1
1.1	Atmospheric Effects of Irrigation	1
1.2	Objectives	6
1.3	Approach	7
2	Global Indicators of Land-Atmosphere Interactions	17
2.1	Introduction	18
2.2	Methods	22
2.3	Results	28
2.4	Discussion and Conclusion	38
3	Diagnosis of Local Land-Atmosphere Feedbacks in India	43
3.1	Introduction	44
3.2	CTP-HI _{low} framework	46
3.3	Methods and Data	48
3.4	Performance of the CTP-HI _{low} Framework for India	54
3.5	Land-Atmosphere Feedbacks and Monsoon	59
3.6	Discussion	66
3.7	Conclusion	68
4	The fate of evaporated water from the Ganges basin	71
4.1	Introduction	72
4.2	Literature Synthesis	73
4.3	Methods	75
4.4	Results	83
4.5	Discussion	92

4.6	Conclusion	97
5	Effects of Irrigation in India on the Atmospheric Water Budget	99
5.1	Introduction	100
5.2	Methods	102
5.3	Results	106
5.4	Discussion and Conclusion	123
6	Synthesis	127
6.1	Atmospheric Effects of Irrigation	128
6.2	Effects on Hydrological Cycle	136
6.3	Ideal Irrigation	137
6.4	Outlook and Recommendations	139
	Summary	159
	Samenvatting	163
	Dankwoord	166
	Publications	167
	CV	169

General Introduction

1.1 Atmospheric Effects of Irrigation

1.1.1 Population and Irrigation Trends

During the 20th century, the human population has increasingly cultivated the earth for agricultural production. More important than the expansion of agricultural areas, the agriculture has become increasingly intensive. During the last 50 years, the use of fertilizers increased five-fold and the irrigated agricultural areas doubled (Foley et al., 2011).

One of the areas with a very high population growth is India. During the 20th century, India's population has grown from about 300 million inhabitants in 1900 to 1.2 billion in 2011 (World Bank and Figure 1.1). This population growth caused an increase in the demand for food. This increased demand caused the agricultural production in India (of which the main crops are wheat and rice) to increase. This increase in production was realised through an increase in agricultural area as well as an increase in productivity, the so-called "green revolution". Apart from food production, the agricultural sectors of India's current economy provide around 17% of GDP and employment to about half the workforce (CIA (2009)).

To secure and manage water supply for the expanding agriculture, irrigation infrastructure (dams, channels, etc.) has been constructed, especially in the Ganges and Indus basins. Around the year 2000, large parts of India were equipped for irrigation as shown in Figure 1.2 (Siebert et al. (2005)). These large scale interventions in the water cycle have made the Ganges and Indus basins among the most highly managed river basins in the world (Biemans (2012)).

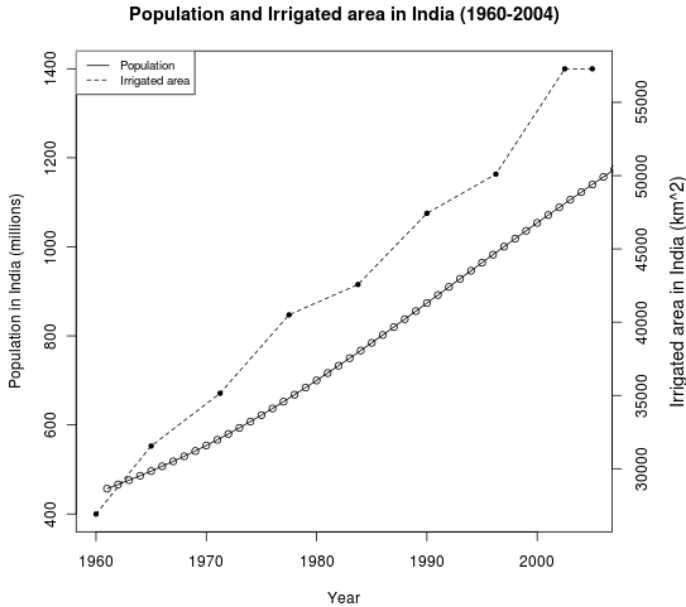


Figure 1.1: *Increasing population and irrigated area in India*

1.1.2 Monsoon Climates and Irrigation Water Sources

In several regions around the world (most notably in West-Africa, Asia and Australia), the atmospheric circulation has a distinct seasonal variability. The origin of this seasonality is the annual cycle of solar insolation, in combination with heating differences between land and ocean. In the season when this insolation is highest, the land surface heats up more than the ocean. This occurs because the ocean has a higher heat capacity than the land, moreover, convection in the ocean can transport the solar heat deep into the ocean. Due to this temperature difference, a thermal heat low develops over the land and atmospheric circulation occurs from the ocean to the land, usually bringing a precipitation peak. During the winter season, the land surface is cooler than the ocean surface and the opposite flow develops; a flow from the land to the ocean, resulting in minimal precipitation.

India has a monsoon climate with a distinct seasonal precipitation. During the dry winter monsoon (December-February), the atmospheric flow brings dry continental

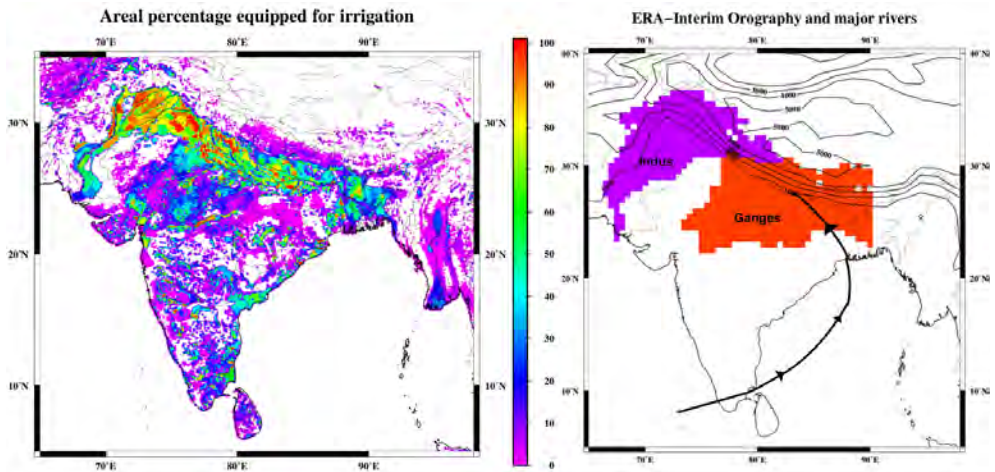


Figure 1.2: Left panel: Fraction of the area that is equipped for irrigation (around the year 2000, Siebert et al. (2005)). Right panel: Ganges and Indus basins and typical monsoon flows.

air from the north, which gives no precipitation. In spring (March-May), the increasing solar insolation heats up the land surface, which leads to high temperatures and an increase in the land-sea temperature contrast. This land-sea temperature contrast induces a flow from the Indian ocean towards the continent, the summer monsoon (from June-August). During this period the atmospheric flow transports moist oceanic air onto the continent, and the majority of the precipitation falls. The large-scale atmospheric flow reverses again during the fall season.

The precipitation can fall as rain and follow the river system towards the ocean directly (and reach the ocean after a couple of weeks). Alternatively, it can be stored on land much longer, either as snow or ice in the Himalaya mountains, or as ground water after infiltration into the soil. During the spring season, rising temperatures cause snow-melt in the mountains and increase the river discharge again. Compared to the total discharge, this melt water is more important in the Indus basin than in the Ganges basin (Immerzeel et al. (2010)).

The water for irrigated crops can come from three sources; precipitation that contributes to the soil wetness and is used by the plant, water that is channeled from rivers and (dammed) lakes, and groundwater. In India, precipitation contributes about 40%, channeled water (including non-local water sources) contributes about 48%, and groundwater contributes 12% to irrigation, respectively (Wada et al. (2012)).

1.1.3 Interaction with the Hydrological Cycle

The land surface part hydrological cycle is affected by (amongst other) irrigation purposes in two ways. Water that has reached the land surface and would under natural conditions flow to the ocean in a couple of weeks, is stored on land for longer. Furthermore, groundwater is subtracted and can either be evaporated and brought into the atmosphere or run-off to the ocean.

To determine effects of these human influences on the hydrological cycle, these were simulated with large scale hydrological models within the EU WATCH FP7 project. These models were run using natural conditions and with human modifications and forced with the same precipitation (Haddeland et al. (2011) and Hagemann et al. (2012)). The effects on the land surface evaporation in south Asia is shown in figure 1.3. The largest effect of the human influence on annual evaporation is found in the dry Indus basin, where it increases with up to 500 mm per year. In the Ganges basin, the increase in evaporation is between 100 and 200 mm per year.

Figure 1.4 shows the annual cycles of precipitation, evaporation and discharge for the Ganges basin for the hydrological model runs. The variability across the models is substantial (shown in the error bars in Figure 1.4), but some results stand out.

The difference in evaporation between the runs is largest during January to May,

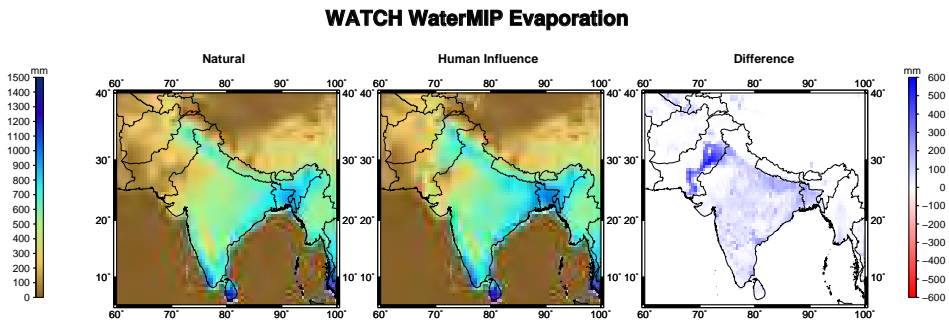


Figure 1.3: Effect of human influence on average annual evaporation (1990-2000) in the three large scale hydrological models of the WATCH large scale model intercomparison for which data were available (Haddeland et al. (2011)).

when the land surface would be dry in the natural run, but is wet in the human impact run due to irrigation, increasing evaporation. During the monsoon season (June-August), the land surface is wet in both runs and the effects on irrigation are minimal.

The discharge into the ocean shows the same seasonal cycle as the precipitation, but with a delay of about a month. The decrease in discharge due to human impacts is

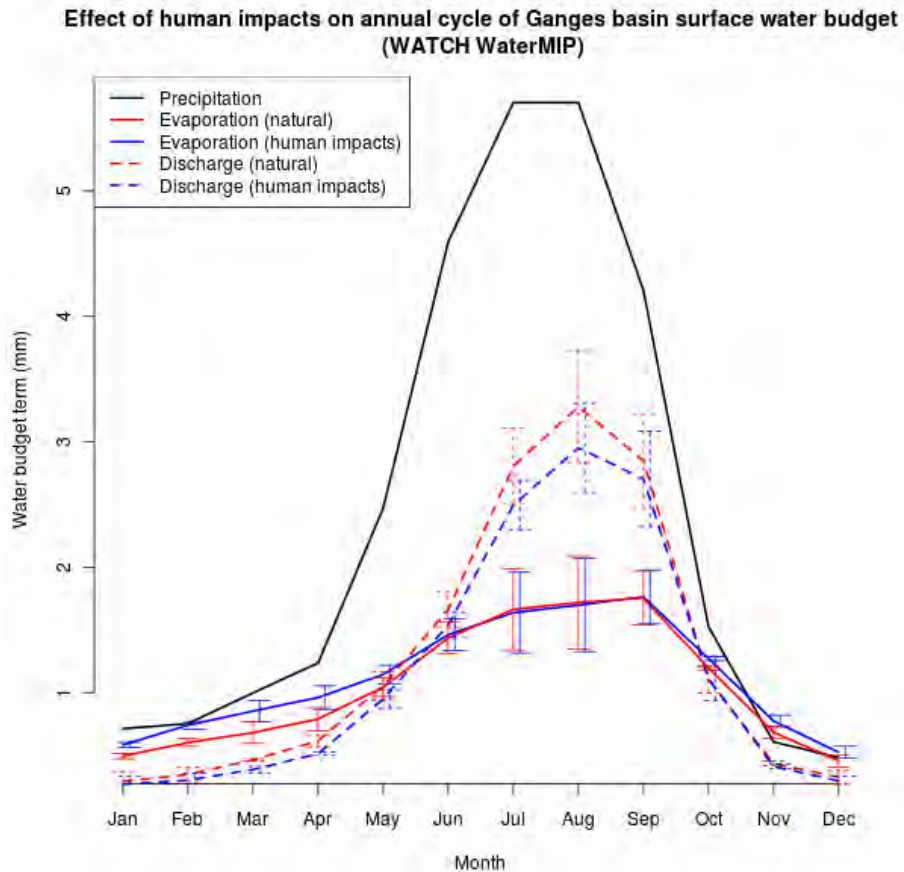


Figure 1.4: Effect of human influence on the annual cycle in the surface water budget in the large scale models of the WATCH large scale model intercomparison (Haddeland et al. (2011)). Error bars show the variability across the models. The same precipitation (Weedon et al. (2011)) was forced for all model runs.

found during the monsoon season.

The effects of the human impacts on the water cycle thus is a shift from the peak discharge during the monsoon season to an increase in evaporation during the five months before the monsoon onset. However, this study ignored the atmospheric effects of the land surface changes. Both model runs were forced with the same precipitation, whereas the changed land surface may have effects on the precipitation. The current research will assess these effects of the land surface on the atmosphere.

1.2 Objectives

The atmospheric effects of irrigation relevant for the water cycle are determined from three perspectives. These perspectives are related to the temporal and spatial scales of the relevant hydrological and atmospheric processes. Moreover, as with many other environmental problems, these perspective influence each other and form a coupled problem.

1.2.1 Local Perspective: Precipitation Triggering

From the local perspective, the irrigation leads to a wetter land surface, which affects the local energy balance. A larger fraction of the incoming net solar radiation will be used for evaporation and a smaller fraction for a sensible heat flux. This change in the energy balance influences the temperature, humidity and height of the atmospheric boundary layer, which subsequently can affect convection, cloud formation and precipitation.

The objectives in this perspectives are to determine **effects of irrigation on the local energy balance and convective precipitation** and whether **the local effect of the land surface on precipitation in India is larger than elsewhere**.

1.2.2 Moisture Recycling Perspective: Ganges Basin Recycling

Generally, irrigation leads to additional evaporation into the atmosphere. The atmospheric flow transports the evaporated moisture away from the evaporation location and it will come back to the land surface as precipitation downwind. The distance traveled through the atmosphere can be small (100 kilometer), which means that the moisture recycles locally and can potentially be reused. It can also be very large, and the moisture is lost for the local resources. The moisture recycling perspective looks at the length and timescales of the atmospheric path of the evaporated moisture and whether the evaporation recycles as precipitation within the river basin.

The objectives from this perspective are to determine **the direction in which additional evaporation is transported and where it leads to additional precipitation**. Moreover, it determines **how this recycling varies seasonally and for different areas in India**.

1.2.3 Large Scale Perspective: Influence on Monsoon Flow

The large scale perspective looks at irrigation on the continental scale. The large scale moistening of the land surface reduces the temperatures and therefore the thermal

low pressure on the continent. The interaction of the land thermal low with the higher oceanic pressures are an important cause of the summer monsoon flow. A decreased land-sea temperature contrast may affect the atmospheric flow patterns on the scale of sea-breezes to monsoon flows.

The objective from this perspective are to determine **the effects of irrigation on the atmospheric flow and how this varies seasonally and spatially.**

1.3 Approach

The three perspectives defined in the objectives have different research approaches. Each perspective has a typical temporal and spatial scale. Usually, the research approach within a perspectives ignores processes on other scales, assuming that these are not dominant. In modeling studies, it may be possible to isolate processes on a certain scale by actively disabling the other processes. Measurements, however, represent the integrated effects of processes at all scales. Sometimes a smart selection of data can isolate processes, for example by studying days when the large scale circulation is small to isolate local effects. However, the reader should keep in mind that some processes act across the perspectives chosen in this study.

For each perspective, table 1.1 shows the approaches taken by previous studies. Within the local perspective, there are statistical approaches that determine whether evaporation is limited by soil moisture or by atmospheric demand (correlation between evaporation and soil moisture) or that determine the probability of afternoon precipitation given the land surface state (that can be dry or wet). There are also model approaches, which range from formulations of the land surface influence on the atmospheric boundary layer development derived from boundary layer theory, to atmospheric boundary layer model runs with wet and dry land surface to an analysis of the soil moisture dynamics in global climate models.

For the moisture recycling perspective, the approaches range from various atmospheric moisture budget models that use atmospheric model output to trace the moisture through the atmosphere. These models can be run on an Eulerian (a fixed grid) or in a Lagrangian mode (a moving grid). Moisture can also be traced directly in an atmospheric model.

For the large scale perspective, statistical approaches exist that compare the atmospheric flow or precipitation in years with a dry and wet land surface. However, the typical approach in the large scale perspective is to use atmospheric models. These models can range from 2D-models (with dimensions of height and length) that simulate an atmosphere along a transect perpendicular to the coast, to 3D regional or global climate models.

This section describes the research approaches for the three perspectives, discussing assumptions and limitations, together with a presentation of earlier work within this

Table 1.1: *Approaches taken in previous studies, for each perspective.*

Perspective	Approach	Description
Local	Statistical Atmospheric Boundary Layer theory Climate model runs	Correlation between surface state and precipitation Determine the influence of land surface in boundary layer model Analyse the co-variability of soil moisture and precipitation for different climate runs
Moisture Recycling	Atmospheric moisture budget (bulk) Atmospheric moisture budget (tracers) Direct tracing in atmospheric model	Use a Eulerian model to trace moisture through the atmosphere Use a Lagrangian model to trace moisture through the atmosphere Explicitly trace moisture in atmospheric model
Large scale	Land surface and precipitation data analysis 3D atmospheric model	Analyse the monsoon strength in wet and dry periods model the three dimensional atmospheric dynamics

approach.

1.3.1 Time and Space scales

Within earth system sciences, usually several processes are involved. Despite the different time and spatial scales of these processes, they may interact and have consequences on totally different scales. An example is the absorption of longwave radiation by CO₂, which is a process on molecular scale and acts on very short time scales. However, the effect of this absorption can influence the local radiation balance, local temperatures, atmospheric moisture content, cloud formation up to global weather patterns. Within the current problem, there are processes involved that act on different time scales. Figure 1.5 shows some of the meteorological and hydrological processes involved in the study of the atmospheric effects of irrigation. The interaction between the surface and the atmosphere occurs on several scales.

On small scales, the atmospheric boundary layer dynamics interacts with the land surface. Convective cells occur on scales of kilometers and hours. These cells are influenced by the land surface moisture patterns, which have a spatial scale of kilometers, but change on weekly-monthly time scales. On large scales, an increased temperature due to global warming affects Himalaya glaciers melting pattern and extent.

1.3.2 Local Perspective: Precipitation Triggering

The local perspective the effect of a wet land surface on the local atmosphere, and especially precipitation, is determined. The approach in this perspective is to analyze

Spatial and Time scales of atmospheric and surface processes

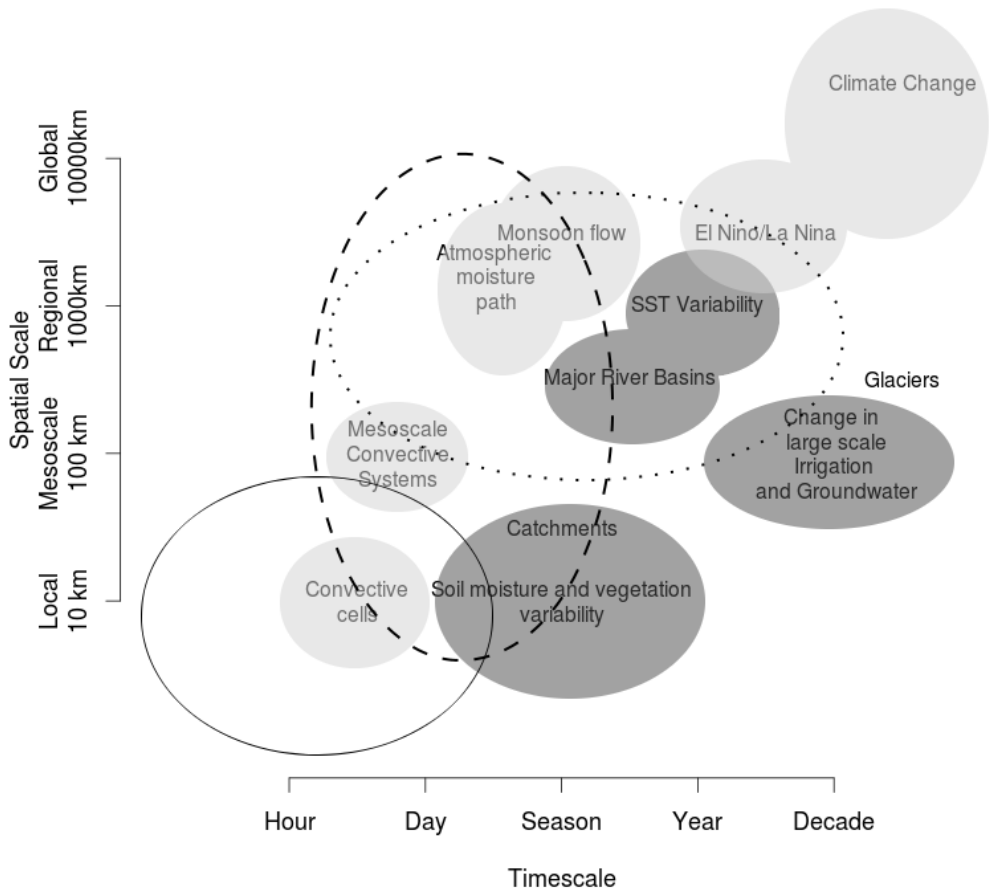


Figure 1.5: Spatial and temporal scales of meteorological (light gray), hydrological and surface (dark gray) processes relevant in the current study. The scales of the local perspective (solid ellipse), moisture recycling perspective (dashed ellipse) and large scale perspective (dotted ellipse) are highlighted.

the atmospheric effects over a length scale of tens of kilometers. This perspective focuses on the local effects of surface wetness on the energy balance of the surface and atmospheric boundary layer and how a change in this balance influences convection.

The atmosphere is treated as a single column in which the large scale circulation is ignored. These assumptions simplify the problem, which makes analysis easier, but are probably only valid for time scales shorter than one day. The scales of the local perspective are highlighted in Figure 1.5.

The interaction between precipitation and soil moisture acts in two ways. The effect of precipitation on soil moisture is quite straightforward; a wetting of the land surface. The reverse effect of the land surface state on precipitation is less straightforward, and whether a wetter land surface leads to more, less, or no change in precipitation depends on the atmospheric conditions (van Heerwaarden et al. (2009)). A wetter land surface increase evaporation, which increases the humidity in the atmosphere. On larger spatial scales, this has to lead to more precipitation. However, on the local scale, this is not necessarily the case. A wetter land surface may reduce the boundary layer of the atmosphere. Due to this reduction, the boundary layer may not reach the lifting condensation level at which moisture starts to condensate and clouds are formed, and convection may not occur. This influence of the land surface on precipitation has been studied extensively using theoretical atmospheric models, precipitation and surface data analysis and sensitivity tests in climate models.

In a large comparison of the land-atmosphere coupling strength in global climate models (GLACE), the precipitation variance was determined for model runs with prescribed and with fully interactive soil moisture dynamics. The difference in the precipitation variance between these runs is the soil moisture-precipitation coupling. Koster et al. (2004) and Koster et al. (2006) found hot-spots of soil moisture-precipitation coupling in the Central US, West-Africa and India for the summer season. Guo et al. (2006) noted that these are the areas of intermediate wetness. There, soil moisture has an influence on evaporation, and evaporation has an influence on precipitation. It must be noted, however, that the variability in coupling strengths across the models was large. These differences across the models can originate from a different representation of the land surface, but other parts of the atmospheric models can also have a significant effect on the land-atmosphere feedbacks within the models. For example, Hohenegger et al. (2009) found a significant influence of the convection parametrization on this feedback.

Starting from theoretical descriptions of the atmospheric boundary layer, Ek and Holtslag (2004) found that the relative humidity at the top of the boundary layer increased with increasing surface wetness, except when the air above the atmospheric boundary layer is very dry. In this case, the contribution of moisture to the boundary layer from the surface is compensated by a moisture reduction due to the entrainment of the drier air from above the boundary layer. De Ridder (1997) linked influence of the land surface to the boundary layer equivalent potential temperature (which is related to the convective activity Kohler et al. (2010)). This analysis showed that a wetter land surface increased the potential for moist convection, except for very dry

atmospheres. Moreover, during situations in which a moist layer of air undercuts a drier layer of air, such as the Indian monsoon, the land surface has a large influence on moist convection.

Using an approach based on a slab model of the atmosphere, combined with data from a atmospheric measurement campaign in Illinois, US, Findell and Eltahir (2003a) analyzed the atmospheric situations under which the land surface has an influence on precipitation. They classified these atmospheric situations using two diagnostics, one based on the humidity and one based on the convective potential in the lower atmosphere. Their results show no influence of the land surface on precipitation for very dry and very wet atmospheric conditions. For intermediate atmospheric wetness, a wetter land surface can lead to more precipitation when the convective potential is slightly positive. However, for strong positive convective potential, a wetter land surface leads to less precipitation.

As a first step in the chain of soil moisture, evaporation, boundary layer, precipitation coupling, Teuling et al. (2009) determined the correlations between evaporation and radiation and between evaporation and soil wetness (previous precipitation) from measurement data. When evaporation correlates well with radiation, it is atmospherically driven, whereas when it correlates well with soil wetness, it is moisture limited. In general, the hot-spots of soil moisture-precipitation coupling is found in the transition areas where evaporation shifts from being radiation limited (temperate and polar areas) to being moisture limited (tropical areas). In India, this transition of evaporation limitation is present and corresponds to the monsoon dynamics (Teuling et al. (2009) and Seneviratne et al. (2010)). In dry periods, evaporation is moisture limited and in wet periods it is radiation limited.

Based on atmospheric reanalysis data, Findell et al. (2011) studied the relation between the fraction of the surface energy budget that is used for evaporation (EF) and the afternoon precipitation for the US. By only taking into days without morning precipitation, the effect of previous precipitation was corrected for. The results showed an relation between the land surface wetness (EF) and the chance of precipitation, for the Eastern US, where earlier results also showed a strong influence of the land surface. However, no relation was found between the land surface and the amount of precipitation. Taylor et al. (2012) derived a relation between the contrasts in land surface in a give area and the afternoon precipitation from satellite data. They found an increased precipitation in areas that are relatively dry compared to their environment (on a scale of 50-100 km), suggesting that there is a negative feedback in the dynamics of local circulations. There was a large difference between this negative feedback diagnosed from the data and diagnosed from models.

By combining several land-atmosphere interaction approaches (the correlation between soil moisture and evaporation, atmospheric moisture recycling and soil moisture memory), Dirmeyer et al. (2009) found an influence of the land surface during India's

pre- and post-monsoon months (March-May and September-November). Based on soil moisture, evaporation and atmospheric data, they found that soil moisture influenced evaporation and moisture recycling during these periods.

Ongoing efforts to determine the coupling of the land surface to the atmosphere focus on determining and intercomparing coupling diagnostics from reanalysis datasets, atmospheric sounding measurements and site measurements (the GEWEX-GLASS LoCo (local coupling) working group, e.g. Santanello et al. (2011a), Ferguson and Wood (2011)). The work presented in chapters 2 and 3 are parts of those efforts.

In chapter 2, the sensitivity of the atmosphere to the surface conditions is determined globally using several land-atmospheric interaction diagnostics. Based on atmospheric reanalysis data, the effect of the land surface on precipitation occurrence as well on precipitation amount is determined. The global patterns in coupling strength are compared to other studies and the relative importance of coupling strength in India is determined.

Subsequently, in chapter 3 the focus shifts to India, where the annual cycle of the sensitivity of precipitation to land surface conditions is studied. A slab model of the atmosphere is forced with measured atmospheric moisture and temperature profiles. This model is run with a wet land surface and a dry land surface. The atmospheric conditions during which these model runs show a different convective precipitation outcome are classified using the framework presented by Findell and Eltahir (2003a), to determine if it is applicable in India. Finally, using a slightly adapted framework, India's spatial and temporal variability in coupling strengths will be determined.

1.3.3 Moisture Recycling Perspective: Ganges Basin Recycling

In the moisture recycling perspective, evaporated moisture is followed along its path through the atmosphere. This will be done until it comes back to the land surface as precipitation. This can be far away (more than thousands of kilometers) and nearby (within 100 km). Even when the moisture recycles locally, there is a difference with the local perspective. The moisture recycling perspective focuses on the moisture budget of the atmosphere, while the local perspective focuses on the energy balance (and thermodynamics).

The moisture recycling perspective has a timescale of less than a month (the mean residence time of moisture in the atmosphere is about two weeks). The spatial scales can be up to thousands of kilometers. These scales are highlighted in Figure 1.5. To determine the moisture recycling effects of irrigation, an atmospheric moisture tracing model has to be used. Several moisture tracing approaches exist, ranging from tracers built into climate models (Bosilovich and Schubert (2002), Numaguti (1999), Koster

(1986)), to models that use the output of atmospheric models for a tracing scheme to determine recycling rates a posteriori (Dirmeyer and Brubaker (1999, 2007), van der Ent et al. (2010), Trenberth (1999), Goessling and Reick (2011)).

Two approaches exist for the schemes that determine the recycling rate based on the output of atmospheric models. In an Eulerian approach, the atmosphere is discretized (usually according to the model definition of the forcing data) into a grid (it can have one or more layers in the vertical). In this scheme, the moisture that evaporated from the region of interest is tagged (the model equivalent of given a dye). For each grid box, a balance is made over the total moisture and over the concentration of the dye (the tagged moisture) every timestep. This balance involves the precipitation, of which a fraction is contributed, via the tagged moisture, by the evaporation from the region of interest.

A second approach is the use of a Lagrangian moisture tracing scheme. In this approach, packets of evaporated moisture are released from the land surface. These packets are followed on their path through the atmosphere. This path is determined by transporting the packet using the three dimensional wind speeds of the forcing data. Again during each timestep, a moisture budget of the packet is made; evaporation from the land surface enters the packet and precipitation falls from the packet, proportionally to these processes in the forcing data.

The two approaches have different assumptions. The Eulerian approach, the horizontal transport is integrated over the vertical layers of the forcing data. Using this integrated flux for transport studies assumes that there is not much vertical variability in the flux. If there is variability, this has effects on the total moisture transport. In the extreme case, the atmospheric flows in two layers are of same magnitude, but opposite direction. This would imply that moisture is transported in both directions. However, if the vertical integral of the horizontal flux is used, the net flow is zero and no moisture is transported away. Moreover, for the Eulerian approach, classical numerical issues (numerical diffusion, numerical stability) have to be accounted for by choosing the right time steps (to obtain Courant numbers around unity). The speed of calculation of the Eulerian approach is high, it decreases with domain size and resolution, but is very applicable on large (global) scales.

The Lagrangian approach releases evaporated moisture into the atmosphere at a certain height. Assumptions for this release height are that the height is random, but proportional to the atmospheric moisture profile in the forcing data (Dirmeyer and Brubaker (2007)). After release, the moisture is traced using the wind patterns of the forcing data. During each timestep, the moisture that is traced is assumed to contribute to the precipitation in the ratio of the precipitation to the total precipitable water at that location and time, regardless of the height of the parcel. The speed of calculation of this scheme is not dependent on domain size (memory use is), but on the source area considered. For source areas larger than the regional scale (around

1000 km), it requires a lot of computation.

A last approach is the explicit tracing of moisture in the atmospheric model. Evaporation from a certain location is tagged as moisture to be traced. During the model simulation, the moisture budget is made not only for the total moisture, but also for the traced moisture. The advantage of this approach is that the effects of all sub-timestep processes on the water budget of the traced moisture are incorporated, so the simulation is more realistic than the post-processing in the Eulerian and Lagrangian schemes. However, a disadvantage is that it is very costly to run the atmospheric model for long times and that the areas from where the evaporation is traced need to be specified before the model run.

Previous studies show a range of recycling ratios estimations for India. Using tracers in a GCM, Bosilovich and Schubert (2002) found that during JJA, about 9% of the precipitation on the Indian mainland originates from evaporation in the same region. Using the same method as used in the current study, Dirmeyer and Brubaker (2007) found 25 year mean recycling ratios at a typical spatial area of $10^5 km^2$ of 2-10%, with a peak during JJA. Yoshimura et al. (2004) followed tagged evaporation from the Indian land surface for the 1998 monsoon season (May-October) and found that the majority of evaporation precipitated again on the Himalaya slopes and in the Indus basin/Pakistan. For Calcutta, they found that 20-30% of the precipitation originated from evaporation from land surfaces. Using bulk methods, van der Ent et al. (2010) found that about 30% of the January land evaporation in India falls again as precipitation over land somewhere, while this is up to 90% during July. Trenberth (1999) used a bulk method to determine recycling ratios and found annual mean recycling ratios for India of less than 10% for a recycling length scale of 500km and 15-20% when a length scale of 1000km is used.

This previous work determined annual mean moisture recycling rates and often used low-resolution global models. The approach in current study will be a more detailed analysis of moisture recycling on the Indian peninsula by looking at spatial and temporal variability of this recycling. To do so, the Lagrangian moisture tracing scheme will be used, because it is not prohibitively expensive to compute for the size of the source areas of interest (the irrigated areas in India). Moreover, this scheme produces a better precipitation pattern and has a better representation of the vertical transport than the Eulerian schemes, which is important given India's orography. In chapter 4 the moisture tracing scheme will be applied to reanalysis data. This chapter describes the current water cycle and does not explicitly incorporate the effects of irrigation. The length and timescales of the atmospheric path of moisture evaporated from two areas with contrasting evaporation are compared. Moreover, the annual cycle of the fraction of moisture that recycles within the Ganges basin is determined and the importance of moisture recycling in the total river basin water balance is determined. In chapter 5, the moisture tracking scheme is applied to four atmospheric models.

These models were run with and without irrigation and their output was used to determine the length and timescales of recycling as in chapter 4, only now to determine the effect of irrigation.

1.3.4 Large Scale Perspective: Influence on Monsoon Flow

The effects of irrigation in the large scale perspective are the interaction with the monsoon flow. One of the causes of this flow is a pressure difference between land and ocean that is caused by differences in surface temperature. This temperature difference builds up during the spring months (March-May), when more solar radiation reaches the earth surface. Due to the higher heat capacity of the ocean, the land surface heats up more than the ocean. An increase in land surface wetness may lead to a decrease in temperature difference between land and ocean, resulting in weaker monsoon flows.

However, many processes on the large scale perspective (time and spatial scales shown in Figure 1.5), such as ocean temperatures (Indian ocean dipole, El Niño/La Niña, surface temperatures on the Tibetan plateau, the typical orography of the Indian orography as well as the dynamics of the inter-tropical convergence range dominate the Indian summer monsoon (Webster et al. (1998)). And it is unclear how important the land surface moisture state in the irrigated areas is.

To determine the large scale effects of irrigation, some studies have used land surface measurements from satellites (determining the greenness of the vegetation) in combination with precipitation patterns. However, the majority of earlier studies have used atmospheric models, ranging from conceptual monsoon models, to meso-scale and global scale models to simulate the effect of irrigation on the atmospheric flow and monsoon strength.

Using satellite data of the land surface greenness (NDVI), Lee et al. (2009) related increased pre-monsoon irrigation to a decreased monsoon precipitation during 1982 to 2003, which they hypothesized was caused by a decreased land-sea contrast. Niyogi et al. (2010) analysed NDVI data in combination with precipitation records of the second half of the 20th century and hypothesized that a decrease in precipitation in northern India is caused by the increased irrigation activity.

In a conceptual monsoon model, Zickfeld et al. (2005) found that once the land-sea pressure (and temperature) contrast falls below a critical value, the amount of moisture transported from sea to land is insufficient to fuel the heat engine that drives the monsoon circulation. In coastal areas, Lohar and Pal (1995) found that irrigation decreased sea breezes, causing reduced low-level moisture supply and a net negative effect of irrigation on precipitation. Douglas et al. (2009) found an influence of irrigation on meso-scale circulations and precipitation patterns. A decrease of precipitation occurred in the coastal zones, but an increase in precipitation in a band just south of

the heavily irrigated Ganges plain.

Douville et al. (2001) found two opposing impacts of a wetter soil; an increase in rainfall over northern India due to larger moisture supply, but also decreasing moisture convergence due to a decreased land-sea surface temperature contrast. Puma and Cook (2010) simulated performed a transient GCM run with increasing irrigation over the 20th century. During the winter month, irrigation increased precipitation slightly in Pakistan and Northern India. However, during the summer monsoon months, precipitation in India's southern and eastern coastal areas decreased with about 1 mm/day due to a decreased monsoon flow. Guimberteau et al. (2012) simulated irrigation in a GCM and found a delay in the monsoon onset date of about a week. The effects of irrigation on the atmospheric flow are not limited to the surface. Lee et al. (2011) found a decreased tropospheric height due to irrigation surface cooling. Moreover, the circulation patterns at the top of the troposphere changed, which might change monsoon activity. Therefore, the irrigation effects could remotely impact Asia's summer monsoon climate.

In chapter 5, an intercomparison of the effect of irrigation on the atmosphere as simulated by four climate models is presented. (Apart from the large scale perspective processes, these climate models also include the processes from the local and moisture recycling perspective.) The effect irrigation on the large scale atmospheric flow will be determined, as well the seasonal and spatial variation.

The results of these three perspectives will be presented in chapter 6. The relative importance of the perspectives will be discussed, as well implications for irrigation patterns. Also, some research perspectives and opportunities for further research will be presented.

Chapter 2

Global Indicators of Land-Atmosphere Interactions

Abstract

The role of the land surface in precipitation triggering and amplification is determined using two soil moisture-precipitation coupling diagnostics. The situations in which soil moisture has a positive influence, a negative influence or no influence on precipitation have been determined from the MERRA and ERA-interim reanalysis datasets.

In the tropics positive feedbacks (a wet land surface leads to more precipitation or a dry land surface leads to less precipitation) occur on up to 30-40% of the days during summertime. Negative feedbacks (a dry land surface leads to more precipitation or a wet land surface to less precipitation) are far less frequent and occur only in very dry areas. Atmospherically controlled situations occur otherwise.

The quality of the soil moisture coupling diagnostics ($\frac{d\theta_e}{dEF}$ (De Ridder (1997)) and CTP-HI_{low} (Findell and Eltahir (2003a))) has been assessed by comparing the positive feedback situations with the triggering and amplification feedback strengths (Findell et al. (2011)). It is shown that de Ridder's $\frac{d\theta_e}{dEF}$, when combined with a minimal boundary layer height, performs well in predicting triggering of precipitation. CTP-HI_{low} performs well for predicting the amount of precipitation. Combining CTP-HI_{low} with a minimal boundary layer height constraint did not improve predictions.

Globally, there are a number of locations where the diagnostics perform well and positive feedback occurs up to 40% of the time. These hotspots include the Southern Brazil, West- and Southern Africa, Central US, India and Mexico. In these areas, a

This chapter is submitted to Journal of Hydrometeorology as Tuinenburg et al. (2012b)

wet land surface can increase the probability of afternoon precipitation by up to 30% and the amount of afternoon precipitation by up to 1 mm.

2.1 Introduction

The coupling of soil moisture (θ) to precipitation (P) and P- θ feedback have been studied extensively over the past decades (see, for example, the reviews by Betts et al. (1996) and (Seneviratne et al., 2010)). Here, we follow Seneviratne et al. (2010) in their definition of 'coupling' and 'feedback'. Coupling is a one-way interaction in which one variable controls the other at least to some extent. Feedback involves a closed loop or two-way coupling or interaction, where both variables control each other. In the context of the present study, θ affecting P or P affecting θ are both expressions of P- θ coupling; P affecting θ upon θ affecting P (a closed loop) is feedback. Studies on P- θ coupling are strongly motivated by the need to understand the impact of soil moisture on weather and climate at many temporal and spatial scales and by the related idea that forecast skill of hydrometeorological models may be improved in particular over land areas where P- θ coupling is strong (Dirmeyer et al. (2009) and Koster et al. (2011)). Also, anthropogenically forced climate change is expected to lead to intensification of the hydrologic cycle (Held and Soden (2006), Bates et al. (2008)). Hydrologic models used to study the impact of such changes on the availability and distribution of terrestrial freshwater resources at global to regional scales are at present typically driven by climatological fields at a given atmospheric reference level, without recourse to any P- θ feedback. The lack of representation of such interactions is considered a possible error source in hydrologic models used for impact studies (Harding et al. (2011)). In this context, assessment of the occurrence and strength of P- θ feedback is thus required both to assess possibilities to improve forecast skills in hydrometeorological models and errors related to missing land-atmosphere interactions in hydrologic models for climate impact studies.

Because of the large range of scales and the suite of complex physical processes involved, the mechanisms that connect P and θ are not entirely clear in spite of the progress made in recent years (Seneviratne et al. (2010)). It is therefore not a surprise that results from atmospheric models vary strongly with regard to the strength and location of P- θ interactions (Koster et al. (2004) and Guo et al. (2006)). Modelled P- θ interactions critically depend on the model parameterizations (Mahanama and Koster (2005), Guo et al. (2006), Lawrence and Slingo (2005)), in combination with model resolution (Hohenegger et al. (2009)). Recent analyses based on observations confirm that the resolution of the present-day global circulation models may be too coarse to properly represent P- θ coupling (Taylor et al. (2011)). Thus, results from modelling experiments regarding P- θ interactions need not necessarily reflect the situation in the real world and therefore need to be used with caution. Nevertheless, modelling

experiments such as the benchmark study by Koster et al. (2004) have resulted in valuable information and guided research in this area.

Using observations to analyse P- θ coupling and feedback suffers from methodological issues too. First, in the real-world earth system it is impossible to prove existence of feedback at large scales using one set of observations: unlike in model experiments it is impossible to shut off one process selectively and repeat the observations without that process. Thus, one has to rely on a set of diagnostics to analyse the atmospheric state in conjunction with the land surface state (Betts (2004)). However, apart from providing insights in the mechanism of land-atmosphere interactions, such diagnostics can at best quantify the likelihood of P- θ coupling and feedback. To date there is no single best set of diagnostics available. Second, observations of key variables in this context, notably of evapotranspiration and soil moisture, are sparse. Even though observation networks and satellite monitoring capabilities have been expanding and improved in the past few decades for evapotranspiration (Wang and Dickinson (2012)) as well as for soil moisture (Dirmeyer (2011)) data records contain many gaps in space as well as in time. Third, statistical analysis of P- θ interaction contains many pitfalls sometimes leading to spurious results (e.g., Wei et al. (2008), Alfieri et al. (2008), Orlowsky and Seneviratne (2010)). In spite of these difficulties, some analyses of P- θ coupling and feedback based on observations have been attempted, although usually with a regional focus and in most cases supported by models calculations (e.g., Boé (2012), Findell and Eltahir (2003a,b), Taylor et al. (2011), Tuinenburg et al. (2011)). Only recently, a first global analysis based on observations has been presented by Ferguson and Wood (2011), who used a suite of remote sensing data to produce a global P- θ coupling classification map. Additionally, based on remotely sensed soil moisture, Taylor et al. (2012) found higher afternoon precipitation over dry areas (relative to the surrounding), especially in West-Africa. However, their analysis produced a wide range of results for different (reanalysis) models.

The GEWEX-GLASS local coupling (LoCo) research, to which this work contributes, attempts to bridge the gap of P- θ interactions, not necessarily reflecting the situation in the real world, and to analyze coupling and interactions at the process level. It includes diagnostics, models and observational approaches, some of which are described above. The goal (and challenge) of LoCo is to distinguish local coupling from large-scale coupling.

Because of the difficulties sketched above, analysis and quantification of P- θ feedback has been proven extremely difficult (Claussen et al. (2004)). The analyses available to date often show contradictory results (Seneviratne et al. (2010)). Relatively little information is available at the global scale and mainly comes from modelling experiments (e.g., Koster et al. (2004), Guo et al. (2006), Zhang et al. (2011)). There are large uncertainties and no reliable global climatology has been constructed as yet. Indeed, when Ferguson and Wood (2011) compared their global P- θ coupling

classification map based on remote sensing data to a similar one based on reanalysis data, marked differences were found between the differing maps and with the previous global studies (apart from some consistencies). Thus, in order to proceed towards a reliable global climatology of P- θ coupling and feedback there is a strong need for alternative analyses, based on alternative data sets and classification methods.

In this research we will present such an alternative analysis at the global scale. We will classify P- θ coupling and feedback in two reanalysis data sets: ERA-Interim (Interim Re-Analysis of the European Centre for Medium-Range Weather Forecast, ECMWF; Dee et al. (2011)) and MERRA (National Aeronautics and Space Administration (NASA) Modern Era Retrospective Analysis for Research and Applications; Rienecker et al. (2011)). Reanalysis products are a merger of up-to-date global weather forecast models with observations, using sophisticated data assimilation procedures to reproduce the atmospheric state as realistically as possible (Dee et al. (2011); Rienecker et al. (2011); Uppala et al. (2005)). Being realistic reconstructions of the weather from the past few decades they are a valuable source of information for analysis of P- θ coupling in spite of some problems (e.g., Betts et al. (2009)). They are therefore increasingly being used in this field of research in regional (Betts (2004), Findell et al. (2011)) to global setting (Ferguson and Wood (2011)).

Our study will also extend the previous global analyses by using two differing classification schemes: the first one is based on the framework proposed by Findell and Eltahir (2003a) and the second one on the diagnostic proposed by De Ridder (1997). These diagnostics are selected here because they include some important mechanisms by which P and θ are coupled. Soil moisture can interact with precipitation directly as well as indirectly. In the direct or recycling mechanisms, a surplus of water vapour entering the atmosphere over wet soils by evapotranspiration is recycled as precipitation. The fraction of recycled water strongly depends on the scale considered and typically amounts to about 10% at a spatial scale of 500 km (Trenberth (1999), van der Ent et al. (2010)). This mechanism can only explain wet positive interaction and feedback, that is, wet soil favouring precipitation. The indirect effect is mediated by the impact of θ on the partitioning of energy between the latent heat flux (λE , with E the water vapour flux and λ the latent heat of vaporization) and the sensible heat flux (H) from the surface (Betts et al. (1996), Betts (2004)). This in turn affects the development of the Atmospheric Boundary Layer (ABL), which may ultimately help to trigger convective precipitation or inhibit it. The indirect mechanism can lead to positive as well as to negative P- θ coupling and feedback, depending on the surface conditions and the atmospheric state (Findell and Eltahir (2003a)). Wet positive feedbacks occur if wet soils favour convective precipitation; dry soils inhibiting convective precipitation imply dry positive feedback. Conversely, negative feedbacks occur if wet soils inhibit convective precipitation or if dry soils favour convective precipitation (Siqueira et al. (2009)).

The indirect mechanism provides the dominant link between P and θ (Schär et al. (1999)), which is also defined as the local coupling (LoCo) process chain (Santanello et al. (2011a), Santanello et al. (2011)). In this mechanism the interaction between the ABL and the free atmosphere is crucial in two ways. First, the state of the free atmosphere just above the ABL critically determines via entrainment the ABL development (Betts et al. (1996), Ek and Holtslag (2004), van Heerwaarden et al. (2009)) and the resulting strength of P- θ coupling (De Ridder (1997), Findell and Eltahir (2003a,b)). Second, the stability of the free atmosphere will determine whether or not the development of the ABL will ultimately lead to convective precipitation (Findell and Eltahir (2003a), Juang et al. (2007), Kohler et al. (2010)). The fact that conditions in the free atmosphere are determined to a large extent by synoptic scale process implies that analysis of P- θ interactions requires considering the connection between local scale and the synoptic scale processes. Alternatively, P- θ coupling classifications could be stratified according to large-scale circulation patterns (Boé (2012)).

The diagnostics utilized in this study acknowledge the crucial role of energy partitioning and ABL development in connection with effects of entrainment. In that way, they also provide a link to the synoptic scale. The CTP-HI_{low} framework has recently been applied in P- θ coupling analyses at regional (van den Hurk and van Meijgaard (2010), Tuinenburg et al. (2011)) and global scale (Ferguson and Wood (2011)). To our knowledge the De Ridder (1997) approach has not yet been attempted in large-scale studies of P- θ coupling. Here, we will provide a comparison of the two diagnostics and analyse their performance (cf. Ferguson and Wood (2011)). This is important in order to be able to assess the uncertainty in the resulting maps. In addition, inclusion of the Findell and Eltahir (2003a) diagnostic set will allow comparison with the aforementioned studies as well.

For our classification we will also extend both sets of diagnostics to account for the crucial role of the Lifting Condensation Level (LCL) in relation with ABL growth (Santanello et al. (2011a)). The LCL has since long been used as a diagnostic in land-atmosphere coupling studies (Betts (2004)). It is defined as the level at which an air parcel that rises dry-adiabatically from the surface becomes saturated. It is a necessary, though not sufficient, requirement that the ABL height (h) reaches the LCL for rising air parcels from the surface to become involved in convection leading to precipitation and therefore for the surface to affect precipitation via the indirect mechanism. While wet soils tend to reduce the LCL, ABL growth is reduced as well. Conversely, dry soils increase the LCL but they enhance ABL growth. The resulting balance between the effect of the land surface state on ABL growth and that on LCL is thus a crucial link in the chain of events leading to P- θ coupling. We will therefore include a comparison between h and the LCL in our classification.

The goal of this research is to determine the effect of soil moisture on precipitation, using two land-atmosphere feedback diagnostics. The frequency of days in which pos-

itive, negative and no feedbacks are expected is determined. Moreover, it is assessed whether precipitation also occurs when expected (for example, when a positive feedback is diagnosed, and the land surface is wet, whether precipitation really occurs). Finally, it will be determined how much additional precipitation the land surface state can contribute.

This research is structured as follows. The methods section (2.2) introduces the diagnostics, the assumptions and data used to derive them, and describes the method of diagnosing the performance of the diagnostics. Section 2.3 presents the frequencies of various feedbacks as diagnosed, the performance of the diagnostics and the amount of precipitation that is dependent on land surface conditions. Section 2.4 presents the discussion and conclusions.

2.2 Methods

This section describes the land-atmosphere feedback diagnostics that are analysed in this research, as well as the data used to derive them.

2.2.1 Diagnostics

The two land-atmosphere diagnostics used in this study describe the relation between the land surface state and convection, based on the temperature and humidity of the lower atmosphere and the land surface fluxes. Both diagnostics have been developed in a one-dimensional setting, which means that any dynamical feedbacks (increased moisture convergence due to convection, etc.) are not ignored.

CTP-HI_{low}

The CTP-HI_{low} framework was introduced by Findell and Eltahir (2003a). It consists of the CTP (the Convective Triggering Potential), which is a measure for the buoyant potential energy in the lower atmosphere (from the surface up to 300 hPa above the surface), and the HI_{low} (the Humidity Index in the lower atmosphere), which is a measure for the humidity in the lower part of the atmosphere (evaluated at 950 and 850 hPa).

CTP is defined in a way similar to CAPE (Convective Available Potential Energy):

$$CTP = \int_{P_{surf}-100hPa}^{P_{surf}-300hPa} g \left(\frac{Tv_{parcel} - Tv_{env}}{Tv_{env}} \right) dz \quad (2.1)$$

HI_{low} is defined as the sum of the dewpoint depressions at 950 hPa and 850 hPa:

$$HI_{low} = (T_{950} - T_{d,950}) + (T_{850} - T_{d,850}) \quad (2.2)$$

Findell and Eltahir (2003a) determined the influence of soil moisture on the triggering of convective precipitation using a slab model of the ABL. For different values of CTP and HI_{low} , they found different influences of the land surface. They created the CTP- HI_{low} framework which is shown in Figure 2.1.

For low values of HI_{low} ($<5K$), the atmosphere is very moist and precipitation trigger-

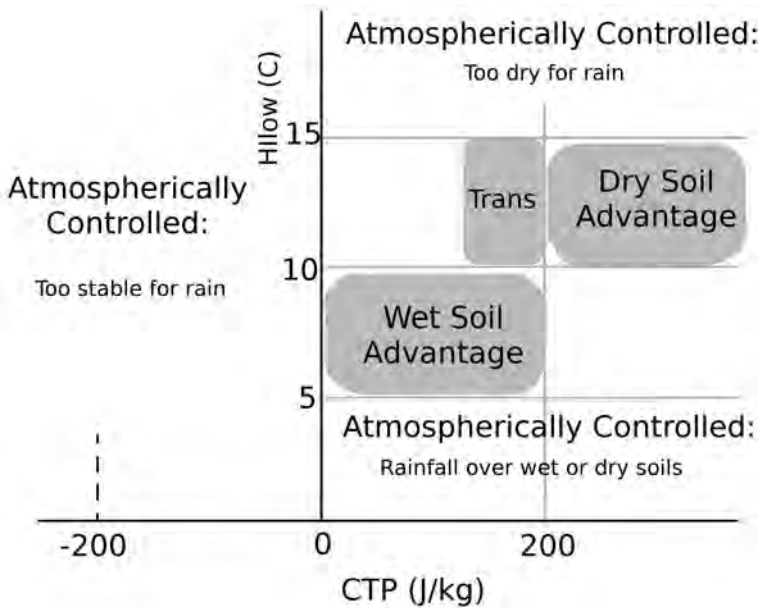


Figure 2.1: The CTP- HI_{low} framework, adapted from Findell and Eltahir (2003a)

ing will occur regardless of soil moisture conditions. For high values ($HI_{low} > 15K$) the atmosphere is too dry and no precipitation will occur regardless of soil moisture condition. For intermediate values, the land surface influences convective precipitation. For $0 < CTP < 200$ and $5 < HI_{low} < 10$, a wet land surface will trigger convection, while a dry land surface will not. This is a positive feedback. For $CTP > 200$ and $10 < HI_{low} < 15$, a dry land surface will trigger convection, while a wet land surface will not. This is a negative feedback.

De Ridder's diagnostic

Using a slab model of the convective ABL, De Ridder (1997) derived an analytical expression that relates equivalent potential temperature (θ_e) in the ABL to evaporative

fraction (EF):

$$\frac{d\theta_e}{dEF} = \frac{1}{2}\Theta_e(t)\left(\frac{1}{(1-EF)^{\frac{3}{2}}} + \frac{1-\mu}{(1-EF)^{\frac{1}{2}}}\right) \quad (2.3)$$

in which:

$$\mu = 2(1+\beta) - \frac{L_v}{c_p} \frac{|\gamma_q|}{\gamma_\theta} (1+2\beta) \quad (2.4)$$

$$\Theta_e(t) = \left(\frac{(R_n - G)\gamma_\theta t}{2(1+2\beta)\rho_a c_p}\right)^{\frac{1}{2}} \quad (2.5)$$

with G the ground heat flux, R_n the net radiation, γ_θ the above-ABL lapse rate of the potential temperature, γ_q the above-ABL lapse rate of specific humidity, ρ_a the density of air, c_p the heat capacity, L_v the latent heat of vaporization and β the scaling between the surface and the ABL top turbulent heat flux (assumed to be 0.3 De Ridder (1997)).

By comparing (latent) heat influx from the surface ($R_n - G$) with the influx from entrainment from above the ABL (γ_θ and γ_q), $\frac{d\theta_e}{dEF}$ (hereafter the Ridder diagnostic) describes the influence of the surface flux partitioning on the potential energy budget of the ABL. De Ridder (1997) found that for almost all reasonable values of μ and Θ_e , $\frac{d\theta_e}{dEF} > 0$. While the Ridder diagnostic describes the relation between θ_e and EF, it depends on EF itself (Equation 2.3). For values of EF approaching 1, the Ridder diagnostic approaches infinity.

ABL Height

Both diagnostics described depend on the moisture and temperature characteristics of the entrained air, which are described by means of the above ABL moisture and temperature lapse rates. CTP is evaluated between 100-300 hPa above the surface. In this study, the lapse rates for the Ridder (γ_q and γ_θ) are diagnosed at these levels as well. These integration bounds have been chosen because they represent the height to which the ABL may penetrate, depending on the surface characteristics (Findell and Eltahir (2003a)).

In addition to evaluating the diagnostics, this study will also compare these diagnostics with the ABL height. This extra criterion assesses whether or not the ABL will be able to transfer signals from the surface to the free atmosphere. If the ABL height does not reach the LCL, influences from the surface cannot have an impact on convection above the ABL.

2.2.2 Data

The diagnostics in this study are evaluated for reanalysis data from 1999-2009. Two reanalysis datasets are used, MERRA (Rienecker et al. (2011)) and ERA-interim (Dee et al. (2011)). For each hemisphere, data for the summer half year are analysed (April-September for the Northern hemisphere and October-March for the Southern hemisphere). The data needed for the analyses are the two dimensional fields of soil moisture, ABL-height, latent heat flux and sensible heat flux, as well as the three dimensional fields of specific humidity and potential temperature. The datasets were acquired at the highest resolution available. The ERA-interim data are available for every 6 hours for all fields with a horizontal resolution of 0.75 degrees and a vertical resolution of 11 levels in the vertical between 950 hPa and 700hPa. The MERRA data have an hourly resolution for the two dimensional variables and a 6-hourly resolution for the three dimensional variables. The horizontal resolution is $2/3 \times 1/2$ degrees and there are 16 levels in the vertical between 950 hPa and 700 hPa.

To determine whether the feedback loop is closed, the soil moisture and precipitation on the days in which a positive feedback is expected are examined. Because the precipitation in the reanalyses does not have the same temporal resolution (hourly vs 6-hourly) and to compare the diagnosed diagnostics to the same precipitation, the precipitation used in this analysis are acquired from the CMORPH dataset (Joyce et al. (2004)), which is available 3-hourly on a horizontal resolution of 0.25 degrees for the domain from 60S to 60N.

For the Ridder diagnostic, thresholds need to be determined, which is done using the ARM-SGP site station data (U.S. Department of Energy as part of the Atmospheric Radiation Measurement (ARM) Climate Research Facility Southern Great Plains site data).

2.2.3 Algorithms

CTP- HI_{low}

CTP and HI_{low} are determined from early morning profiles, when the solar radiation has not yet influenced the atmospheric conditions. As the reanalysis datasets have a temporal resolution of 6 hours, for each location the value closest to 6 AM local time was taken from the reanalyses data. Thus, the difference with 6 AM is at most three hours. Based on the humidity and potential temperature profiles, Equations 2.1 and 2.2 are applied. As the integration bounds, the pressure levels in the model were chosen that were closest to those in the definition.

De Ridder's $\frac{d\theta_e}{dEF}$

The lapse rates used in equation 2.3 are determined from the same timesteps as those for the CTP and HI_{low} , but are diagnosed between 900 hPa and 800 hPa. EF is determined from the mean latent and sensible heat fluxes around noon. Following De Ridder (1997), values in equations 2.3, 2.4 and 2.5 were: $L_v = 2500000 J/kg$, $t = 40000 s$, $\rho_a = 1.225 kg/m^3$, $c_p = 1003.5 J K g^{-1} K^{-1}$ and $\beta = 0.3$.

For the CTP- HI_{low} framework, strict boundaries for feedback categories were defined by Findell and Eltahir (2003a) (see Figure 2.1). For the Ridder diagnostic, such thresholds were not yet available. Here, we have derived a suitable threshold from the relation between EF and precipitation observed at the ARM SGP site. At this site, good atmospheric profile measurements as well as good surface flux observations were available.

Figure 2.2 shows the slope of a linear regression between EF and CMORPH afternoon precipitation for the ARM SGP site per $\frac{d\theta_e}{dEF}$ bin. It is based on the Ridder diagnostic values derived from the profiles measured at the site. The green lines show the outcome of a t-test to test whether the slope of the regression between $\frac{d\theta_e}{dEF}$ and the precipitation is significantly different from zero.

For low values of $\frac{d\theta_e}{dEF}$, there is no significant relation between $\frac{d\theta_e}{dEF}$ and EF. For

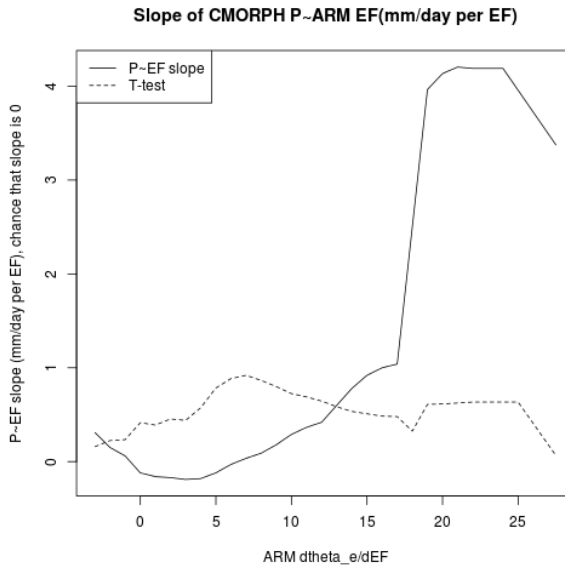


Figure 2.2: The slope of a linear regression between CMORPH precipitation and evaporative fraction (EF) from the ARM SGP site for different values of $\frac{d\theta_e}{dEF}$.

values of $\frac{d\theta_e}{dEF} > 20$, there is a positive relation between $\frac{d\theta_e}{dEF}$ and EF. Therefore, in the remainder of this paper, a threshold for a positive influence of the land surface on precipitation of $\frac{d\theta_e}{dEF} > 20$ will be used for positive feedbacks.

For negative feedbacks a threshold of $\frac{d\theta_e}{dEF} < 0$ is chosen because values of $\frac{d\theta_e}{dEF}$ smaller than -5 K/(-) do not occur in practice.

2.2.4 Indicator Evaluation

Comparing the soil moisture state with precipitation raises the question whether the soil is wet because of the precipitation or whether there is precipitation because the soil is wet. To isolate the effect of soil moisture state on precipitation, we classify days only when there is no morning (CMORPH) precipitation ($< 1\text{mm}$). For these days, the early morning soil moisture state is determined and compared to the afternoon (CMORPH) precipitation. Following Findell et al. (2011), the dependence of precipitation on EF is determined using two measures, the triggering feedback strength (TFS) and the amplification feedback strength (AFS). TFS is the relation between EF and probability of precipitation. AFS is the relation between EF and amount of precipitation.

To assess the ability of the diagnostics to determine the influence of the land surface on precipitation and precipitation triggering, the TFS and AFS are determined from three data subsets. First, TFS and AFS are determined for the days in the dataset without morning precipitation. Next, TFS and AFS are determined for the days in the datasets without morning precipitation and with a positive feedback (CTP-HI_{low} and the Ridder). In addition, AFS and TFS are calculated for the same subset of days, but with the additional restriction of a ABL height larger than 1000m. When the ABL does not reach 1000m, we assume that the signal from the land surface is not transferred to the free troposphere. We define the quality of the diagnostic as the difference between TFS and AFS based on the different datasets. If the diagnostics perform well, then the subset of days with positive feedbacks is expected to have a higher TFS and AFS than the TFS and AFS based on the subset of all the days.

Triggering Feedback Strength

TFS is the conditional probability of afternoon precipitation occurrence on EF (Findell et al. (2011)). It is defined as the slope of the probability of precipitation versus EF. For each grid cell, the data are split into ten equal bins of EF, for which the (conditional) probability of precipitation (probability of $P > 1\text{mm}$) is determined. Subsequently, the slope of this probability with EF is determined to give the increasing probability of precipitation (triggering) with EF. The slope is multiplied by the

standard deviation of EF (σ_{EF}):

$$TFS = \sigma_{EF} \frac{\partial p(\text{precip})}{\partial EF} \quad (2.6)$$

For further details about the derivation of TFS, the reader is referred to Findell et al. (2011).

The TFS is determined for all the data as well as for a subset of the positive feedback cases for each diagnostic. The difference between these calculations assesses the added value of the diagnostic in predicting the influence of the land surface on precipitation triggering.

Amplification Feedback Strength

The conditional probability of the amount of afternoon precipitation on EF, the amplification feedback strength is similar to the TFS, but the expectation of precipitation is determined instead of the probability of precipitation (Findell et al. (2011)):

$$AFS = \sigma_{EF} \frac{\partial E(\text{precip})}{\partial EF} \quad (2.7)$$

This will again be done for all the data, as well as for a subset of the positive feedback cases. The difference between the sets assess the added value of the diagnostic in predicting the influence of the land surface on the amount of precipitation.

2.3 Results

2.3.1 Positive Feedback

Figure 2.3 shows the fraction of days in the summer season (April-September for the northern hemisphere, October-March for the southern hemisphere) diagnosed as days with positive feedback, in the MERRA and ERA-interim reanalyses, respectively.

The different nature of the two diagnostics used can be seen in the different patterns in Figure 2.3. CTP-HI_{low} is exclusively defined by the characteristics of the ABL-layer, while the Ridder diagnostic also depends on the surface state. The areas where the CTP-HI_{low} shows the largest fractions of positive feedbacks are located in regions with a transition between a wet atmosphere and a dry atmosphere (HI_{low}=5-10K). In contrast with the Ridder diagnostic, which shows high fractions of positive feedback situations in areas which have a high EF. Due to the strong dependence on EF, the Ridder diagnostic is high in tropical areas which have high EF. Also, as noted by De Ridder (1997), the Ridder diagnostic increases with decreasing μ (equation 2.4).

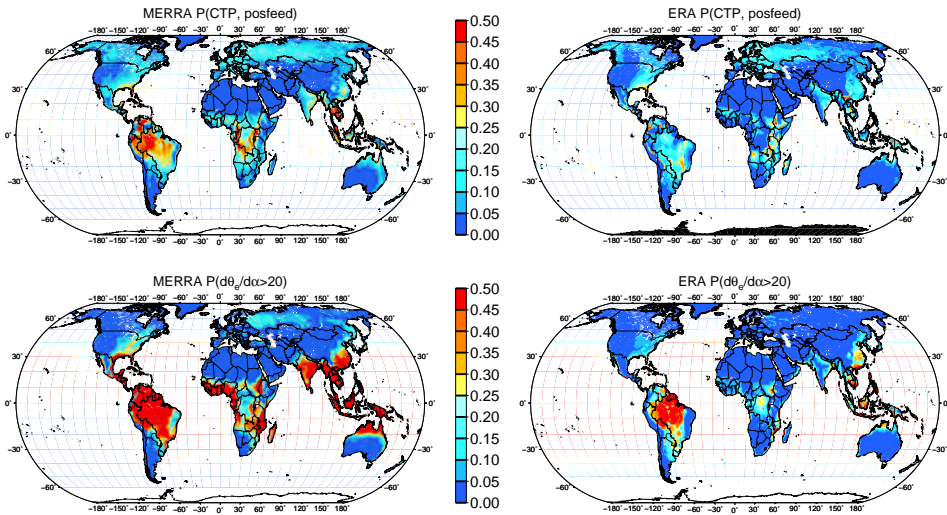


Figure 2.3: Fraction of days of the summer season (April to September for the Northern Hemisphere, October to March for the Southern Hemisphere) during which a positive soil moisture-precipitation feedback is expected for two diagnostics and two datasets. The upper row shows the positive feedback situations based on the CTP-HI_{low} framework, while the lower row shows the positive feedback situations based on the Ridder diagnostic. The left column shows the results for the MERRA reanalysis dataset, while the right column shows the same analysis based on the ERA-interim data.

Negative values of μ are found in areas with a large vertical moisture gradient γ_q , notably coastal areas where the moist marine air undercuts drier air flows. An example of the latter situation is the coastal region of the southeast US.

Apart from the difference between the diagnostics, there is also a large difference between the data sources. For CTP-HI_{low}, there are notable differences in positive feedback frequencies in Africa and South-America. ERA-interim has higher frequencies in east Africa, while MERRA has higher frequencies in West and Central Africa. In South-America, a similar shift is noted, with ERA-interim showing more positive feedback situations in the South-Eastern part and MERRA more in the Amazon.

For the Ridder diagnostic, the patterns of the frequencies are roughly the for the datasets. Although the frequencies based on the MERRA dataset are much higher than those based on the ERA-interim data, both datasets show positive feedbacks in the Amazon, India, China and Indonesia. However, the MERRA dataset shows a signal in the eastern US and West Africa, whereas the ERA-interim datasets only gives a signal in Central Africa.

The differences in positive feedback frequencies for the Ridder diagnostic between ERA-interim and MERRA are due to generally lower values of the Ridder diagnostic in ERA-interim than in MERRA. This is shown in Figure 2.4 where the average values of the Ridder diagnostic is shown for the two datasets. The Ridder diagnostic patterns of the mean value are similar, with larger values in South America, India, China, Indonesia and the eastern US. However, in Central Africa, ERA-interim yields higher values than in the rest of the continent, while MERRA yields higher values in West- and East-Africa. The mean values in ERA-interim generally are lower than those in MERRA and are just below the $\frac{d\theta_e}{dEF}=20\text{K}/(-)$ threshold. This explains the difference between the frequencies from the datasets in Figure 2.3. Apart from the different models driving the reanalyses, the differences in $\frac{d\theta_e}{dEF}$ may be due to the difference in temporal resolution. As the Ridder diagnostic strongly depends on the surface fluxes, a good temporal representation of these fluxes is essential. In this respect, MERRA's hourly resolution is a lot better than ERA-interim's 6-hourly resolution.

Figure 2.5 shows the frequency of positive feedbacks with the additional constraint

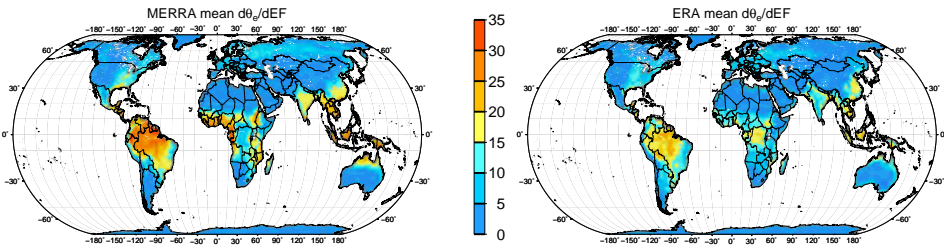


Figure 2.4: Mean $\frac{d\theta_e}{dEF}$ during the summer season, derived from MERRA and ERA-interim.

of a ABL height higher than 1000m. The additional constraint does not have a very large impact on the frequencies, compared to Figure 2.3. The patterns are similar, but in some of the areas (Amazon, Central Africa) with frequent occurrence of positive feedbacks using the Ridder, the ABL height of 1000m is not reached (probably due to very wet land surface) and the frequencies are lower.

2.3.2 Negative Feedback

Figure 2.6 shows the fraction of days with negative feedback situations (a dry land surface will promote precipitation, while a wet land surface will inhibit precipitation) for both datasets, using both diagnostics.

The difference between the diagnostics found for to the positive feedbacks in section 2.3.1 are also clear for the negative feedbacks. In the CTP- HI_{low} framework, negative feedback occurs if the lower atmosphere is fairly dry ($HI_{low}=10\text{-}15\text{K}$) while there is

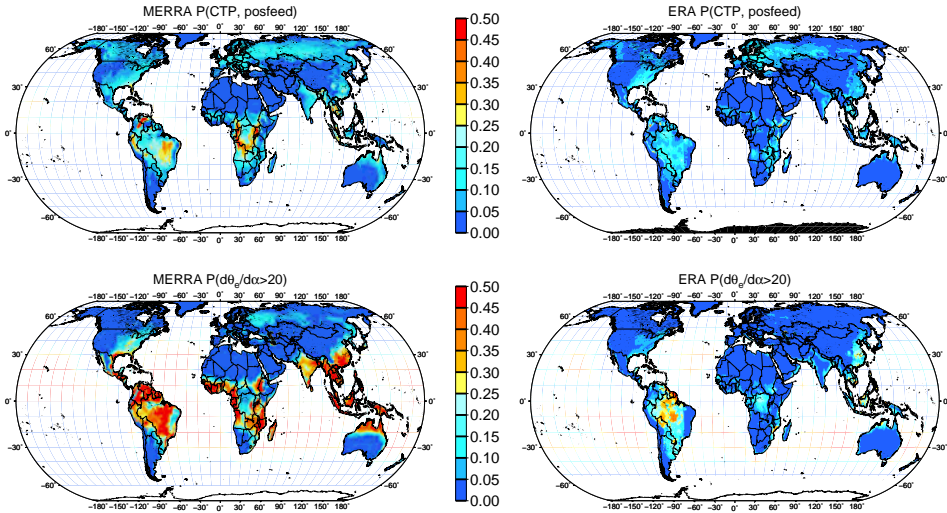


Figure 2.5: Fraction of days of the summer season (April to September for the Northern Hemisphere, October to March for the Southern Hemisphere) during which (1) a positive soil moisture-precipitation feedback is expected for two diagnostics and two datasets and (2) the maximum ABL height exceeds 1000m. The upper row shows the positive feedback situations based on the CTP- HI_{low} framework, while the lower row shows the positive feedback situations based on the Ridder diagnostic. The left column shows the results for the MERRA reanalysis dataset, while the right column shows the same analysis based on the ERA-interim data.

The difference between the diagnostics found for to the positive feedbacks in section 2.3.1 are also clear for the negative feedbacks. In the CTP- HI_{low} framework, negative feedback occurs if the lower atmosphere is fairly dry ($HI_{low}=10-15K$) while there is sufficient buoyant energy in the lower atmosphere ($CTP > 180J/kg$). On the other hand the Ridder diagnostic can only be negative when EF is small and $\mu > 2$ (in equation 2.4), which only occurs if $\frac{|q|}{\gamma_{\theta}}$ is negative or very small.

For both MERRA and ERA-interim, negative feedback situations are very rare in the CTP- HI_{low} framework. Frequencies between 0.01 and 0.05 are found in the eastern US, South-Western South America, India and Western Russia. The MERRA reanalysis also predicts some negative feedbacks in central Africa, but this is not the case for the ERA-interim data.

For the Ridder diagnostic, negative feedbacks are more frequent, but confined to the very dry desert areas. The patterns are very similar for the datasets.

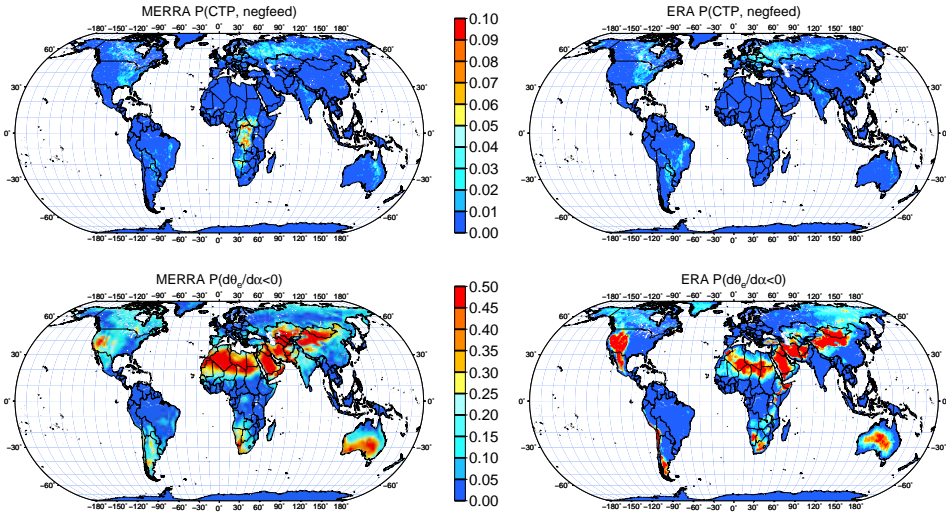


Figure 2.6: Fraction of days of the summer season (April to September for the Northern Hemisphere, October to March for the Southern Hemisphere) during which a negative soil moisture-precipitation feedback is expected for two diagnostics and two datasets. The upper row shows the negative feedback situations based on the CTP- HI_{low} framework, while the lower row shows the negative feedback situations based on the Ridder diagnostic. The left column shows the results for the MERRA reanalysis dataset, while the right column shows the same analysis based on the ERA-interim data.

2.3.3 Triggering and Amplification Feedback Strength

In this section we compare the diagnosed positive feedback strengths with the triggering and amplification feedback strengths (TFS and AFS). The TFS and AFS are calculated based on all the data as well as based on the data for which a positive feedback is expected. Both TFS and AFS are expected to be larger for the subset of positive feedback cases than for all the data. Therefore the quality of the feedback diagnostic can be assessed from the differences in the increase from the datasets.

Figure 2.7 shows the TFS for the different data subsets. The top row shows the TFS based on all the data. TFS values are positive almost everywhere, with high values notably in West-Africa, Southern-Africa and China. Much higher values are obtained for MERRA than for ERA-interim. Similar to Findell et al. (2011) (who use a different dataset and left out days with negative CTP), relatively high values are found in Mexico and the Western US, but these values are lower than in other regions in the world. The TFS also is high in dry areas, which might be caused by a few precipitation events, for which the TFS can be sensitive.

AFS is depicted in Figure 2.8. Again, the top row is based on all the data. The AFS shows hotspots in classical feedback regions (West-Africa, West India (East India has negative AFS) and Central/eastern US), as well as in Southern Africa and Australia in both datasets. Again the results are similar to those of Findell et al. (2011). In South-America and Central Africa, the datasets diverge. Here, MERRA shows more positive feedbacks than ERA-interim. As with the TFS, the AFS show high positive and negative values in dry areas, which are sensitive for individual precipitation events.

CTP-HI_{low}

The skill of CTP-HI_{low} in predicting the triggering of convection is limited. The panels in the second row of Figure 2.7 show the TFS based on cases with a CTP-HI_{low} positive feedback. These figures are dominated by negative values, with the exception of West-Africa, India, coastal China and Western Brazil/Bolivia.

When the AFS based on the data with (CTP-HI_{low}) positive feedback is compared with the AFS based on all data (second row in Fig. 2.8), added value (positive values) is obtained for India, coastal China and (of lower magnitude) in the eastern US in both datasets. In West-Africa and the Amazon, the AFS based on the positive feedback data is higher in MERRA, but mixed values are found in ERA-interim.

CTP-HI_{low} and ABLH

The third row in Figure 2.7 shows the difference between TFS based on (CTP-HI_{low}) positive feedback cases and a ABL layer height higher than 1000m and based on the positive feedback alone (regardless of ABL height). For both datasets, negative and positive values are scattered. For ERA-interim, the added value of diagnosing the ABL height is present in China, India and some parts of the Amazon, although the latter also shows negative values. Including ABL height is only beneficial in India and China for the MERRA data.

The added value of combining CTP-HI_{low} with ABL layer height for the amount of precipitation (AFS) is limited. Values in the third row of Figure 2.8 are scattered. However, some positive values are found in South-America, the eastern US and India.

Ridder

The difference between TFS based on positive feedback cases from the Ridder diagnostic and based on all data is very different between MERRA and ERA-interim (fourth row in Fig. 2.7). For MERRA, uniformly high values are found in the east-

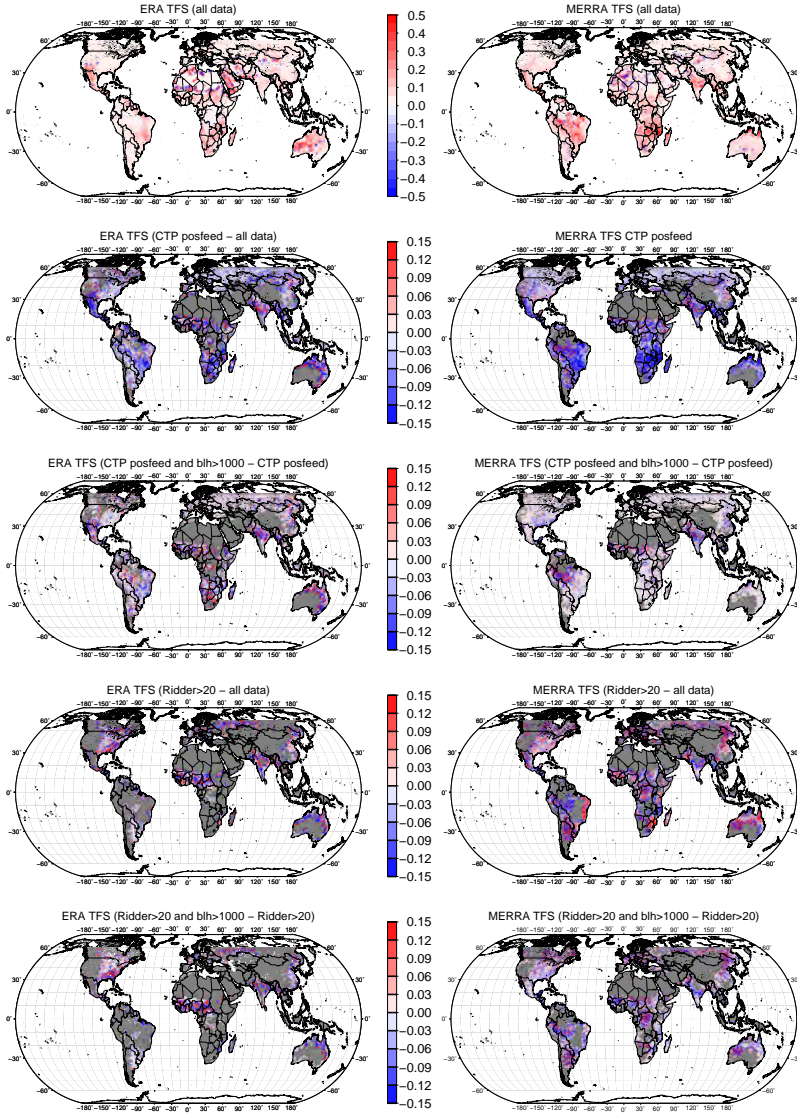


Figure 2.7: Triggering Feedback Strength (TFS, Findell et al. (2011)) based on ERA-interim (left column) and MERRA (right column) surface fluxes and atmospheric profiles and CMORPH afternoon precipitation. The units of TFS are probability of precipitation per (dimensionless) EF. The top row shows the TFS based on all the data in which no morning precipitation occurred. The second shows the difference of TFS based on days with a positive feedback based on $CTP-HI_{low}$ and that based on all data. The third row shows the difference between TFS based on days with a positive feedback ($CTP-HI_{low}$) and a ABL higher than 1000m and based on days with only a positive feedback. The fourth and fifth rows are similar to the second and third rows, only the feedbacks are based on the Ridder diagnostic.

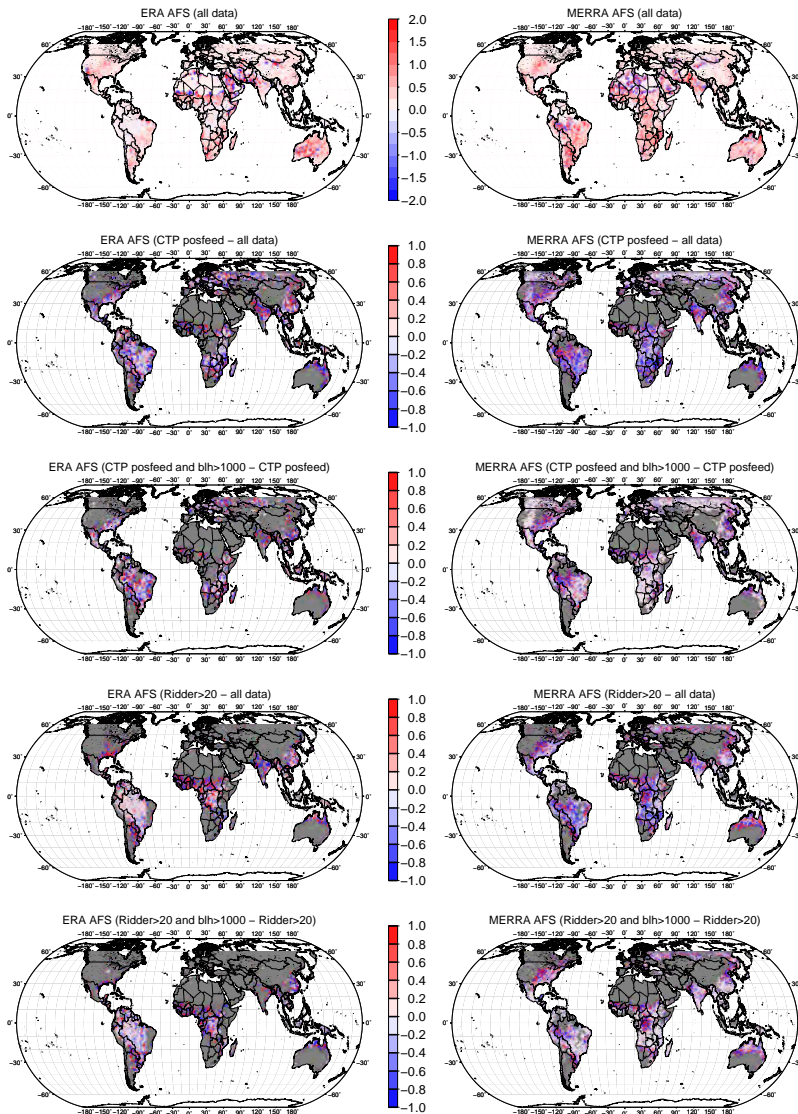


Figure 2.8: Amplification Feedback Strength (AFS, Findell et al. (2011)) based on ERA-interim (left column) and MERRA (right column) surface fluxes and atmospheric profiles and CMORPH afternoon precipitation. The units of AFS are amount of precipitation per (dimensionless) EF. The top row shows the AFS based on all the data in which no morning precipitation occurred. The second shows the difference of AFS based on days with a positive feedback based on CTP- HI_{low} and that based on all data. The third row shows the difference between AFS based on days with a positive feedback (CTP- HI_{low}) and a ABL higher than 1000m and based on days with only a positive feedback. The fourth and fifth rows are similar to the second and third rows, only the feedbacks are based on the Ridder diagnostic.

ern US and China, whereas ERA-interim shows such high values in South-America, Central- and West-Africa, India and the eastern US.

For AFS, there are also large differences between the datasets. ERA-interim yields high values in Central Africa, China, and the Southern US. For MERRA, the added values of the Ridder diagnostic is not present, with a lot of negative values and otherwise scattered values.

Ridder and ABLH

The combination of the Ridder diagnostic and the ABL height shows improvements in TFS compared to using only the Ridder diagnostic (last row in Fig. 2.7). For both datasets, TFS values are higher for the subset of data with the ABL height included. This is the case almost everywhere, with the exception of West-Africa, where adding the ABL height constraint decreases the TFS for MERRA.

2.3.4 Triggering and Amplification of Precipitation

Figure 2.9 allows to examine the relation between EF and afternoon precipitation in more detail for four regions (see upper panel of Figure 2.10) that have a high TFS and AFS in both datasets. For these regions (India, Mexico, South-East Brazil, South-East Africa), EF is considered in bins of width 0.1 (-). For each EF bin, the mean afternoon CMORPH precipitation is determined, as previously, only for days in which the morning precipitation was small ($< 1mm$). To test whether the relationship between EF and precipitation for positive feedback days is different than for other days, this was done for the subsection of days with a positive feedback and for the subsection of days without a positive feedback (the rest of the days). This procedure was followed for both diagnostics and both datasets (given eight curves per region).

Differences in absolute precipitation values between the positive feedback cases and the non-positive feedback cases are likely to occur from different precipitation regimes, i.e. positive feedback cases are more likely to occur during wetter periods. Therefore, to determine the effect of changes in EF on precipitation, the derivative of precipitation against EF (the slope in Figures 2.9) has to be assessed, rather than the absolute precipitation values.

The panels in Figure 2.9 show the resulting relations between EF and afternoon precipitation for all four locations. Generally, precipitation is low for low EF fractions and increases to EF fractions of about 0.7, whereafter precipitation decreases. The legend of Figure 2.9 shows the slope of a linear regression between EF and afternoon P for all subsets of data.

For India and Mexico, the slopes of the regression of precipitation against EF for the positive feedback cases are different from those for the rest of the cases, while

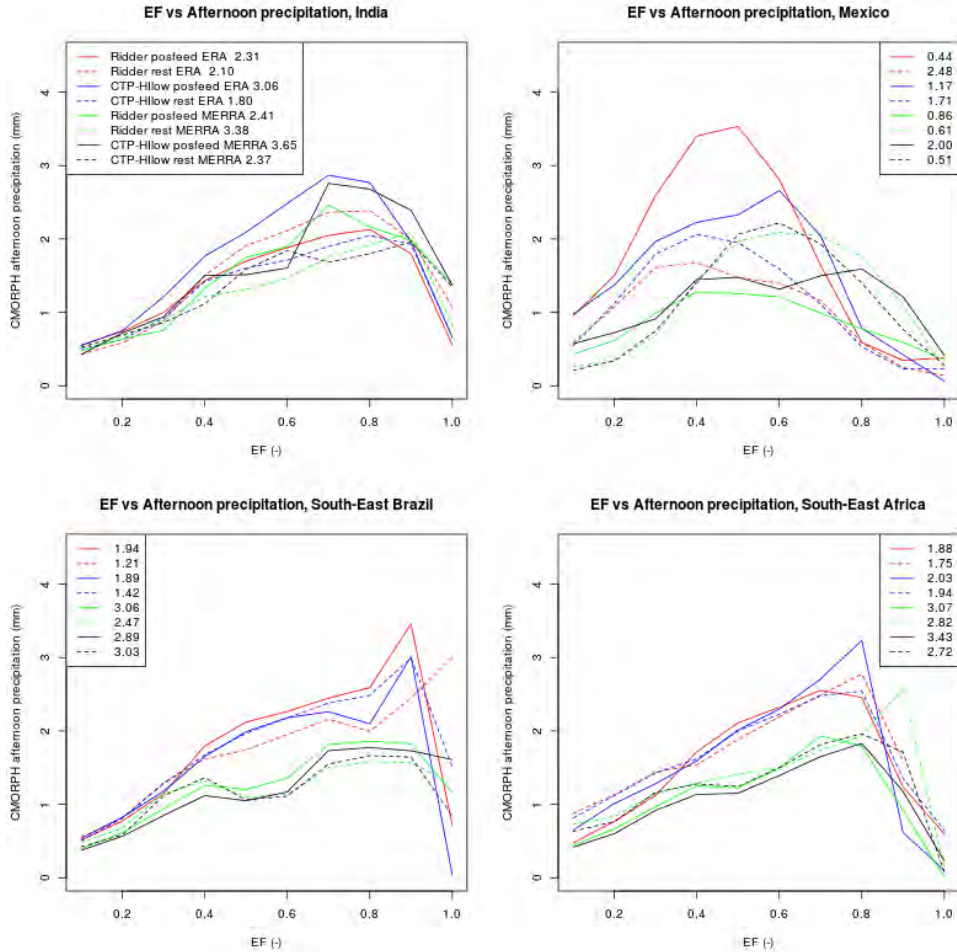


Figure 2.9: The relation between EF and afternoon precipitation. Each panel shows four curves per diagnostic for MERRA and ERA-interim; a linear regression between EF and CMORPH afternoon precipitation for the cases with a predicted positive feedback and the same linear regression for the other cases, as well as a curve showing the mean precipitation per EF bin (bin size is 0.1), again for the positive feedback cases and for the rest of the cases. All panels show the results for the areas indicated in Figure 2.10. The numbers in the legend show the value of a linear regression between EF and afternoon precipitation.

for southeast Brazil and southeast Africa, there is no significant difference between the curves. In India, positive feedback cases have a higher $\frac{dP}{dEF}$ over the domain of $EF < 0.7$, while for Mexico the $\frac{dP}{dEF}$ is higher only for $EF < 0.5$.

Figure 2.9 shows that the relation between EF and precipitation does not show a linear behaviour. Moreover, the differences in $\frac{dP}{dEF}$ between positive feedback cases and other cases are generally largest for EF values between 0.3 and 0.8. In this EF range, the maximum $\frac{dP}{dEF}$ difference is about 2 mm/EF, which means that for positive feedback days a large increase in EF due to land surface changes, could enhance precipitation with about 25%. The $\frac{dP}{dEF}$ difference between positive feedback cases and non-positive feedback cases generally is larger for CTP-HI_{low} than for the Ridder diagnostic. This means that the CTP-HI_{low} framework selects the cases in which the land surface promotes precipitation better than the Ridder diagnostic.

2.3.5 Common Patterns Among Diagnostics

Figure 2.10 shows the mean TFS and AFS for ERA-interim and MERRA. Although TFS and AFS are a bit noisy, the patterns resemble those found in earlier studies; the transition zones between wet and dry regions. Also, TFS and AFS show extreme values in dry regions. This is probably due to single (or a small number of) events and do not represent significant feedbacks. For TFS, values up to 0.06 occur around the world, but higher values are present in large parts of Africa, the western part of South-America, Mexico, the eastern US, India, China and Australia. Coastal areas generally show lower TFS than inland areas, which is also true for the CTP-HI_{low} frequency patterns (Figure 2.3). The large frequencies of positive feedbacks that are found using the Ridder diagnostic in coastal and very wet areas do not have high TFS values.

The mean AFS in Figure 2.10 shows mostly similar patterns as the mean TFS. Notable differences are the central US and Argentina, where AFS is relatively high while TFS remains low. Like the TFS patterns, the AFS patterns resemble the CTP-HI_{low} diagnostic more than the Ridder diagnostic.

2.4 Discussion and Conclusion

This study assesses the influence of the land surface wetness (soil moisture, or EF) on the triggering of precipitation. We use two diagnostics: the Ridder diagnostic and CTP-HI_{low} to evaluate data from two reanalyses (MERRA and ERA-interim). Both diagnostics suggest that during most of the summer half year, the land surface has no influence of precipitation; this is the atmospherically controlled regime. Positive relations between soil moisture and precipitation are diagnosed marginally in the subtropics, but up to 30% of the time in the tropics. Negative feedbacks (which means that drier land surfaces lead to more precipitation) are far less frequent and only

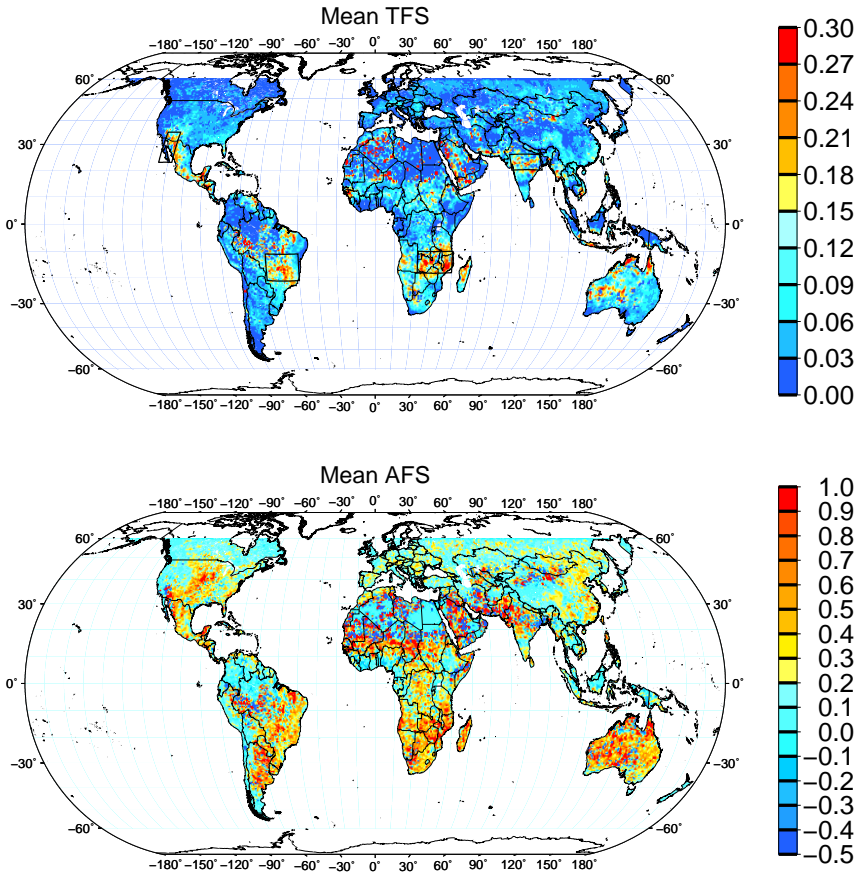


Figure 2.10: Mean triggering feedback strength (top panel) and amplification feedback strength (bottom panel) over ERA-interim and MERRA data, using CMORPH precipitation data.

obtained with the Ridder diagnostic in very dry (desert) areas.

Due to the different physical background of the diagnostics, feedbacks are obtained in different regions. $CTP-HI_{low}$ is sensitive to the humidity of the lower atmosphere, giving positive feedbacks for fairly high (but not too high) specific humidities and negative feedbacks for specific humidities that are slightly higher than for the positive feedbacks (see Figure 2.1). On the other hand, the Ridder diagnostic is sensitive to the surface flux partitioning, giving positive feedbacks for wet surfaces with high evaporative fractions and negative feedbacks for dry surfaces with low evaporative fractions. Therefore, $CTP-HI_{low}$ will diagnose more frequent feedbacks in areas that are slightly drier (and consequently a bit further away from the coast) than the Rid-

der diagnostic will do. Due to the high values of the Ridder diagnostic for high EF, the predicted frequencies of positive feedbacks are very high in wet areas such as the Amazon, Central Africa and South East Asia.

Following Findell et al. (2011), the land-atmosphere interactions were diagnosed in two stages. First, the triggering feedback strength (TFS), determining the influence of the land surface on probability of precipitation, was derived. Secondly, the amplification feedback strength (AFS), determining the influence of the land surface on the expected amount of precipitation, was derived. The global patterns of TFS and AFS show high values in the transition areas between dry and wet, but large differences occur between the datasets.

The TFS and AFS were used to determine the added value of the diagnostics in predicting positive feedbacks. For days with a positive feedback, the TFS and AFS was determined and compared to the TFS and AFS based on all data. The Ridder diagnostic (which is dominated by surface characteristics), when combined with the condition of a ABL higher than one kilometer, shows skill in predicting the triggering of precipitation. The CTP-HI_{low} framework showed better skill in predicting the amount of precipitation, especially in India, China and the East of the United States. Combining the CTP-HI_{low} framework with the ABL constraint showed little improvement.

Large differences occur between the two reanalysis datasets used in this study (MERRA and ERA-interim). The results confirm the large differences in feedbacks found in the same datasets by Taylor et al. (2012), who found negative feedbacks for MERRA and positive feedbacks for ERA-interim. In the present study, these difference may have multiple causes. The differences may be due to surface characteristics, land surface models, soil type and layering as well as to data nudging and data assimilation. Also, the resolution between the datasets is different. Although the horizontal resolution is similar, MERRA has more levels in the vertical than ERA-interim, which leads to a better diagnosis of the moisture and temperature lapse rates in MERRA. More importantly, the temporal resolution of the surface fluxes is different, hourly for MERRA and 6-hourly for ERA-interim. Therefore, the midday EF can be better diagnosed from MERRA as the daily cycle in surface fluxes is better resolved.

In Southern Brazil, Southern- and West-Africa, India, China and Mexico, positive feedbacks are diagnosed from both datasets and TFS and AFS are high. These are the areas where positive feedbacks occur and the land surface can have an influence on both the triggering and the amount of precipitation. Typically for these areas, a wetter land surface leads to a 20%-30% increase in afternoon precipitation probability and an average increase of 0.5-1mm of afternoon precipitation for an increase over the entire EF range. Additionally, in the Central US and Argentina, the amplification feedback is present (up to 1mm increase in afternoon precipitation), but triggering feedback is not. That is, in these regions, the land surface only has an effect on the

amount of precipitation, not on the triggering.

Most of the areas with positive feedbacks are located in the transition zones between dry and wet climates, as predicted by Koster et al. (2004) and Guo et al. (2006). However, in areas with very wet (Central Africa) and very dry (Australia) climate, positive feedbacks are diagnosed as well. For the US, using different datasets, our TFS and AFS values differed from those of Findell et al. (2011). Using MERRA and ERA-interim (which agree on TFS and AFS signals for the US), the positive feedback areas are diagnosed more in the Central US, compared to the positive feedbacks in the eastern US found by Findell et al. (2011), who use the NARR reanalysis.

For areas in Figure 2.10 (upper panel), the relation between EF and precipitation has been studied in depth. This relation is not linear; typically, precipitation increases with EF until a maximum at EF values of around 0.7-0.8, after which the precipitation decreases with EF again. This suggests that even if a positive influence of the land surface is expected based on $CTP-HI_{low}$, the Ridder diagnostic, TFS or AFS, the actual effect of a wetter land surface may depend on the location on the actual EF and the current land surface state.

This study very much presents a 'model world', because it depends heavily on the two reanalysis datasets used. Taylor et al. (2012) showed that the coupling between land surface and precipitation is very different among models and between models and remotely sensed products (which also depend on models and assumptions). The approach taken here is to determine the common patterns across the diagnostics and datasets. This is done because the required observations (vertical temperature and moisture profiles and surface fluxes) are not available globally at the required resolution.

To overcome the data availability issues, future efforts of the LoCo working group will focus on testing diagnostics for the densely monitored ARM SGP site and possibly FLUXNET sites, for which high-quality data are available. However, measurements sites are predominantly located in temperate areas, whereas the current research suggests that most of the sensitivity is to be found in the tropics.

We conclude that the two land-atmosphere diagnostics in this study can have added value, especially in studying atmospheric conditions on sub-seasonal time scales (individual days to months). For longer periods, statistical approaches (which can not be used with a limited amount of data) like the TFS and AFS may be useful. The $CTP-HI_{low}$ diagnostic shows frequency patterns that resemble the TFS and AFS better, while the Ridder diagnostic shows unrealistic values in wet areas. However, the Ridder diagnostic (when combined with a ABL height) shows some skill in predicting the triggering of precipitation.

Diagnosis of Local Land-Atmosphere Feedbacks in India

Abstract

Following the convective triggering potential-humidity index (CTP-HI_{low}) framework by Findell and Eltahir (2003a), the sensitivity of atmospheric convection to soil moisture conditions is studied for India. Using the same slab model as Findell and Eltahir, atmospheric conditions in which the land surface state affects convective precipitation are determined. For India, CTP-HI_{low} thresholds for land surface-atmosphere feedbacks are shown to be slightly different than for the USA.

Using atmospheric sounding data from 1975-2009, the seasonal and spatial variations in feedback strength have been assessed. The patterns of feedback strengths thus obtained have been analyzed in relation to the monsoon timing. During the monsoon season, atmospheric conditions where soil moisture positively influences precipitation are present about 25% of the time. During onset and retreat of the monsoon, the South and East of India show more potential for feedbacks than the North. These feedbacks suggest that large scale irrigation in the South and East may increase local precipitation.

In order to test this, precipitation data (from 1960-2004) of the period of about three weeks just before the monsoon onset date has been studied. A positive trend in the precipitation just before the monsoon onset is found for irrigated stations. It is shown that for irrigated stations, the trend in the precipitation just before the monsoon onset is positive for the period 1960-2004. For non-irrigated stations, there is no such

upward trend in this period. The precipitation trend for irrigated areas might be due to a positive trend in the extent of irrigated areas, with land-atmosphere feedbacks inducing increased precipitation.

3.1 Introduction

The interaction between the land surface and atmosphere has multiple pathways, among which the coupled water and energy cycles. Different feedbacks can occur when land and atmosphere interact (Brubaker and Entekhabi (1996), Eltahir (1998)). Understanding these feedbacks is important to explain past climatic changes, improve seasonal weather forecast and assessments of the impact of land use scenarios on the climate.

Positive feedbacks occur when a given land surface state enhances itself in magnitude or persistence. For example, a wet surface can induce precipitation, while a dry surface cannot. In case of a wet land surface, evaporation is not limited by available soil moisture, and latent heat is released into the atmosphere. This moisture flux increases the specific humidity of the atmospheric boundary layer (ABL). If this moisture rises to layers of conditional instability, latent heat release can result in convective precipitation, increasing soil wetness. By contrast, a dry land surface limits evaporation by moisture availability. The smaller moisture flux is insufficient to induce convection, and no precipitation occurs, so the land surface stays dry.

Negative feedbacks occur when dry surfaces lead to precipitation and wet surfaces inhibit the formation of rain. This can occur when a potential instability is present above the ABL top. The larger sensible heat flux from dry surfaces leads to a larger ABL growth. The ABL may entrain the stable layer, reach the unstable air above and trigger convection, while no convection would occur with wet surface conditions. Feedbacks between land and atmosphere are hard to measure directly in manipulative experiments, because it is usually not feasible to make fully controlled changes to the land surface state. An approach is to simulate the influence of the land surface using models. At the global scale, Koster et al. (2004) and Koster et al. (2006) inter-compared GCMs to determine the sensitivity of temperature and precipitation to the land surface state. They found hotspots of coupling of soil moisture to precipitation for boreal summer (JJA) in West-Africa, the Mid-West of the United States and India. Guo et al. (2006) analyzed the model runs of Koster et al. (2006) and concluded that the hotspots of coupling were located on transition zones between dry and wet climates. In wet climates, soil moisture is plentiful and evaporation is controlled by atmospheric demand. In dry climates, the typical variations in evaporation are too small to affect precipitation. Between these extremes, evaporation is large enough to influence precipitation, but the magnitude still depends on soil moisture.

Another approach is the analysis of correlation between soil moisture, evaporation

and moisture recycling ratios. Dirmeyer et al. (2009) and Dirmeyer and Brubaker (2007) did this globally while others focused on regional analyses (Bisselink and Dolman (2008) and Findell and Eltahir (1997)).

On a local scale, De Ridder (1997) studied the theoretical relationship between land surface and convective precipitation and found that the potential for convective precipitation increased with evaporative fraction, except in very dry conditions. Based on this work, Findell and Eltahir (2003a) (hereafter FE2003a) used a slab model to determine the relative influences of surface and entrainment fluxes on convective precipitation. They found that under certain atmospheric conditions, the soil moisture conditions can trigger or prevent precipitation, while under other conditions, the land surface condition was irrelevant. For the USA, they created a framework to classify atmospheric conditions, from which feedbacks can be diagnosed without the need to perform model runs.

In this study, we focus on India, one of the hotspot coupling regions identified by Koster et al. (2006). India has a number of distinct seasons. During January to May, the predominant flow is from the North, bringing dry and cool conditions. By May, the land surface has been heated by increased solar radiation, which causes rising air masses over land. These draw in moist oceanic air, that brings the summer monsoon rains that provide the majority of annual precipitation (Barry and Chorley (2003)). These monsoon rains last until September-October, after which the cool season starts. Feedbacks are expected for the onset and retreat periods, because they resemble the transition zones between dry and wet climates of Guo et al. (2006). Moreover, India is an interesting case to study land-atmosphere feedbacks because of the large scale modification of the land surface. India has become one of the most heavily irrigated areas in the world (Siebert et al. (2005)), due to rising population and demand for agricultural products.

GCMs have been used to study the influence of soil moisture on the Indian monsoon. Webster et al. (1998) noted that soil moisture characteristics are important in determining monsoon structure. Meehl (1994b) and Meehl (1994a) modified surface conditions and found a correlation between a stronger Indian summer monsoon and the land-sea temperature contrast, but also between wet soil conditions and Indian summer monsoon precipitation. Douville et al. (2001) note that rainfall increases over northern India as a consequence of wetter surface conditions, but as the land-sea contrast decreases, the increased water recycling is balanced by a decreased moisture convergence.

Dirmeyer et al. (2009) found increased moisture recycling ratios during the onset and especially the retreating phases of monsoons. For India, the correlations between soil moisture state, evaporation, soil moisture memory, and moisture recycling ratios were all positive during MAM and SON. During SON, soil moisture memory was the highest, about 20 days (the time the auto-correlation of soil moisture was above

the 99% confidence level). These positive correlations indicate the possibility of land-atmosphere feedbacks, but do not exclude other processes, such as vegetation changes and interaction.

On a smaller scale Lohar and Pal (1995) used a 2d model and observed decreased sea breezes as a result of irrigation for south West Bengal. The smaller sea breeze reduced low level moisture supply making the net effect of irrigation on precipitation negative. Lee et al. (2009) related remotely sensed increasing trends in pre-monsoon irrigation to decreasing trends in monsoon precipitation for 1982-2003. They hypothesized that the decreased land-sea contrast is the cause of this relationship.

In the present study, we apply the FE2003a method of determining local land-atmosphere feedbacks with two main goals:

- Test whether the approach of FE2003a and Findell and Eltahir (2003b) can be applied to India, and what possible adaptations of their framework need to be done.
- Determine what feedbacks (from soil moisture to convective precipitation) can be expected for India, how they vary spatially and how they relate to monsoon onset and retreat, and whether more precipitation is found in irrigated areas with positive feedbacks.

Three hypotheses are put forward. 1) The CTP- HI_{low} framework can be used for India, so the potential for feedbacks can be determined quickly for long periods without the need to perform model simulations. 2) Soil moisture influences precipitation during the monsoon onset and retreat, because these are the periods in the year that resemble the transition zones between wet and dry climates (Guo et al. (2006) and Dirmeyer et al. (2009)). 3) Precipitation is sensitive to large-scale irrigation in these periods.

The structure of this paper is as follows. In section 3.2, the framework developed in FE2003a that is used to assess the feedbacks is introduced, while section 3.3 presents the approach to determine the feedbacks and the data used. Section 3.4 will show how this framework can be used for India, after which the relation between feedbacks and monsoon will be discussed in section 3.5. Section 3.6 and 3.7 present the discussion and conclusions.

3.2 CTP- HI_{low} framework

To determine the effect of soil moisture on precipitation, this study uses the CTP- HI_{low} framework, proposed by FE2003a. Based on two atmospheric indicators (CTP and HI_{low}), this framework predicts whether the land surface has an influence on the occurrence of convective precipitation. More precisely, it assesses the sensitivity of

the atmosphere, in terms of convective potential (CTP) and moisture content (HI_{low}), to variations in energy partitioning at the land surface.

FE2003a hypothesized that certain atmospheric conditions favour rainfall over wet soils while other conditions favour rain over dry soils. To test this, they forced a slab model with atmospheric sounding data from the summers of 1997-1999 from Illinois, USA (station ILX). The model was run once with wet soil moisture conditions (85%) and once with dry soil moisture conditions (15%), which resulted in three groups of soundings:

1. Atmospherically controlled cases (no difference between wet and dry soil)
2. Positive feedback cases (precipitation on wet soil, no precipitation on dry soil)
3. Negative feedback cases (no precipitation on wet soil, precipitation on dry soil)

They found the atmospheric layer between 950 and 700 hPa to be critical in triggering convection. Two indicators of stability and humidity, the convective triggering potential (CTP) and humidity index in the lower level of the atmosphere (HI_{low}) were developed into a framework to diagnose the land surface influence.

3.2.1 Convective Triggering Potential

The CTP has a similar definition as the convective available potential energy (CAPE), but the integration bounds are different:

$$CTP = \int_{P_{surf}-100hPa}^{P_{surf}-300hPa} g \left(\frac{Tv_{parcel} - Tv_{env}}{Tv_{env}} \right) dz \quad (3.1)$$

Tv_{parcel} is the virtual temperature of a parcel that is lifted moist adiabatically from the level 100hPa above the surface, while Tv_{env} is the temperature of the observed profile. CTP (in $J kg^{-1}$) measures the buoyancy of rising air, originating from the temperature difference with its environment. Positive values indicate (conditional) instability between 100 and 300hPa above the surface. When the ABL reaches this height, there is energy available to start deep convection. The values of 100hPa and 300hPa above the surface represent the layer that can just be reached by the daytime ABL. Because surface conditions affect the ABL growth, they control whether or not this critical region is reached.

3.2.2 Humidity Index

The humidity index in the lower level of the atmosphere, HI_{low} , is based on the humidity index by Lytinska et al. (1976), which is designed to determine the possibility

of rain for an atmospheric profile. This humidity index is defined as the sum of the dewpoint depressions at 500, 700 and 850hPa. FE2003a defined HI_{low} as:

$$HI_{low} = (T_{950} - T_{d,950}) + (T_{850} - T_{d,850}) \quad (3.2)$$

in which T is the temperature and T_d the dewpoint temperature. For high humidities, $HI_{low} < 5K$, while values of $HI_{low} > 20K$ indicate low humidity. Lytinska et al. (1976) found a threshold for precipitation of HI (three level humidity index) $< 30K$, while FE2003a found HI_{low} (two level humidity index) $< 15K$ as precipitation threshold.

3.2.3 Framework for land surface influence

Fig. 3.1 illustrates the CTP- HI_{low} framework, including the original thresholds for feedbacks. FE2003a found the groups of soundings for which the model resulted in a positive feedback to have $CTP=0-200 \text{ J kg}^{-1}$ and $HI_{low}=5-10 \text{ K}$. For the negative feedbacks, they found $CTP>200 \text{ J kg}^{-1}$ and $HI_{low}=10-15K$, while the atmospherically controlled cases lay outside these bounds; cases with $HI_{low} < 5$ had precipitation for dry and wet soils, while cases with $HI_{low} > 15$ showed no convection over either soil condition. Between $CTP=80-200 \text{ J kg}^{-1}$ and $HI_{low}=10-15K$, a transition zone was defined in which any outcome was possible.

Since the defined framework is based on slab model results, it has a local viewpoint with a limited number of processes taken into account. Omitted processes that are potentially relevant for land-atmosphere interactions include effects of orography, wind shear and synoptic systems that affect atmospheric conditions after collection of the early-morning data.

3.3 Methods and Data

Our study proceeds along the following steps:

1. Test the framework applicability for India, using a slab model with a limited sounding dataset (methods in 3.3.1, results in section 3.4)
2. Use the optimised framework to classify a much larger sounding dataset, and analyse the results for India's different seasons (methods in 3.3.2, result in section 3.5a-d):
3. Test whether large scale irrigation affects pre-monsoon rainfall in India (methods in 3.3.3, result in section 3.5e):

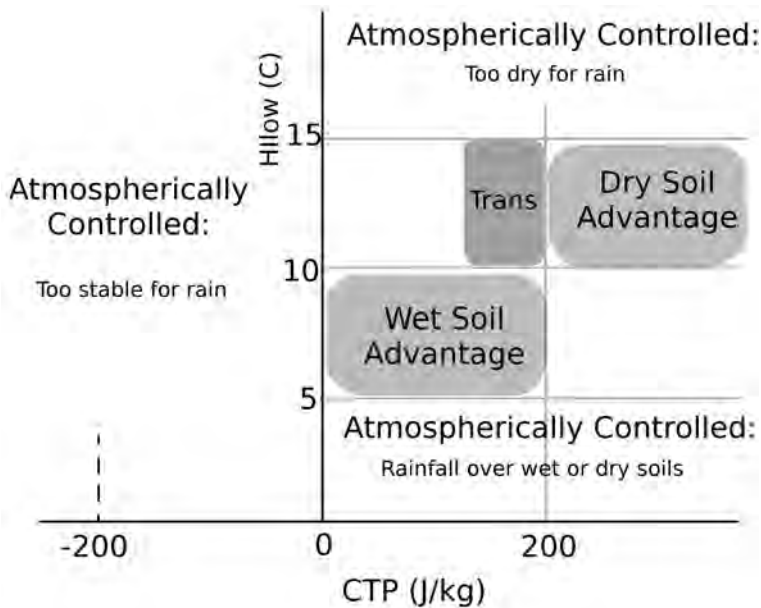


Figure 3.1: $CTP-HI_{low}$ framework, regions in which wet soils and dry soils promote precipitation, as well as transition regions (in which the outcome is unsure) are shaded. Figure from FE2003a.

3.3.1 Framework validation

The $CTP-HI_{low}$ framework that was developed by FE2003a (section 3.2), was based on measurements from locations in the USA. To test whether this framework is valid in India, the slab model used by FE2003a was slightly modified and forced with atmospheric soundings from India. The slab model simulations are repeated for India because early morning CTP values are higher than in the USA (up to 500 J kg^{-1} for India, up to 350 J kg^{-1} for Illinois, USA) and because incoming shortwave radiation is higher for India than for the USA.

FE2003a used the slab model developed by Kim and Entekhabi (1998a) to investigate the coupled exchange of water, heat and momentum between the land surface and atmosphere. The main assumptions of the model physics and boundary conditions are:

- perfect mixing of the ABL
- a cloud-free ABL
- no change in overlying air masses during the simulation
- constant soil moisture during the simulation

Kim and Entekhabi (1998a) assumed constant potential temperature and moisture lapse rates above the mixed layer. FE2003a modified the model to acquire the lapse rates from the early morning sounding measurement, so that entrainment is determined by observed lapse rates of potential temperature and specific humidity.

Apart from determining the entrainment, the sounding is used to initialize the model at sunrise. After the simulation of the daily ABL evolution three outcomes are possible; no convection, shallow clouds and deep convection. No convection occurs when the ABL height does not reach level of free convection (LFC). Shallow, non-precipitating clouds are assumed to form when the ABL height reaches LFC, but at the same time depth of convection (DOC) stays below 5km or CAPE below 400 J kg^{-1} . Deep convection with precipitation is assumed to occur when LFC is reached and $\text{CAPE} > 400 \text{ J kg}^{-1}$ and $\text{DOC} > 5\text{km}$.

FE2003a compared slab model results to data from the Flatland ABL Experiment field campaign in Illinois (Angevine et al. (1998)). This showed varying correspondence between model and measurement (Findell (2001)), but the model was not optimized to fit these observations because it was used as an analytical tool. The model used in the present study determines incoming solar radiation based on the day of year and the geographic location of the atmospheric sounding. This differs from FE2003a, who took the radiative forcing constant for the entire boreal summer season. For further explanation of the model, the reader is referred to Kim and Entekhabi (1998a), Kim and Entekhabi (1998b), Findell (2001) and FE2003a.

For each sounding, a dry and wet soil run (15 and 85% soil moisture) were compared to determine what kind of feedback occurs. This resulted in four possible feedback classes (as in FE2003a, see section 3.2): positive feedback, negative feedback, atmospheric controlled (rain) and atmospheric controlled dry. For each of these classes, the statistics of the maximum modeled ABL depth, as well as an average sounding are calculated to test the appropriateness of the height intervals chosen for computing CTP and HI_{low} . Next, we determine the mean and standard deviations of CTP and HI_{low} for the positive and negative feedback model outcomes to check the separation of these groups in CTP- HI_{low} phase-space. For the same reason, the classification success/fail rate using the original FE2003a thresholds is determined and optimised classification thresholds for India are determined. To check for intra-regional variation in optimal CTP and HI_{low} thresholds the same analysis is also done per station.

3.3.2 Feedback Classification

After the validity of the framework for India has been tested and its parameters adapted where appropriate, the potential influence of the land surface on precipitation is predicted for different periods and regions.

To determine which kind of feedback dominates for a given period in the annual cycle,

CTP and HI_{low} values are calculated from a much larger set of soundings. Based on these values, the framework is used to classify the feedback potential of all soundings. The obtained classification only presents the possibility of land surface influence on precipitation, since no models are actually run to determine the differences between atmospheric conditions with a dry and wet soil.

The resulting classification data are then analysed along a number of lines. First, for three stations representative of India geographic extremes, average monthly values of CTP and HI_{low} are computed to illustrate its annual dynamics. Next, frequencies of occurrence of positive or negative feedbacks are computed for various periods (from a fortnight up to 2 months) preceding the climatological monsoon onset date in a particular year, during the monsoon and after the monsoon cessation date. The actual onset and retreat dates for each year are computed from the IMI (see next section). These frequencies are determined over all India and per station. Finally, from the latter spatial patterns in feedback frequencies for these periods are plotted and interpolated on a map.

3.3.3 Determination of Pre-Monsoon Irrigation Influence

After we have established when and where the land surface is *potentially* important, it remains to be seen whether an actual soil moisture anomaly really does affect actual precipitation. Precipitation data of the sensitive periods will be analysed to see if there is any difference in precipitation between irrigated (more than 25% of the 0.08 degree gridcell equipped for irrigation) and non-irrigated (less than 25% of the 0.08 degree gridcell equipped for irrigation) sites. As will be shown in section 3.5, the potential for positive feedbacks is maximal in a one-month period before the monsoon onset. Then, a wet land surface is expected to increase precipitation. We assume that anomalously early rain may be enhanced by positive feedback. However, we must distinguish between anomalously early rain due to large scale circulation changes and due to local feedbacks. We determine the former from the wind field based all-India Monsoon Index (IMI), and the latter from actual rainfall itself. Fig. 3.2 shows a schematic overview of the procedure used. Next, we describe the procedure in more detail.

For each station, the climatological monsoon precipitation onset (marked t_{MSpc} in Fig. 3.2) is assumed to be the average date when the cumulative precipitation climate has reached 15% of the total average annual precipitation. For the period 1960-2004, this corresponds to the onset date as suggested by O'Hare (1997).

The climatological monsoon circulation onset (marked t_{MSic} is determined by the average date that sign change of the 10-day moving average of the IMI changes from negative to positive. IMI is defined (Wang and Fan (1999)) by the 850 hPa zonal wind averaged over ($5^{\circ}N$ - $15^{\circ}N$ $40^{\circ}E$ - $80^{\circ}E$) minus that averaged over ($20^{\circ}N$ - $30^{\circ}N$,

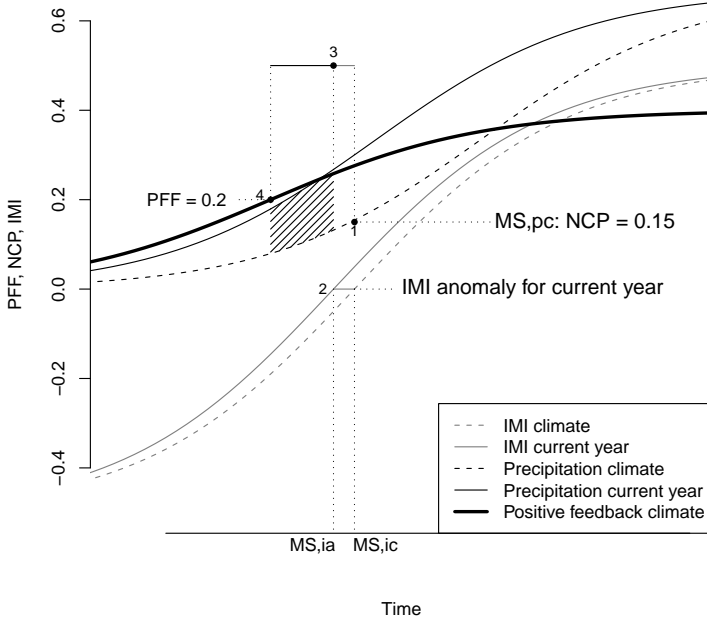


Figure 3.2: Schematic of the pre-monsoon onset period over which the precipitation anomaly is calculated. The positive feedback fraction (PFF), normalized (by yearly total) cumulative precipitation (NCP) and Indian monsoon index (IMI) are plotted against time. The climatological start of the monsoon season based on precipitation ($t_{MS,pc}$), the climatological start of the monsoon season based on IMI ($t_{MS,ic}$) and the start of the monsoon season in the current year based on the IMI ($t_{MS,ia}$) are indicated. t_{fb} is the start of the feedback period before the monsoon onset. (Curves do not reflect actual data.)

60°E-90°E). This meridional shear of zonal winds depicts the intensity of the Indian monsoon trough and associated southwesterly monsoon. During summer monsoon wind patterns, the IMI is positive, while it is negative during the rest of the year. Climatologically, the IMI becomes positive by end May. In order to determine the anomalous large-scale circulation effects on the monsoon onset date, the anomaly of the IMI in the current year ($t_{MS,ia}$) is calculated: $t_{MS,ic} - t_{MS,ia}$. The difference (marked 2 in Fig. 3.2) is subtracted from the climatological monsoon precipitation start ($t_{MS,pc}$). The resulting date is assumed to be the start of the monsoon season, corrected for anomalies in the large scale circulation (marked 3 in Fig. 3.2). Then, the climatologically average period sensitive to feedbacks preceding the mon-

soon onset date is defined as the difference between the date t_{FB} in which the 10-day moving average fraction of positive feedback situations is larger than 0.2 and the climatological monsoon precipitation onset t_{MSpc} ; i.e. the period between markers 3 and 4 in Fig. 3.2. This period is different for each station. The fraction threshold of 0.2 is based on the classification by FE2003b, who use this threshold to classify stations as subject to predominantly positive feedbacks.

Then we determine the precipitation anomaly due to feedback (P_{FB} in mm) in the period before the monsoon onset (shaded area in Fig. 3.2) as:

$$P_{FB} = \int_{t_{FB}}^{t_{MAp}} P_{year} - P_{climate} \quad (3.3)$$

In which $t_{MAp} = t_{MSpc} - (t_{MSic} - t_{MSia})$ is the monsoon onset date corrected for the large scale circulation. This resulting pre-monsoon precipitation anomaly is determined for all stations, for each year from 1960-2004. Differences in trends in P_{FB} between irrigated and non-irrigated stations then confirms our hypothesis that positive feedbacks over irrigated areas may enhance rainfall.

3.3.4 Data

The data used in this study are from radiosondes launched at 0 UTC (5-7 AM local time) from 62 meteorological stations in India from the period 1975-2009, and were acquired from the university of Wyoming¹. The differences in local time for the early morning soundings will not to have a big influence on the analysis, because the ABL is unlikely to have reached the levels at which CTP or HI_{low} are evaluated (pressure level > 950 hPa).

The data are used for two purposes; a small subset of these data to force the slab model to test the framework and a much larger subset to determine a climatology of potential feedback situations. For both purposes, the sounding data are filtered on number of vertical levels. For the model forcing data, soundings with less than 20 vertical levels in the lower 400 hPa are filtered out, resulting in 4024 suitable soundings from 29 stations. The filtering for the data to determine the climatology was less strict, radio soundings with at least 10 levels below the 600 hPa level are selected. However, stations that had less than 1000 usable soundings for this period are not taken into account. This selection resulted in 30 stations with an average of 6500 soundings per station (195000 soundings in total, see Fig. 3.3 for stations).

The Aphrodite 0.25 degree gridded dataset (Yatagai et al. (2009)) is used as precipitation data. The precipitation values of the grid cell in which a station is located were aggregated into daily precipitation timeseries for each station for the period 1960-2004. Furthermore, the global map of irrigated areas (Siebert et al. (2005)) is

¹<http://weather.uwyo.edu/upperair/sounding.html>

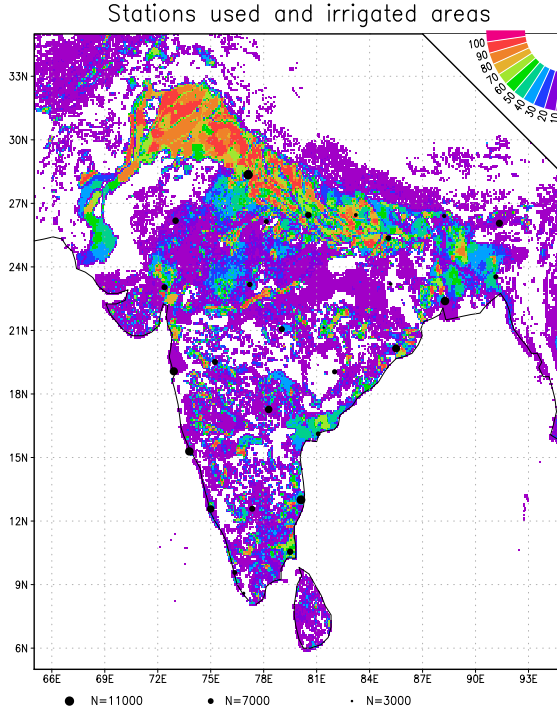


Figure 3.3: Distribution of sounding stations used to determine the atmospheric conditions for feedbacks, the shading shows the fraction of irrigation (Siebert et al. (2005)). The size of the markers indicates the number of soundings available.

used to determine the fraction of area suitable for irrigation of the 0.08 degree grid cell in which each station is located.

In order to determine the yearly anomaly in monsoon onset, the all-India Monsoon Index (IMI) (Wang and Fan (1999)) is calculated from daily NCEP/NCAR reanalysis data (Kalnay et al. (1996)) for 1960-2004.

3.4 Performance of the CTP- HI_{low} Framework for India

This section tests framework performance for India, based on the results of the slab model runs with soundings from Indian stations. The distribution of CTP and HI_{low} values for the model outcomes will be compared to the thresholds for feedbacks found

by FE2003a. Furthermore, we will quantify the predictive capacity of the framework. Thresholds for feedbacks will be changed to optimize this predictive capacity.

For 81% of the soundings, the slab model simulations diagnosed an atmospherically controlled situation. However, in 19% of the simulations, surface conditions determined the occurrence of convection.

The average atmospheric profiles of different model outcomes are shown in Fig. 3.4. The positive feedback and atmospherically controlled wet cases have higher specific humidities in the lowest 100 hPa than the negative feedback and atmospherically controlled dry cases. Between 900-850 hPa, the moisture profiles of the positive and negative feedback model outcomes are different as well. The positive feedback cases show a decline of specific humidity, while the negative feedback cases show an increased moisture content from 900 to 850 hPa. Above 850 hPa, the positive, negative and dry profiles show similar specific humidities. Moisture differences between the model outcomes are maximal at the levels at which HI_{low} is evaluated (950 and 850 hPa). Moisture measures based on the dewpoint depression evaluated at various levels were tested, but were unable to distinguish better between the model outcome categories. Therefore, HI_{low} is considered to be an adequate measure.

The mean potential temperature profiles of the model outcomes (Fig. 3.4) show an approximately constant slope for the atmospherically controlled wet and positive feedback cases. The negative feedback and atmospherically controlled dry cases show lower potential temperature lapse rates between 1000-900 hPa and higher lapse rates between 900-700 hPa. Thus, CTP (evaluated between 900 and 700 hPa) diagnoses the instability at the levels where positive feedback and atmospherically controlled wet outcomes differ from negative feedback and atmospherically controlled dry outcomes. The surface conditions have an impact on the ABL height, with average maximum simulated heights of 1200m over wet soils and 2000m over dry soils (Fig. 3.5). The difference in ABL height between wet and dry soil runs confirms that the layer between 1-2 km above the ground is the one that is susceptible to entrainment by the ABL. Therefore, it was tested whether a modified version of the CTP, with integration bounds of 100 and 200 hPa above the land surface improved the classification framework. This appeared not to be the case because the majority of the soundings did not have enough observation levels between 1 and 2 km above the surface to calculate the wet adiabat reliably.

Fig. 3.6 shows the CTP- HI_{low} values for cases in which the soil moisture affected the model outcome, the cases with positive or negative soil moisture feedback. In agreement with the results for the USA in FE2003a, positive feedback cases generally occur if $CTP < 250 \text{ J kg}^{-1}$ (mean: 135 J kg^{-1} , standard deviation: 120 J kg^{-1}), while negative feedbacks cases occur if $CTP > 250 \text{ J kg}^{-1}$ (mean: 276 J kg^{-1} , standard deviation: 138 J kg^{-1}). However, we find higher HI_{low} values for positive and negative feedbacks than proposed by FE2003a. The bulk of the positive feedback cases have

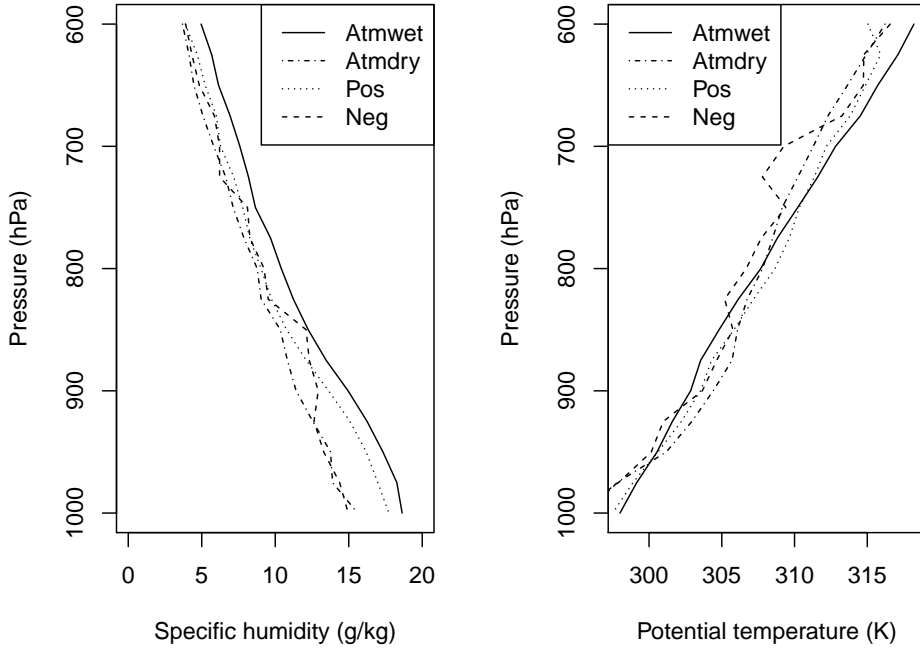


Figure 3.4: Mean (measured) specific humidity and potential temperature profiles of the soundings that resulted in the slab model outcome categories atmospherically controlled wet (*Atmwet*), atmospherically controlled dry (*Atmdry*), positive feedback (*Pos*) and negative feedback (*Neg*).

HI_{low} values of up to 13 K (mean: 9.9 K, standard deviation: 3.6 K). The majority of negative feedback cases have HI_{low} values of 10-16 K (mean: 13.8 K, standard deviation: 7.4 K), slightly higher than the thresholds found by FE2003a.

This distribution of positive and negative feedbacks (Fig. 3.6) suggests that different thresholds for feedbacks should be adopted for India. An optimization showed the best prediction of the model results with positive thresholds of $CTP=0-200 \text{ J kg}^{-1}$ and $HI_{low}=7-12 \text{ K}$ and negative thresholds of $CTP>200 \text{ J kg}^{-1}$ and $HI_{low}=11-16 \text{ K}$. The model runs are also analysed for the individual stations. For positive feedbacks, the mean values for CTP varied between 108 and 183 J kg^{-1} and for HI_{low} between 8.6 and 11.9 K, while for negative feedbacks CTP ranged between 191 and 305 J kg^{-1}

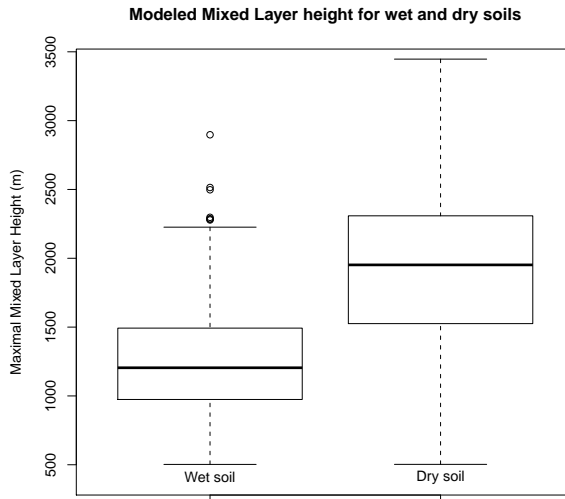


Figure 3.5: Standard box-plot (with box indicating lower and upper quartiles, bar in box indicating the median, whiskers indicating the range of the data (maximized at 2.5 quartiles of the median), and dots indicating outliers) of the slab model results showing the differences in modeled mixed layer height (m) between the runs with wet and dry soils for model runs in which the soil moisture determined the model outcome.

and HI_{low} between 10.5 and 16.1 K. No relationship was found between the location (for example North-South gradient) of a station and the mean CTP- HI_{low} values from the slab model results. Therefore, henceforth, the CTP and HI_{low} thresholds are assumed to be equally valid for all stations in India.

A cross table of model results versus predictions of the framework (table 3.1) shows that about 70% of the soundings is correctly classified (framework diagnosis is the same as slab model outcome) by the framework when using the original FE2003a thresholds. When a particular feedback is modeled for a sounding, the framework diagnoses that same feedback in 47% of the cases for positive feedbacks and in 34% of the cases for negative feedbacks. A positive feedback diagnosed by the framework is only simulated with the model in 30% of the cases, this is 21% for negative feedbacks. When these original (FE2003a) thresholds are used, the occurrence of both positive and negative feedback situations is overestimated. Positive feedbacks are diagnosed in 20% of the cases by the framework, while only in 13% of the cases by the model. For negative feedbacks, these figures are 8.6% for the framework and 5.4% for the model.

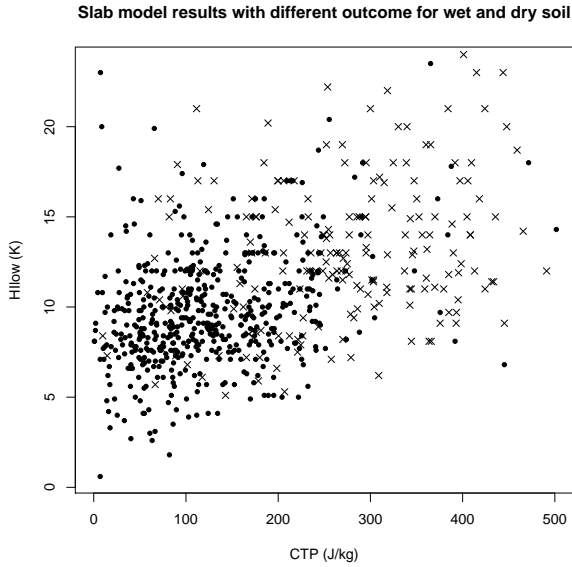


Figure 3.6: Slab model results in $CTP-HI_{low}$ framework for India (all stations) showing only the cases with different outcomes for different surface conditions. Dot markers show positive feedbacks (wet soils promote precipitation), while cross markers show negative feedbacks (dry soils promote precipitation).

With the new thresholds, 76% of the soundings are correctly classified. The relevant

Table 3.1: Comparison of feedbacks as determined by the slab model and predicted by the framework, using the same thresholds for feedbacks as FE2003a. Overall, 70% of the soundings are correctly classified. 47% of the modeled positive feedback cases are determined as positive feedback by the framework, while 29% of the cases classified as positive feedback actually are modeled as positive feedback. For negative feedbacks these figures are 34% and 21%, respectively.

	Framework prediction:			
	Positive	Negative	Atmospheric Controlled	Total
Model Prediction:				
Positive	244	41	235	520
Negative	20	74	123	217
Atmospheric Controlled	554	231	2502	3287
Total	818	346	2860	4024

cross table (table 3.2) shows that 49% of the positive feedback model outcomes are classified as such by the framework, while 41% of the situations classified as positive feedback are modeled as such. For the negative feedback these figures are 34% and 23%. Using the new thresholds, the fraction of feedback cases is better estimated. The framework predicts 15% of the cases to have a positive feedback (13% in the model) and 7.7% of the cases to have a negative feedback (5.4% in the model).

The model results suggest that the CTP- HI_{low} framework can be used for the Indian

Table 3.2: Comparison of feedbacks as determined by the slab model and predicted by the framework, using the optimized thresholds for feedbacks for the Indian data. Overall, 76% of the soundings are correctly classified. 49% of the modeled positive feedback cases are determined as positive feedback by the framework, while 41% of the cases classified as positive feedback actually are modeled as positive feedback. For negative feedbacks these figures are 34% and 23%, respectively.

	Framework prediction:			
	Positive	Negative	Atmospheric Controlled	Total
Model Prediction:				
Positive	254	30	236	520
Negative	19	73	125	217
Atmospheric Controlled	344	209	2734	3287
Total	617	312	3095	4024

continent. It predicts positive feedbacks better than negative feedbacks. Compared to the study for the USA (FE2003a), different HI_{low} thresholds have to be used to classify feedbacks. Using these adjusted thresholds, the predictive performance of the framework increases, especially for positive feedback situations. In the remainder of this study, $CTP=0-200 \text{ J kg}^{-1}$ and $HI_{low}=7-12 \text{ K}$ will be used to classify positive feedbacks, and $CTP=200-500 \text{ J kg}^{-1}$ and $HI_{low}=11-16 \text{ K}$ for negative feedbacks. Furthermore, the transition zones (Fig. 3.1) as defined by FE2003a, are assumed to be atmospherically controlled and are not considered separately.

3.5 Land-Atmosphere Feedbacks and Monsoon

In this section, we will determine the prevalence of atmospheric conditions for which feedbacks are expected for India's different seasons. First, we investigate the climatological yearly cycle of feedback potential for different stations. Next, we test how the feedbacks relate to the summer monsoon timing, with special attention paid to the relation with onset and retreat. It must be stressed that as we use the framework to

classify atmospheric situations, this section only discusses chances of feedback occurrence. Finally, we will test whether this feedback potential actually has an effect on precipitation by comparing irrigated and non-irrigated sites.

3.5.1 Seasonal CTP- HI_{low} Cycle

India's regions have differing yearly CTP- HI_{low} cycles. Fig. 3.7 shows these cycles for stations in the north (New Delhi, 28.35°N, 77.12°E), south (Thiruvananthapuram, 8.29°N, 76.57°E) and east (Kolkata, 22.39°N, 88.27°E).

The differences in the yearly cycles of these three stations follow the large-scale

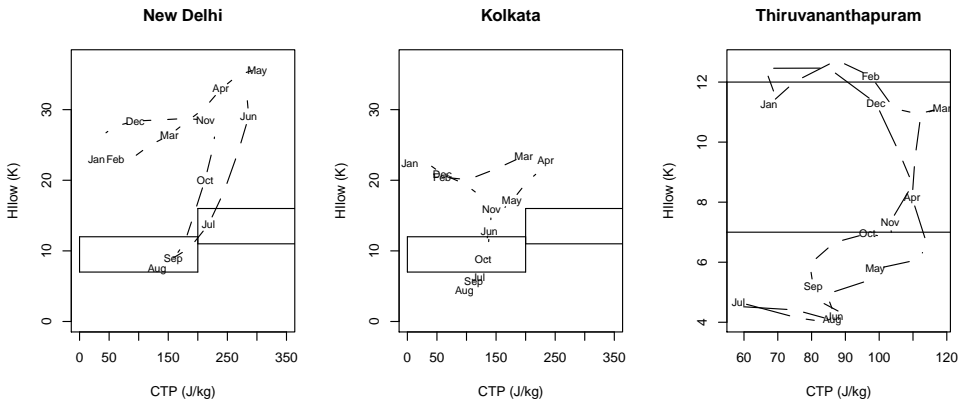


Figure 3.7: Average yearly cycle of CTP and HI_{low} values for stations New Delhi, Kolkata and Thiruvananthapuram, based on the period 1975-2009. The cycle has been smoothed with a 10-day kernel filter. A value is plotted every decad, with the first decad of the month indicated with the month abbreviation. The CTP- HI_{low} regions for which feedbacks are expected are indicated with boxes. Note the different scale for the Thiruvananthapuram plot.

differences in climatic regime. New Delhi has a very dry pre-monsoon season, with $HI_{low} > 20$ from November to June. CTP-values increase during this period, due to increasing solar radiation and consequent increased surface heating. New Delhi has a monsoon season from July to September, with average $HI_{low} = 8-15$ K. These months have the most precipitation and the most potential for feedbacks. After the monsoon season, HI_{low} values increase again and from October to January, less incoming radiation decreases the CTP values again.

Kolkata shows a similar increase in CTP during January to April, but the presence of marine moist air decreases HI_{low} values earlier. The monsoon season starts in June, with $HI_{low} < 7$ K during July to September. After the monsoon season, a similar pat-

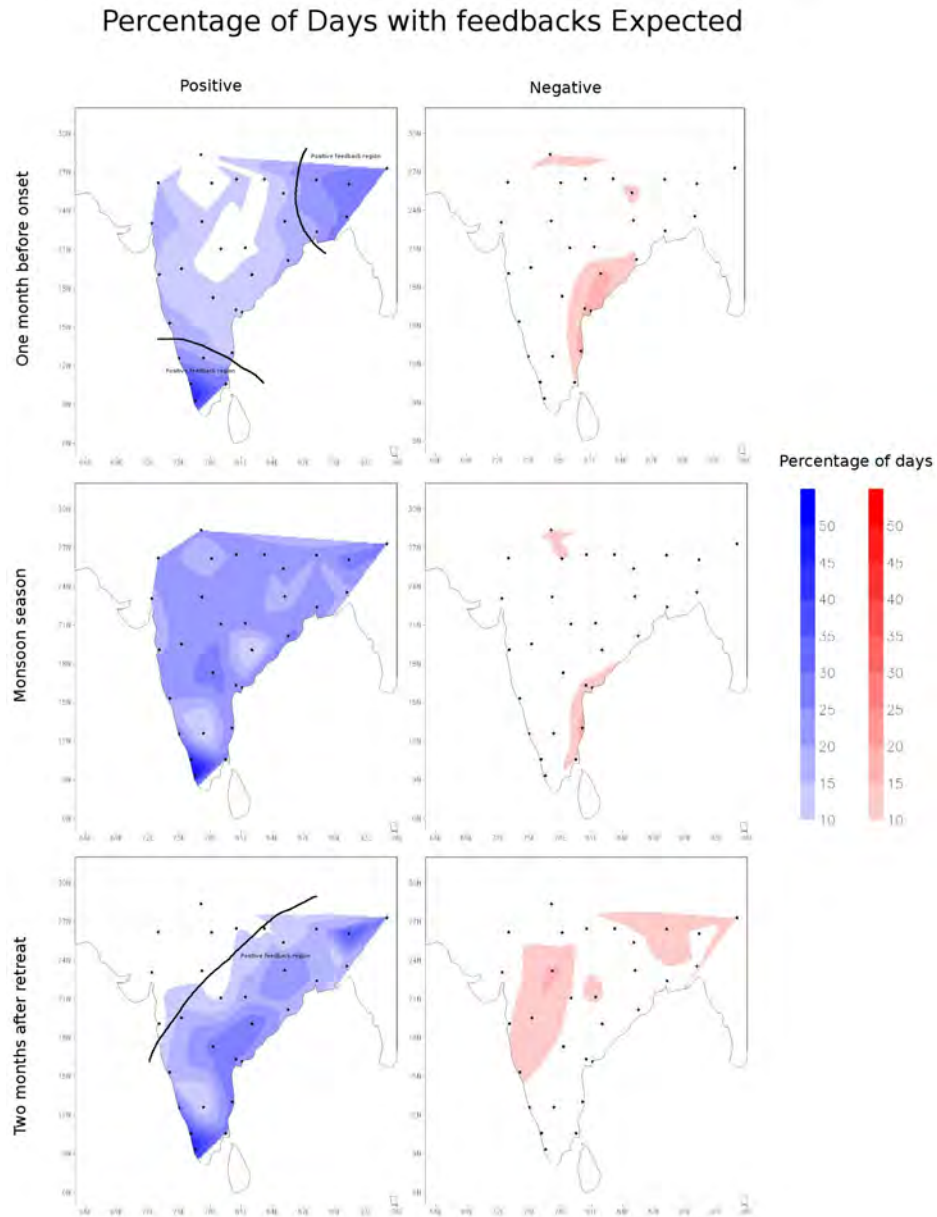


Figure 3.8: Interpolation of percentage of positive (left column) and negative (right column) feedbacks from one month before the monsoon onset until the onset date (top row), during the monsoon season (middle row) and in the two months after the monsoon retreat (lower row). Feedbacks are diagnosed by applying the modified CTP- HI_{low} framework to the soundings for all stations. Stations are indicated with black markers. Note that the onset and retreat dates are not the same for all stations, so the integration periods are different for all stations in all rows.

tern is found as for New Delhi, with a dry incoming air (increasing HI_{low} values) and subsequent decrease in radiation (lower CTP values). For Kolkata, the period just before and just after the monsoon season has the highest feedback potential. Thiruvananthapuram has a much moister climate, with smaller seasonal CTP- HI_{low} variation. During the monsoon season (May-October), HI_{low} values are so small that precipitation occurs regardless of land surface. From November to April, HI_{low} values are higher, showing the most potential feedbacks in these months.

3.5.2 Monsoon Onset

The contours in Fig. 3.9 depict the average onset date of the monsoon, varying from end of May to early July. The upper panels in Fig. 3.8 show the fraction of positive and negative feedbacks in a period of one month before the climatological monsoon onset (as documented by O'Hare (1997)).

The percentage of days with positive feedback varies between 0 and 20% in central and north west India. The south and north-east/Bangladesh have the largest probabilities of feedbacks, with fractions between 20% and 40%. Table 3.3 shows the percentages of positive, negative and atmospherically controlled cases for a two week and one month period before the monsoon for all stations in India and for the three regions indicated in the contours in Fig. 3.8 (upper left panel). With non-atmospherically controlled fractions higher than 30%, the south and northeast have the largest probability for the occurrence of feedbacks. In these regions, the positive feedback situations are much more likely than negative feedback situations.

In the rest of India, the fraction of days with potential for feedbacks is considerable,

Table 3.3: Feedback expectations for a two week and a one month period before the monsoon onset, for soundings from all stations in different regions in India (see Fig. 3.8, upper left panel, for the delineation of these regions).

Period		All India	South	North-East	Rest of India
2 Weeks	Atm	73.0	66.7	69.2	74.8
	Pos	18.5	28.0	23.8	15.9
	Neg	8.5	5.3	7.0	9.3
1 Month	Atm	75.7	67.6	68.4	78.2
	Pos	17.0	27.6	23.7	14.3
	Neg	7.3	4.8	7.9	7.5

but both positive and negative feedbacks occur, so no clear classification can be made.

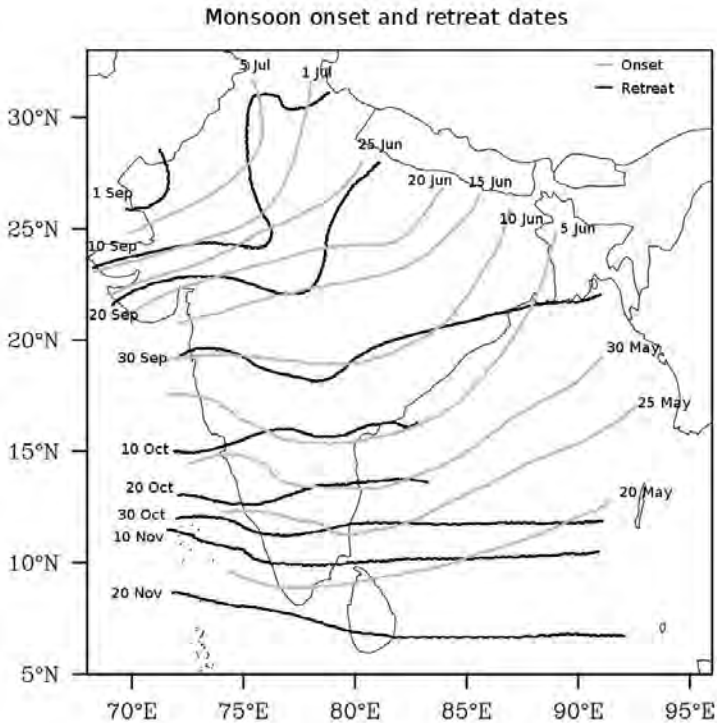


Figure 3.9: Average climatological monsoon onset and retreat dates after O'Hare (1997). There is a north-south gradient in the monsoon length, with longer monsoon seasons in the south than in the north.

3.5.3 Monsoon Season

The length of the monsoon season (the difference between onset and retreat dates, Fig. 3.9) varies from about six months in the south to about two months in the north. The middle row in Fig. 3.8 shows the fraction of positive and negative feedback situations during the monsoon period. For almost all the stations, the percentage with positive feedback is 20-25%, with an average value of 23% for all stations. Negative feedbacks during the monsoon occur only 5% of the time. Atmospherically controlled cases (precipitation regardless of the land surface conditions) are found for 71% of the soundings.

Two stations have a small fraction of feedback situations, Jagdalpur (19.1°N, 82.0°E) and Bangalore (12.5°N, 77.3°E). Both are dominated by atmospherically controlled wet conditions.

Table 3.4: Feedback expectations for a two weeks, one month and two months period after the monsoon retreat, for soundings from all stations in different regions in India (see Fig. 3.8, lower left panel, for a delineation of these regions).

Period		All India	North	South and East
2 Weeks	Atm	67.9	72.8	64.6
	Pos	21.9	14.8	26.7
	Neg	10.2	12.4	8.7
1 Month	Atm	71.0	77.7	66.3
	Pos	19.5	10.9	25.5
	Neg	9.5	11.4	8.2
2 Months	Atm	75.8	83.5	70.6
	Pos	16.6	8.1	22.4
	Neg	7.6	8.4	7.0

3.5.4 Monsoon Retreat

During the monsoon retreat, considerable potential for feedbacks is also present. However, the situation in the north of India is quite different from that in the south and east. The northern region has some potential for feedbacks in the two weeks after the monsoon retreat, with positive and negative feedbacks equally likely. Table 3.4 shows the percentages of positive, negative and atmospherically controlled cases for a two week, a one and two month period after the monsoon for all stations in India and for the two regions indicated in the contours in Fig. 3.8 (lower left panel). Atmospherically controlled situations prevail after about one month after the retreat.

In the south and east, potential for positive feedbacks after the monsoon retreat is much stronger. In the two months after the monsoon retreat, the feedback situations (of which the majority positive) represent about 30% of the cases, as shown in Fig. 3.8, lower panels. The duration of the period during which feedbacks are expected is longer than during the monsoon onset, suggesting that land surface changes can have a larger influence during the retreat period than during the onset period.

3.5.5 Influence of Irrigation on Pre-Monsoon Precipitation

The effect of land-atmosphere feedbacks cannot be determined from precipitation records alone, since at a given moment, only one land surface state is present. However, for India, the irrigation extent has doubled between 1960 and 2004 (see trend in Fig. 3.10), giving different land surface conditions over time for the same sites. Fig. 3.10 shows the trends in precipitation in the pre-monsoon period that is sensitive to positive feedbacks (probability of positive feedbacks higher than 0.2), for stations in

irrigated regions and in non-irrigated regions (part of 0.08 degree gridcell suitable for irrigation larger/smaller than 25%). The length of this period is different for each station, but on average it is 23 days.

The irrigated stations show an upward trend of 0.7% of the annual precipitation

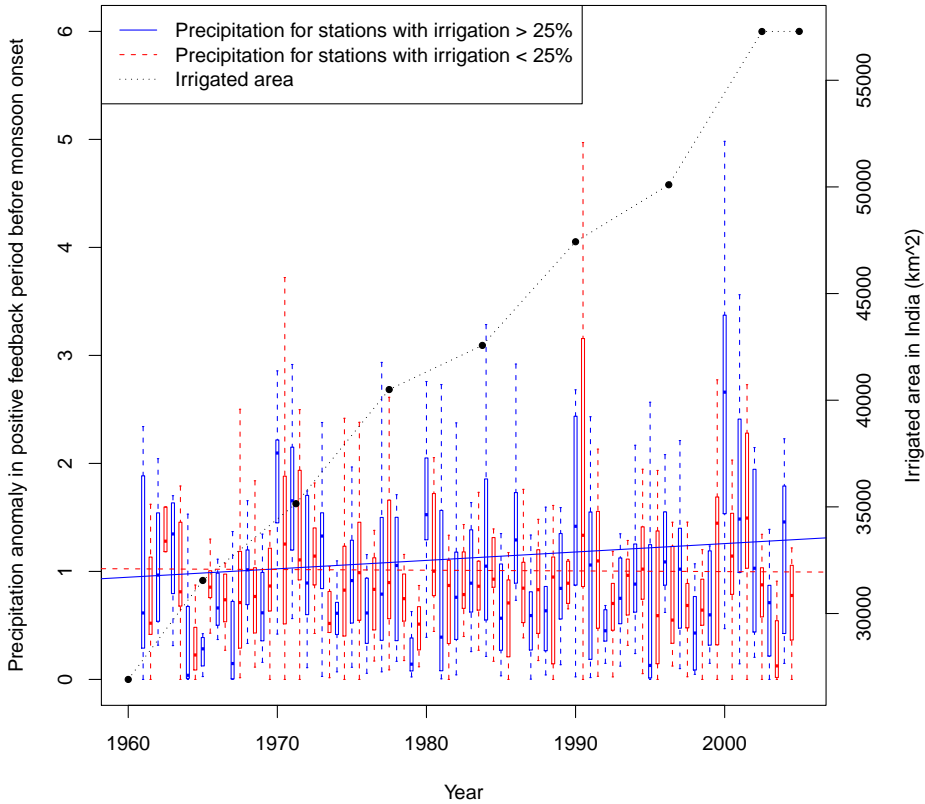


Figure 3.10: Relative deviation from the 1960-2004 precipitation mean in the period with positive feedbacks before the monsoon onset for irrigated (blue) and non-irrigated (red) sites from 1960-2004. The period before the monsoon onset is different for each site, but constant in time. The irrigated sites show an upward trend (0.0077 ± 0.0042 of yearly precipitation, this trend is significant from zero at the 93% confidence level), while the non-irrigated do not (-0.0006 ± 0.0033 of yearly precipitation). Total irrigated area in India (Siebert et al. (2005)) is plotted on the right axis.

per year in the period considered, while the non-irrigated stations show almost no trend. The trendlines of irrigated and non-irrigated stations are different at the 93%

confidence level. While the irrigated trend is different from zero at the 93% confidence level, the non-irrigated trend is not statistically different from zero. The upward trend in the irrigated areas results in about 30% more pre-monsoon rainfall over the 1960-2004 period. This increase in pre-monsoon precipitation for the irrigated stations corresponds to about 1-3% of the annual precipitation.

3.6 Discussion

In this study, the importance of local feedbacks from land surface state to convective precipitation has been quantified for India using the existing CTP- HI_{low} framework (FE2003a). It was shown that this framework, that was proposed for the USA, can be applied to India as well. However, some adaptation of the classification thresholds will improve the performance in these tropical conditions. By forcing a slab model with atmospheric soundings from India, feedbacks were found for higher values of HI_{low} than those proposed for the USA.

Using the acquired thresholds for feedbacks, a much larger number of soundings can be efficiently classified without running a model. Overall, the framework predicts 76% of the atmospheric situations correctly. However, two types of errors are made: not all situation that show feedbacks in the model are classified as having a feedback by the framework, and not all situations that are classified as having a feedback, show this feedback in the model. For the chosen feedback thresholds for India, the number of cases falling in these error categories are similar. Therefore, the framework does not over- or underestimate the number of cases in which there is a feedback situation. However, when considering individual soundings classified as having a feedback, the chances of misclassification are significant (about 60% of positive feedback classification actually are atmospherically controlled and about 50% of the modeled positive feedbacks are not classified as such). The framework classifies about half of the feedbacks that occur in the model. In the original study by FE2003a, the predictive capacity of the framework is not quantified, so it is unknown whether the framework performs differently for India than for the USA. However, it is shown that by using different thresholds for feedbacks for different regions, the prediction error is reduced. Therefore, for new regions where the framework is to be applied, models should be used to re-assess the feedback thresholds. Alternatively, given enough computing resources one might skip the classification and use the model only to evaluate the soundings.

Apart from optimizing the framework thresholds, alternative measures have been used to classify the soundings. However, changing the levels and ranges at which CTP and HI_{low} are evaluated did not improve the framework predictions. Moreover, the slab model was also run with soil moisture between 15% and 85% of the maximum soil moisture. However, no significant relation was found between the soil moisture per-

centage at which the model result changed from precipitation to no precipitation or vice versa and CTP or HI_{low} .

In our approach, a simple model that might lack important processes is used to determine land-atmosphere feedbacks. Advection, orography and flows that originate from land surface heterogeneity are not included in our simple model. These processes are important for the feedbacks that are considered here, but are not taken into account. To test the effect of those processes on land-atmosphere feedbacks, a 3D atmospheric model should be used.

Application of the framework showed that there is significant potential for local positive feedbacks from the land surface state to convective precipitation, the opposite negative feedbacks are less predominant. This means that wet surface conditions can enhance local precipitation. The potential for these local feedbacks varies both spatially and seasonally for India.

The yearly CTP- HI_{low} cycle shows the signature of the monsoon dynamics. From about a month before the onset of the monsoon, India's south and east and Bangladesh show a potential for positive feedbacks. HI_{low} values are in the positive feedback range in these areas due to advected moisture from the nearby ocean, while CTP values are positive due to increased insolation. So, areas with wet surface conditions favour convection and can trigger pre-monsoon convective rains. In the remainder of India, HI_{low} values are slightly higher and positive and negative feedbacks occur in equal ratios (see table 3.3).

During the monsoon season, the probability of positive feedbacks is high throughout India. Feedbacks during the monsoon period might be important in regions in that receive the majority of precipitation from convective storms. These regions are found in the rain shadow of mountain ranges and during monsoon breaks (periods of up to two weeks during which the prevailing monsoon flow pattern stops)(O'Hare (1997)). During the period two months after the monsoon retreat, atmospheric situations for which positive and negative feedbacks can be expected are present in about the same quantities in north India. During that same period, positive feedbacks can be expected in a region extending from the south, through a strip along the Bengal coast, to the east.

When the summer monsoon has completely retreated, dry atmospherically controlled situations start prevailing, with no convection regardless of surface conditions. These conditions persist throughout the winter months (January-March), during which the land surface conditions are not expected to trigger rainfall.

These results are in agreement with the positive correlations between soil moisture, recycling ratio and evaporation for MAM and SON reported by Dirmeyer et al. (2009). As in the present study, Dirmeyer et al. (2009) concluded that soil moisture is important during the monsoon onset and retreat phases, although their integration period of three months is quite large in comparison with onset and retreat. During the monsoon

season, we find the same land-atmosphere coupling patterns as Koster et al. (2004), but additional sensitive regions are found in east and south India and Bangladesh. We plan further research using reanalysis data to get a better spatial and temporal feedback description, and to compare this with other diagnostics (recycling ratios, correlation between soil moisture and precipitation, etc.).

Although we find positive local feedbacks for large parts of India in the monsoon season, the reduction of the land-sea contrast can affect the large scale monsoon flow and act as a large scale negative feedback, as suggested by Lee et al. (2009). Regional scale atmospheric models could assess the relative importance of local and large scale feedbacks.

Determining the actual importance of land-atmosphere feedbacks from precipitation data alone is complicated. The signal from both large scale processes and local feedbacks are present in the data. Moreover, when relating the potential for feedbacks to the monsoon onset, local feedbacks may already have influenced the precipitation data from which the onset date is determined. The determination of monsoon onset date by the large scale wind pattern (IMI) can at least partly circumvent this problem.

In the period before the monsoon onset, surface conditions are mostly dry. Therefore, large scale irrigation is expected to influence precipitation just before the monsoon onset. Since there has been an increase in irrigation in India during the entire 20th century, the pre-monsoon precipitation is expected to have increased in irrigated areas. This is confirmed in Fig. 3.10, which shows the difference in trends of pre-monsoon precipitation between irrigated and non-irrigated areas. In the 1961-2004 period, there has been an increase in pre-monsoon precipitation in irrigated areas that corresponds to 1-3% of annual precipitation. This is a modest amount compared with the total annual precipitation, but it is significant in a period of small precipitation amounts, and may be important for, e.g., crop germination.

Further examination of precipitation data could determine how well the trends in pre-monsoon precipitation follow the irrigation trends, as well as the influence of irrigation during the monsoon and post-monsoon season.

3.7 Conclusion

This study applied the CTP- HI_{low} framework to India to determine the influence of land surface on convective precipitation. The framework can be applied to India, but HI_{low} thresholds to determine cases with feedbacks was higher than in the original study for the USA. With the new thresholds for feedbacks applied to atmospheric situations in India's climatology, the periods around the monsoon season and the monsoon season itself showed the largest percentages (of up to 40%) of days with

potential for local feedbacks.

Using the framework improves the feedback potential prediction with about 30-40%, compared to a classification without prior knowledge. However, for a significant fraction of the soundings the classification is incorrect. Efforts to make the framework more physically realistic, for example by limiting the integration of definitions of CTP and HI_{low} to the simulated ABL depth, did not improve this classification. There seems to be a limit to the predictive capacity of a framework with only two indicators. However, the advantage of the framework is that large timeseries can be analysed quickly.

The feedback potential follows India's monsoon dynamics. During January to April, the atmosphere is too dry for the land surface to induce precipitation. However, in the period before the monsoon onset, positive feedbacks are found in the south and east. During the monsoon season, all of India has atmospheric conditions in which a wet land surface can trigger precipitation more than 20% of the time. After the monsoon retreat, a region extending from the South to the East shows these atmospheric conditions more than 20% of the time.

The effect of these feedbacks just before the monsoon onset was tested by comparing the extent of large scale irrigation with the pre-monsoon precipitation. Irrigated areas show an increasing pre-monsoon precipitation trend, while non-irrigated areas lack this trend. This suggests that irrigation increases precipitation in these periods. This precipitation increase corresponds to about 3% of the annual precipitation, but falling in the month before the monsoon onset, it may represent a significant contribution to water resources.

We conclude that the CTP- HI_{low} framework is a good method to efficiently determine the potential for local land-atmosphere feedbacks. Periods and regions where feedbacks are potentially important can be determined easily. Because of the limitations in the framework, a three dimensional model that takes into account more processes should be used to study the land atmosphere feedbacks in more detail. This is beyond the scope of the present paper and is a subject of further study.

Chapter 4

The fate of evaporated water from the Ganges basin

Abstract

This research studies river basin moisture recycling rates in order to determine the atmospheric part of the water cycle and the influence of the land surface there on. For river basins in India (Ganges and Indus), the fraction of evaporation that falls again as precipitation in the same river basin (the moisture recycling) is determined. Furthermore, the seasonal variance of moisture recycling and the fraction of precipitation that originates from evaporation from the same river basin is quantified.

Using a quasi-isentropic moisture tracking scheme, evaporation from land surfaces in India is tracked through the atmosphere until precipitation brings it back to the land surface. This scheme is forced with ERA interim reanalysis data from 1990-2009. With the information about the atmospheric paths of water vapor, the distance between evaporation and precipitation location is determined. To get an approximation of the influence of land-use on the atmospheric moisture budget, the atmospheric paths of water vapor from two bordering areas with different evaporative regimes are compared.

Results show a strong annual cycle in the recycling ratio. For the Ganges basin, the recycling ranges from 5% during the winter months (Nov-Mar) to 60% during the June-July-August (JJA) season. The comparison of two focus areas in the Ganges basin with a difference in March-August evaporation shows that during the pre-monsoon months (March-May), up to 70% of the the evaporation difference between the two

areas, recycles within the Ganges basin. Analysis of the soil moisture nudging terms in ERA-Interim compared to independent irrigation data strongly suggest this evaporation difference can be attributed to large scale irrigation.

The importance of basin moisture recycling for precipitation shows an annual cycle as well. An annual average of 4.5% of Ganges precipitation originates from water evaporating in the Ganges basin. During the dry winter monsoon, any precipitation originates from sources outside the basin. During March-April-May (MAM) and Oct-Nov, 10% of the precipitation originates from evaporation within the basin. During the summer monsoon season, the large influx of moisture from the Indian ocean dominates the precipitation and recycling is 5% of precipitation.

4.1 Introduction

During the 20th century, population pressure and demand for agricultural products has increased on the Ganges plains. As a consequence, between 1900 and 2000, irrigation extent has increased five-fold in India (from 12 to 58 million hectare)(Siebert et al. (2005)). Two sources supply the water used for this irrigation; a channeling system that diverts water from the Ganges river onto the fields and the pumping of ground water. These human activities have substantially changed the natural water cycle in India, for example by pumping to the surface up to 150 mm ground water per year (for India south of the Himalayas, around the year 2000)(Wada et al. (2010)), increasing the surface moisture available for evaporation. Siebert and Döll (2010) analysed not only ground water subtraction, but also surface water use and found that irrigation consumes up to 1 mm surface and ground water per day in most parts of India for 1998-2002.

The water on these irrigated fields either infiltrates or evapo(transpi)rates, with a small fraction of irrigation water being part of the harvested crop. During times of the year in which the soil would normally be dry, irrigation increases evaporation. This increased evaporation has two related effects: a change in the land surface energy balance and an increased release of moisture to the atmosphere.

Combined, these changes can increase or reduce precipitation and change flow patterns. The effects of surface moisture conditions on the Indian climate, and especially the monsoon flow, has been subject of different studies. On the global circulation model (GCM) scale, Koster et al. (2004) found a hot-spot of soil moisture-precipitation coupling in India. However, in a follow up study, again using GCMs, Koster et al. (2011) found that soil moisture initializations did not increase the precipitation forecasting skill in India. Douville et al. (2001) found two opposing impacts of a wetter soil; an increase in rainfall over northern India due to larger moisture supply, but also decreasing moisture convergence due to a decreased land-sea surface tempera-

ture contrast.

In coastal areas, Lohar and Pal (1995) found that irrigation decreased sea breezes, causing reduced low-level moisture supply and a net negative effect of irrigation on precipitation. Lee et al. (2009) related increased pre-monsoon irrigation to a decreased monsoon precipitation during 1982 to 2003, which they hypothesized was caused by a decreased land-sea contrast. Using a one-dimensional slab model and therefore only assessing the local effect of the land surface, Tuinenburg et al. (2011) noted that from one month before the monsoon onset until two months after the monsoon retreat, a wet land surface increases the triggering of convection.

The evaporated water becomes part of the atmospheric part of the water cycle and is transported downwind. If the water precipitates nearby the evaporation site, it is recycled within the area and can potentially be reused. If it precipitates far downwind, it is lost for the local water resources. The time- and length-scales of the atmospheric part of the water cycle depends on precipitation, evaporation and wind patterns, which vary throughout the year. Methods to quantify the atmospheric part of the water cycle and estimates for India are discussed in Section 4.2.

This research investigates the fate of the evaporated water from two areas with different hydro-meteorological conditions on the Ganges plains in India, and its seasonal and inter-annual variance addressing the following research questions:

- What happens to the water evaporated from the Ganges plain and how do different hydro-meteorological regimes affect the fate of the water?
- What are the temporal and spatial aspects of the atmospheric water cycle over India?
- What is the importance of water recycling within India's river basins?

This paper is structured as follows. Section 4.2 gives an overview of previous literature on moisture recycling and methods to derive recycling rates. Section 4.3 presents the methods used, with subsections on the data used, the details of the water tracing model and accounting of trajectories into river basin recycling. Section 4.4 presents the results, with subsections on the downwind footprint of evaporation, basin recycling, importance of recycling for basin precipitation and temporal aspects of the recycling. Sections 4.5 and 4.6 present the discussion and conclusions.

4.2 Literature Synthesis

Several studies have quantified moisture recycling rates. These recycling rates are defined as the fraction of precipitation in a particular domain (for example a 300x300km square area) that originates from evaporation in the same domain. In other words it

is the fraction of precipitation that comes from moisture from local sources. This is opposed to advected precipitation, which originates from non-local sources (moisture evaporated outside the area considered). An analogue definition is used for evaporation recycling; the fraction of evaporation from an area that precipitates again in the same area. Apart from climatological reasons, recycling rates are dependent on the size (or length scale) of the region considered. For small regions, down to a single point, the recycling ratios decrease to zero, while for large regions, up to the entire globe, the recycling ratios approach one. Therefore, comparing recycling ratios from previous studies is difficult, as the size of regions considered differs.

Most studies use analytical bulk models to quantify recycling ratios. Burde and Zangvil (2001a) provide a good overview of these models and their different assumptions. These assumptions usually are: (1) the use of time averaged data represents the non-linearities that occur on shorter time scales, (2) the changes in atmospheric moisture storage is constant over long time periods and (3) the atmosphere is assumed to be well mixed. These bulk recycling models have become more complex over time, ranging from one-dimensional time and space averaged models to two-dimensional models that take into account variances in space and time (Budyko (1974), Brubaker et al. (1993), Burde and Zangvil (2001b), Schär et al. (1999)).

As an alternative to the bulk models, methods have been developed to tag evaporated water and track its path through the atmosphere and determine the region where the tagged water precipitates. Within a GCM, Numaguti (1999) and Bosilovich and Schubert (2002) tagged water evaporating from (large) areas and determined which fraction of precipitation consisted of this tagged water. The drawbacks of using water tracers in GCMs is that it is computationally and data storage intensive. Moreover, the source regions to be considered have to be determined beforehand and new regions can only be assessed doing new model runs. Although these water tagging methods are more computationally expensive than the bulk methods, they provide a better representation of the time varying aspects of the moisture recycling, especially the nonlinear terms (Dirmeyer and Brubaker (2007)).

To circumvent these drawbacks of tracers in atmospheric model, Dirmeyer and Brubaker (1999) used a evaporation tagging method, forced with reanalysis data, to determine the origin of precipitation in the Mississippi basin during 1988 and 1993. Using the same method (quasi-isentropic calculation of water vapor trajectories backwards in time, QIBT), Dirmeyer and Brubaker (2007) established global climatologies of moisture recycling (within an area of about 300x300 km), based on NCEP reanalysis (Kanamitsu et al. (2002)). The advantage of the QIBT method is that it can be used as post-processing to atmospheric models, and that accounting of source regions can be defined after the simulation. Therefore, Dirmeyer and Brubaker (2007) were able to calculate recycling per grid cell, as opposed to the more broadly defined regions (such as oceanic versus land evaporation) used in the GCM tracer studies.

Previous studies show a range of recycling ratios estimations for India. Using tracers in a GCM, Bosilovich and Schubert (2002) found that during JJA, about 9% of the precipitation on the Indian mainland originates from evaporation in the same region. Using the same method as used in the current study, Dirmeyer and Brubaker (2007) found 25 year mean recycling ratios at a typical spatial area of $10^5 km^2$ of 2-10%, with a peak during JJA. Yoshimura et al. (2004) followed tagged evaporation from the Indian land surface for the 1998 monsoon season (May-October) and found that the majority of evaporation precipitated again on the Himalaya slopes and in the Indus basin/Pakistan. For Calcutta, they found that 20-30% of the precipitation originated from evaporation from land surfaces. Using bulk methods, van der Ent et al. (2010) found that about 30% of the January land evaporation in India falls again as precipitation over land somewhere, while this is up to 90% during July. Trenberth (1999) used a bulk method to determine recycling ratios and found annual mean recycling ratios for India of less than 10% for a recycling length scale of 500km and 15-20% when a length scale of 1000km is used.

All these studies took a global perspective and did not study the temporal aspects of moisture recycling or the effect of land use (change) on moisture recycling.

4.3 Methods

The current research will study the atmospheric path of water vapor evaporated from the Indian subcontinent, and especially the Ganges plain (see Fig. 4.3 for domain, basins and orography of the Indian sub-continent). Forced with ERA-interim reanalysis data, the quasi-isentropic trajectory method of Dirmeyer and Brubaker (1999) is used to determine the path of the evaporated water through the atmosphere. However, the process is reversed and forward trajectories have been calculated instead of the backward trajectories determined in the original method.

In the first part of the study, two 2×3 degree areas with contrasting hydro-meteorological conditions are compared, in the Northerly area A annual evaporation is higher than in the Southerly area B, while annual precipitation is lower in area A than in area B. Figure 4.2 shows the hydro-meteorological conditions and the locations of both areas. Additional reasons to select these particular areas, are that they are close together, so that large scale wind patterns are not very different and that the monsoon onset and retreat dates are similar for both areas. The output of the water trajectory model is used to determine the differences between recycling from areas with higher (area A) and lower (area B) evaporation.

In the second part of the study, the output of the trajectory model is analysed for the Indian sub-continent. For different river basins, the importance of river basin moisture recycling for the river basin water budget is determined. For the Ganges basin, an additional analysis is done. The basin is divided into two equally sized parts,

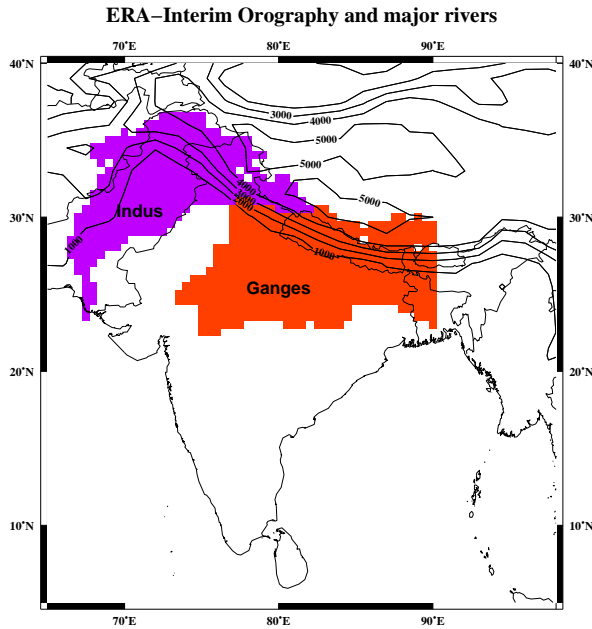


Figure 4.1: Contourplot of the orography in the ERA interim dataset (in meters). The Ganges and Indus rivers basins are shaded.

one with a fraction of irrigated area smaller than the median and one with a fraction higher than the mean. The differences in basin recycling are determined for both parts of the basin to get a first order estimate of the effect of irrigation on moisture recycling. While recognizing that irrigation is not explicitly included in ERA interim, in section 4.3.3 we will explore to what extent it is included through the soil moisture nudging term.

The focus is on river basin moisture recycling, as this is the unit most relevant for hydrology. Moreover, water that recycles within the river basin can potentially be reused as resource.

4.3.1 Water trajectory model

The water trajectory model used tracks the water that evaporates from the earth surface along its path through the atmosphere, to where it precipitates. The trajectory model is schematically shown in Figure 4.3.1. It is a version of the model used by Dirmeyer and Brubaker (2007), modified to do forward trajectories for evaporation instead of backward trajectories for precipitation.

During every reanalysis (6-hour) time step, the evaporation from a grid cell is fol-

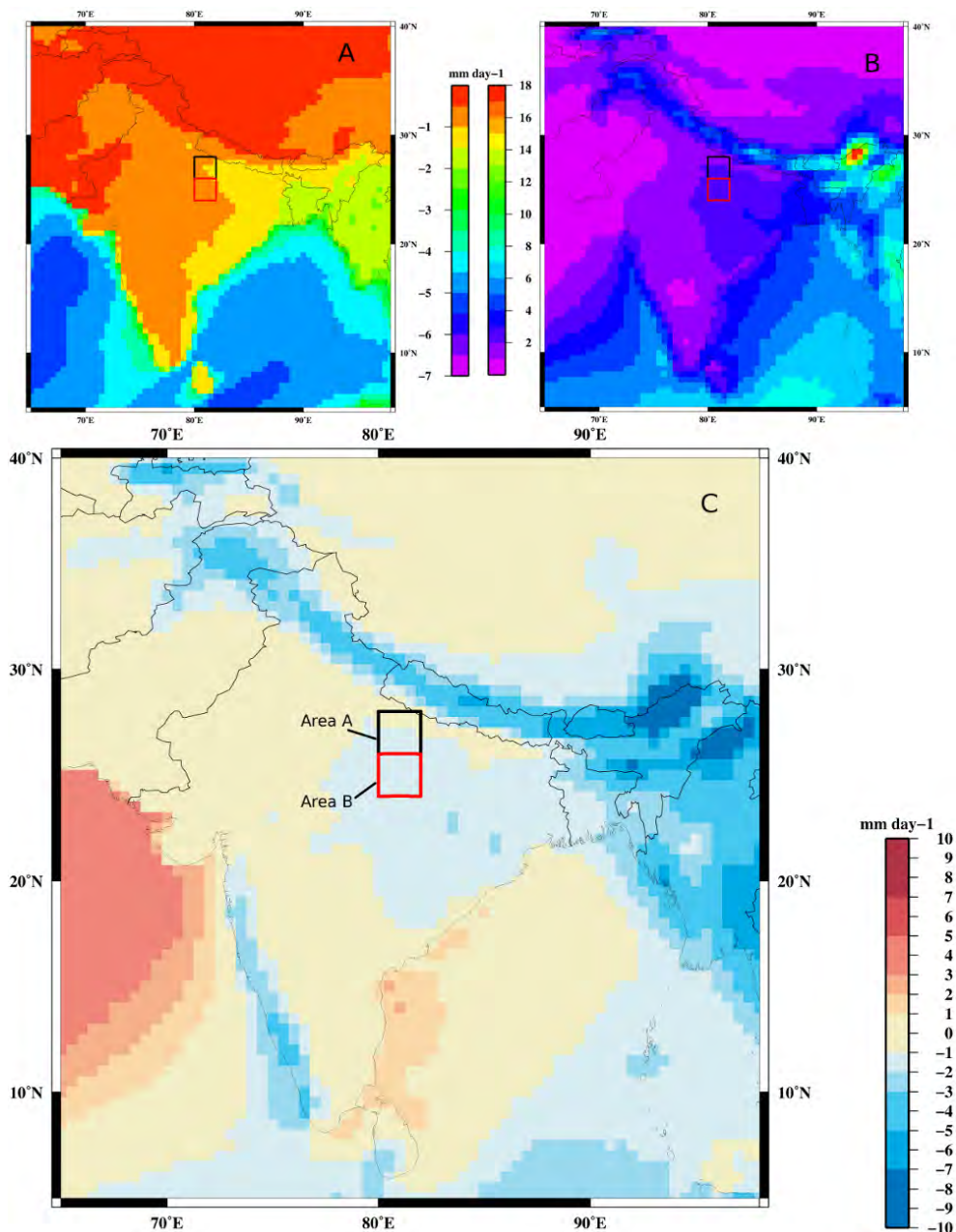


Figure 4.2: Annual mean values of evaporation (a), precipitation (b) and evaporation-precipitation (c), in mm/day based on ERA-interim for 1990-2009. Two areas that are the focus in this research are indicated, the area in the black rectangle has annual mean $E = 1.0$ mm/day, $P = 2.0$ mm/day and $E - P = -1.0$ mm/day. The area in the red rectangle has annual mean $E = 0.9$ mm/day, $P = 2.2$ mm/day, $E - P = -1.3$ mm/day.

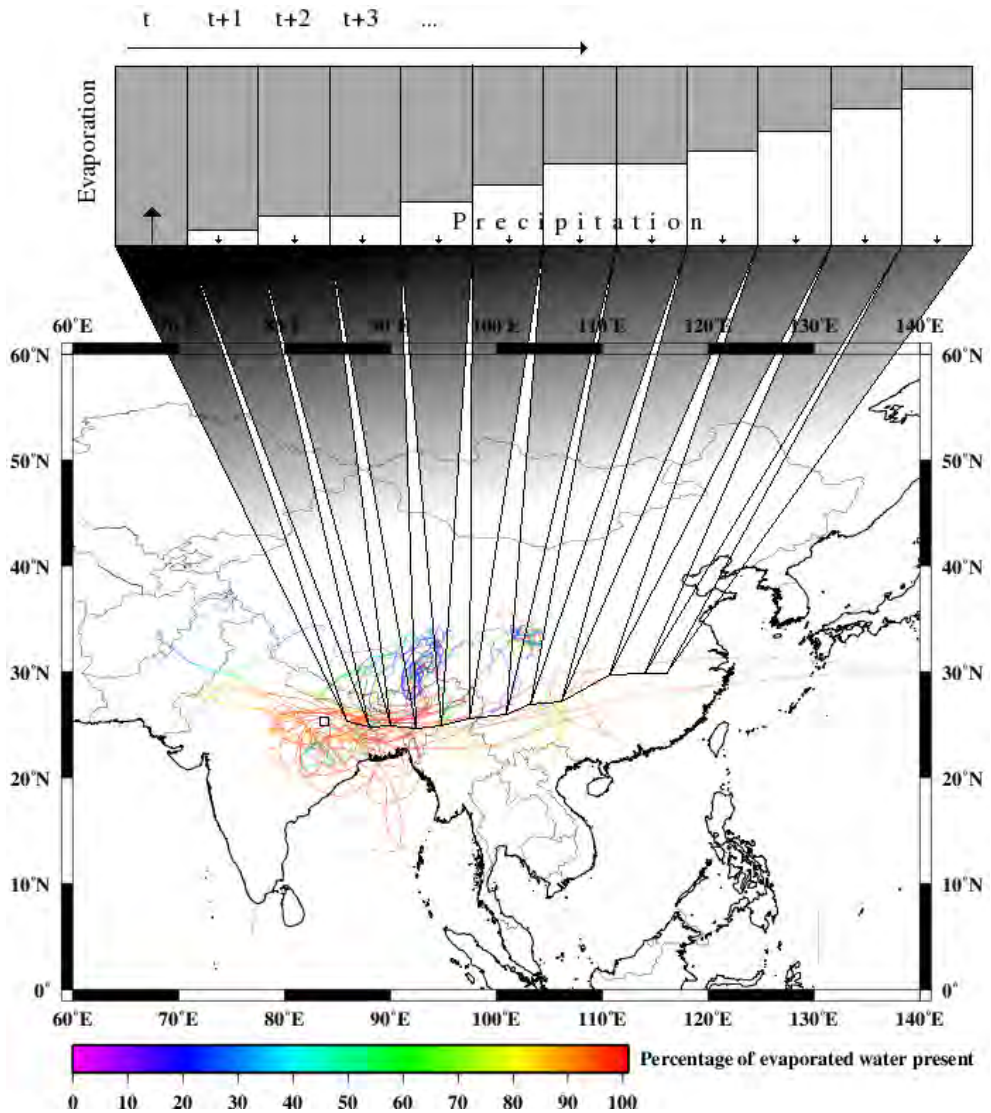


Figure 4.3: Trajectories of evaporated water from the irrigated area in MAM, the color of the line-segment represents the amount of originally evaporated water still present. The cartoon represents the scheme of the water allocation in the trajectory model, based on Dirmeyer and Brubaker (2007). Once water is evaporated ($Time = t$), all the water is still present in the parcel. As the parcel is tracked ($Time > t$), water precipitates out of the parcel and less of the originally evaporated water remains in the parcel.

lowed by means of a number of virtual parcels. These parcels are released from random (latitude and longitude) locations within the grid cell. After evaporation from the surface, the model assumes the evaporated water vapor is mixed through the atmospheric column with the same distribution as the water vapor already present. Therefore, the starting height of the parcels is chosen at random, but scaled with the vertical specific humidity profile (resulting in an average starting height at 200 hPa above the local topography). According to Dirmeyer and Brubaker (2007), this is probably the weakest assumption of the method. However, tests with parcel releases from the surface did not show significantly different results. When the starting position of a parcel is known, its path through the atmosphere is calculated using the three dimensional reanalysis wind speeds. The wind speeds at the location of the parcel is obtain by a linear interpolation between the surrounding grid cell and pressure level values. To obtain an accurate and smooth path of the parcel, the reanalysis wind speeds have been linearly interpolated in time to 36 minute time steps (one tenth of a six-hour period), during which wind speeds are assumed to be constant.

When the parcel is just released, it contains all the evaporated moisture from the source location. However, during every reanalysis time step, evaporation (from the surface, into the parcel) reduces the fraction of moisture from source location present in the parcel. Similarly, the precipitation (out of the parcel, onto the land surface) allocates a fraction of the moisture from the source area to the precipitation in the current location of the parcel. The model assumes a perfect mixing of moisture in the atmospheric column. Moisture at any level is equally likely to precipitate and evaporated moisture is mixed perfectly in the column, although weighted by the humidity profile. Therefore, the amount of precipitation attributed to the moisture from the source area is:

$$A_{x,y,t} = P_{x,y,t} \frac{W_{parcel,t} E_{source,t}}{PW_{x,y,t}} \quad (4.1)$$

where A is the attribution, P the precipitation, W_{parcel} the amount of water in the parcel and PW the precipitable water (all in mm). E_{source} is the fraction (dimensionless) of water in the parcel that evaporated from the source area. When the parcel is just released ($t = 0$), W_{parcel} is equal to the amount of water that has evaporated from the source area during the starting time step and $E_{source} = 1$. Then, as a consequence of evaporation into the parcel during every time step the amount of moisture in the parcel is updated:

$$W_{parcel,t} = W_{parcel,t-1} + (E_{x,y,t} - P_{x,y,t}) \frac{W_{parcel,t-1}}{PW_{x,y,t}} \quad (4.2)$$

where E is the evaporation in mm. The fraction of source water in the parcel updates as:

$$E_{source,t} = \frac{E_{source,t-1} W_{parcel,t-1} - A_{x,y,t}}{W_{parcel,t}} \quad (4.3)$$

As a consequence the amount of source water present in the parcel ($E_{source,t}W_{parcel,t}$) decreases with precipitation along the path of the parcel. The parcel is followed until less than 5% of the source water is still present, or the parcel has been tracked for 30 days, or the parcel leaves the 15W-120E,5S-75N domain. Figure 4.3.1 shows a subset of trajectories of water parcels launched from one of the focus areas of this study. Some evaporation is transported far away and no precipitation falls out of the parcel (trajectory-sections plotted in red), while others rain out quickly (trajectory-sections plotted in blue).

For each 1 degree grid cell, ten parcels were released during every reanalysis time step (6 hours). This repetition of the procedure is done to account for differences in starting locations within the grid cell and subsequent different pathways of the parcel. Tests with more parcel releases showed no substantially different mean pathway.

This process is repeated for all one degree grid cells in the Indian sub-continent (5-40N, 60-100E), for each time step in the 1990-2009 dataset. This resulted in a database which related evaporated water to patterns of downwind allocated water ($A_{x,y,t}$).

4.3.2 Basin Recycling

The output of the trajectory model used described in section 4.3.1 is a relation between evaporation at a source location and a spatial distribution of precipitation attributed to that evaporation. In the majority of moisture recycling studies, a typical length or spatial scale is used to calculate recycling rates. For example, it is determined how much evaporation recycles within a 300x300km area. A drawback of this approach is that recycling rates are dependent on this length or spatial scale. Dirmeyer and Brubaker (2007) fitted recycling rates for different length scales to a power law (equation 4.4) for different study areas.

$$\rho = aA^b \quad (4.4)$$

in which ρ is the recycling rate (%), A is the size of the area under consideration and a and b are parameters to be fitted. For their study areas, Dirmeyer and Brubaker (2007) found $b = 0.462$, with a small variance (and significantly ($p=0.001$) different from 0.5 (the square relation between distance and area)), and concluded that this slope factor can be used universally. So, when a recycling ratio is determined for a region of a given size, a can be determined by using equation 4.4 and the obtained recycling ratio can be converted to a recycling ratio for a source region of a different size. By comparing the typical length scales of the trajectories calculated in the current research, the validity of eq. 4.4 for India will be determined. For this, the length scales have to be converted to an cumulative area value by taking the square root and cumulative value of the atmospheric water path length scale probability calculated.

The scaling law for recycling is important to interpret results of moisture recycling studies at different scales. However, the determination of recycling rates in a square or rectangular area neglects the link to the land surface hydrology which uses the river basin as its unit. These rivers basins are usually not rectangular. The shape of the river basin and its orientation to the dominant atmospheric flows are important factors affecting river basin moisture recycling. As this study focusses on land uses in the Indian river basins and their influence on the atmospheric water balance, the recycling ratios in this study will be based on the river basin. This will make the results more comparable to outputs of large scale hydrology models, and (hopefully) more relevant to the hydrological community. We define the basin recycling rate as the fraction of water that falls as precipitation in the same river basin as it evaporated from.

4.3.3 Data

The water trajectory model needs to be forced with atmospheric wind and humidity data and surface fluxes. These data can come from free running climate models (GCM output) or from constrained weather prediction models (reanalysis data). The advantage of using the GCM data is that the moisture budgets close, no water is created or removed in the model run. This is not the case with reanalysis data, in which the 'analysis term' adds or removes moisture to nudge the model state to the atmospheric measurements. On the other hand, this data assimilation means the representation of the actual atmospheric state is better in the reanalysis data.

In the current study, the water trajectory model is forced with ERA interim reanalysis data (Dee et al. (2011)) from 1990-2009, with a native horizontal resolution of 1 degree lat/lon. The three dimensional fields of wind speed (u,v,w) and specific humidity (q) are used from seven vertical levels (500, 600, 700, 775, 850, 925 and 1000 hPa). The two dimensional fields used are evaporation and (total) precipitation. All the input data is linearly interpolated to a horizontal resolution of 0.5 degrees and a temporal resolution of 36 minutes. We recognize that this may mean that sub-grid non-linearities in moisture transport, precipitation and evaporation (due to convection, strongly varying wind patterns, etc.) are misrepresented.

As a first order quality check, the ERA interim precipitation in the two focus regions is compared to CRU version 2.10 (Mitchell and Jones (2005)) and Aphrodite version 10 (Yatagai et al. (2009)) precipitation.

The basin data are based on the drainage direction map DDM30 (Döll (2002)). This map is based on a hydrologically corrected 1-km digital elevation model and has a resolution of 30'.

Irrigated area size is determined from the GMIA (Siebert et al. (2005)), which is the fraction of 0.08 degree grid cell that is suitable for irrigation (see Fig. 4.3.3). For

the annual cycle in irrigation water supply, Siebert and Döll (2010) is used. Based on the global high resolution monthly irrigated and rain-fed crop areas from the MIRCA2000 database (Portmann et al. (2010)) and the Global Crop Water Model (GCWM, Siebert and Döll (2010)), this data set provides the monthly evapotranspiration of water extracted from rivers, lakes and aquifers ('blue' water) for irrigated agriculture and that of water from the soil ('green' water) for the situation around 2000. To test the effect of irrigation on the ERA-interim data, the ERA-interim soil moisture data from four soil layers is analysed (covering 0-288 cm depth).

For the reanalysis moisture data (both in the soil and the atmosphere), the anal-

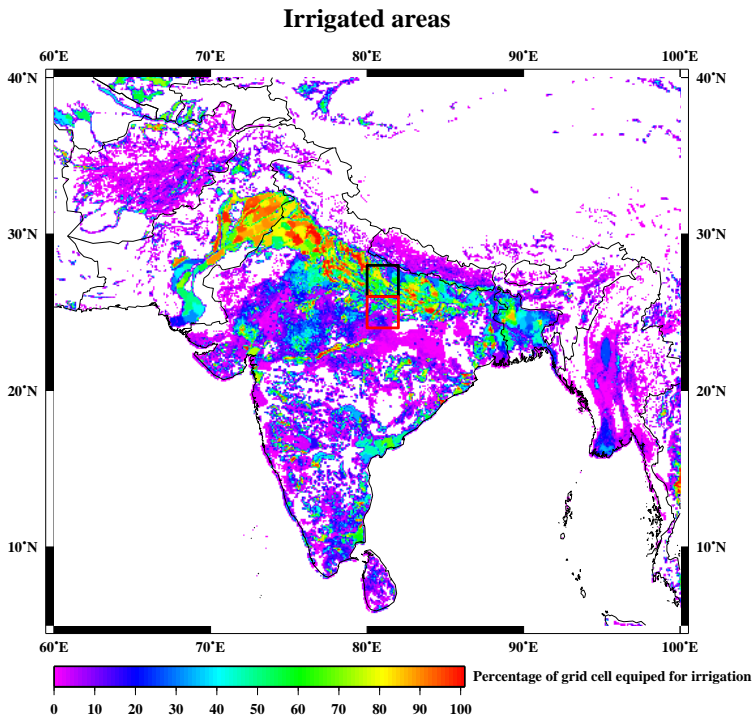


Figure 4.4: Fraction of grid cell (0.08 degree) equipped for irrigation (Siebert et al. (2005)) in the Ganges basin.

ysis increment is determined by subtracting the reanalysis moisture at the start of the model simulation with the moisture in the previous model run (started 12 hours earlier), valid for the same time. The moisture difference between these two model states is the amount of water that is added to or subtracted from the system due to the reanalysis process.

4.4 Results

4.4.1 Downwind precipitation footprint of evaporation

Figure 4.5 shows the average yearly evaporation cycle for areas A and B in Figure 4.2. During about half the year (August to March), evaporation from both areas is similar. However, from March to August, evaporation from area A is about 0.5 mm per day higher. The most distinct difference in evaporation occurs during the MAM period, when evaporation from area A is higher than from area B. This difference cannot be explained by differences in precipitation in this period. Precipitation amounted to 0.28 (0.22, 0.27) mm/day in area A and 0.49 (0.53, 0.46) mm/day in area B, for ERA interim data (with Aphrodite and CRU numbers added in brackets)). The precipitation difference between the two areas can be explained by their different location relative to the monsoon onset; the monsoon arrives earlier in the area that is more to the south. These rainfall data show that a) the analyzed rainfall compares well with two alternative observed precipitation datasets, and b) that differences in precipitation cannot cause the differences in evaporation because of the opposite sign of the two.

The results from the water tracking model show the spatial distribution of where

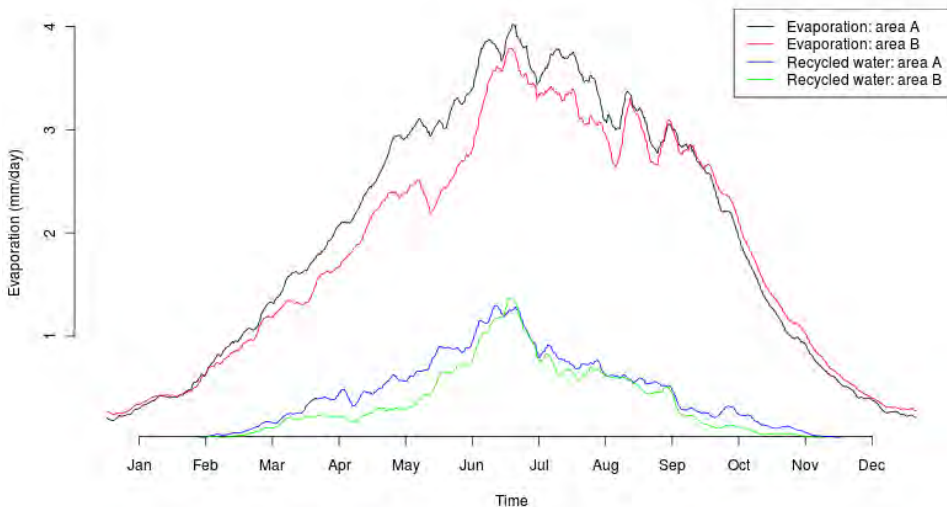


Figure 4.5: Average yearly cycle of ERA-interim evaporation and recycled evaporation within the Ganges basin (basin recycling) calculated using the trajectory scheme (discussed in section 4.4.3) for areas A and B (figure 4.2) for 1990-2009.

this evaporated water precipitates after its path through the atmosphere. Therefore, we focus on this period to observe the differences in the water cycle due to irrigation. For area A, the downwind precipitation distribution or footprint (MAM) is shown in Figure 4.6A. During MAM, the majority of evaporated water is transported in the direction of the Himalaya mountain range and either precipitates there, or flows around it and precipitates on the Tibetan plateau. However, there is also a fraction of evaporation that is transported further away, primarily in the direction of the Bay of Bengal and onward to south-east Asia and eastern China.

As the total evaporation from area B is less during MAM (see Fig. 4.5), the total integrated area of the footprint of area B (Fig. 4.6B) is smaller than that of area A. Despite the different size of the footprint, the shape is similar to the one from the area A, with the majority of evaporation ending up on the slopes of the Himalaya's and on the Tibetan plateau and out of the Ganges river basin (see section 4.4.3)

Figure 4.6C shows the difference between the footprints of the two areas for MAM. So, this is the footprint of the difference of evaporation between the study areas. It shows that of the additional evaporation, the majority is transported towards the Tibetan plateau.

4.4.2 Description of the Atmospheric Water Path

The paths of the evaporated water through the atmosphere are different for the two focus areas. Fig. 4.7 shows the distribution of distances between evaporation and precipitation sites for evaporation from both areas for different times of the year. During all seasons, the majority of evaporation precipitates again within 3000km of the evaporation site. Distinct peaks are found at the distance from the evaporation sites where mountain ranges are located, these peaks might be slightly different for area A and B due to the different (around 200km) locations of these areas. During December-January-February (DJF), the water is transported furthest away, the third peak (precipitation falling in south-east Asia) is large and there is more precipitation falling at large distances (>3000km) than in the other seasons. The difference between the focus areas is minimal.

During MAM, the distribution shifts towards the shorter distances; more water is transported to the Himalaya's and precipitates there. Subsequently, during JJA, the flow direction has reversed compared to DJF and the majority of evaporation is transported towards the North and precipitates within 1500km. The tail of the distribution (>3000km) has much lower values than during the other seasons. During JJA, there is a difference between area A and B, with evaporation from area B being transported further away from its source location than the evaporation from area A, by a distance roughly equal to the distance between the two source areas relative to the mountains North of these. As the summer monsoon retreats, the atmospheric moisture transport

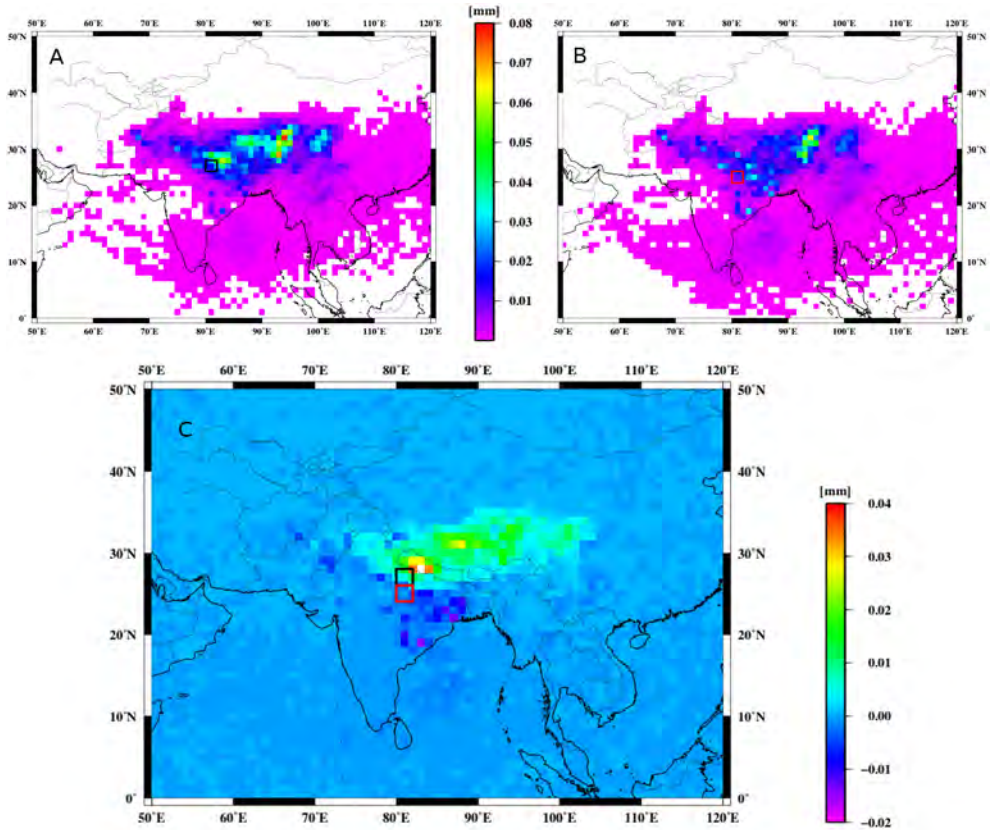


Figure 4.6: Footprints of areas in Figure 4.3.3 for MAM for 1990-2009, based on ERA-interim. Area A (A), area B (B) and difference between them (C). Units are millimeters of evaporation from the source area, so the areal sum is equal to the total MAM evaporation in the source region. In general, the difference between the footprint shows positive values, however there is an area on the southern side of area B where the values are negative values due to the different locations of the two focus areas. As area B is located south of area A (Fig. 4.3.3), evaporation originating there is more likely to be transported southward

lengths increase during September-October-November (SON). However, there is still the difference in transportation lengths between the two areas.

Fig. 4.8 shows the probability density functions for the atmospheric residence times for water evaporating from the focus areas. These residence times are determined by noting the time of evaporation of a water parcel and during each time step of the water trajectory an accounting of how much water precipitated out of the parcel at that timestep. The probability density functions shown in Fig. 4.8 is the weighted

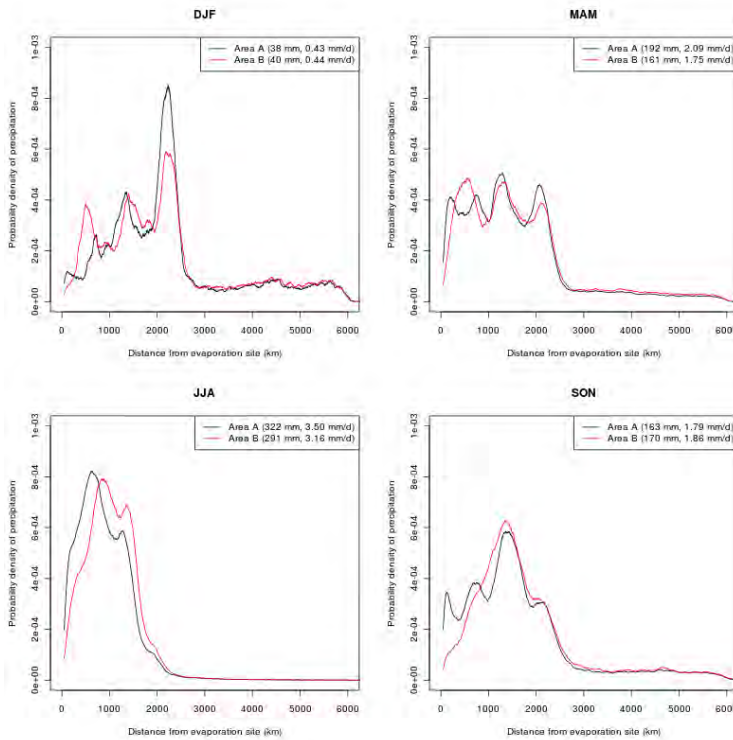


Figure 4.7: PDF's of distance between evaporation and precipitation locations for evaporation from areas A and B (see Fig 4.3.3), 1990-2009 mean for DJF, MAM, JJA and SON. Data is normalized to total evaporation from both areas. Daily and seasonal sum of evaporation for both sites is indicated in the legend.

sum over all parcel released from the areas over a given period.

For DJF, the residence times do not differ between. The distribution is skewed towards lower residence times, with a peak at about 5 days and is slowly declining towards longer residence times. During MAM, the atmospheric residence time distributions for evaporation from both areas show a more pronounced peak at about 4 days. Evaporation from area A has slightly lower residence times than from area B, a part of which might again be explained by the different locations of the areas. JJA shows broader peaks, but the difference in residence times is larger than during any other season. Evaporation from area A shows a peak at residence times of 3 days, while that from area B has a peak at about 6 days. These differences in residence times for JJA correspond to the differences in distances travelled by the parcels (Fig. 4.7), but cannot be explained by the small differences between the starting locations of the parcels.

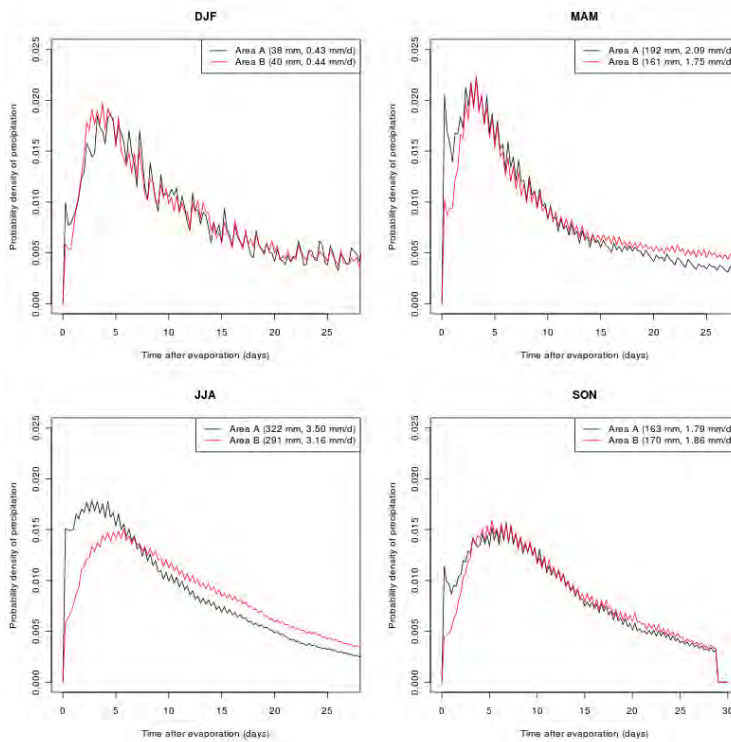


Figure 4.8: PDF's of atmospheric residence times for evaporation from areas A and B (see Fig 4.3.3), 1990-2009 mean for DJF, MAM, JJA and SON. Data is normalized to total evaporation from both areas. Daily and seasonal sum of evaporation for both sites is indicated in the legend.

During the retreating phase of the summer monsoon, the difference in residence times between the evaporation from the two areas decreases. However, the residence times for parcels from area A are still a bit lower than those from area B. As the southerly monsoon flows disappear or become weaker, the residence times increase again.

4.4.3 Basin recycling

The downwind footprints of evaporation from both areas (Fig. 4.6A and 4.6B) show the spatial distribution of precipitation due to evaporation. In addition to these full spatial distributions, it is relevant to determine which fraction of evaporation ends up as precipitation within the Ganges basin. This basin recycling of evaporation shows the potential importance of the land surface as a source of precipitation in the river basin, as well as the potential to re-use evaporated water within the basin.

The lower two curves in Fig. 4.5 (green and blue curves) show the yearly cycle of the amount of evaporated water that precipitates again within the Ganges basin for the areas A and B. During the (boreal) winter monsoon (NDJF), the atmosphere is so dry that only very little precipitation occurs and practically all the evaporation is transported out of the river basin area. During MAM, the prevailing wind direction becomes southerly and some pre-monsoon precipitation occurs. Therefore, basin recycling ratios increase and about 30% of the evaporation is recycled. The recycling peaks at about 40% during June/July and falls again after August, when the summer monsoon flow weakens.

Throughout the year, the basin recycling rates are similar for both areas. However, during MAM, when evaporation from area A is higher, the basin recycled water is also higher. A large fraction (of up to 70-80%) of the additional evaporation in area A (compared to area B) recycles within the river basin. This means that from the additional evaporation, a large fraction can potentially be reused within the river basin.

The annual cycle of basin recycling shown in Fig. 4.5 only shows the basin recycling rates for the two focus areas. Figure 4.9 shows the fraction of evaporation that ends up in the Ganges basin for the Indian sub-continent for February and June. Again, during the dry winter monsoon Fig. 4.9B, recycling ratios are below 10%. Due to the northerly flow, the transportation of evaporation from the ocean to the Ganges basin is almost non-existent, and some (only around 5%) of the evaporation from Pakistan and the Indus valley is transported to the Ganges basin and precipitates there. During the wet summer monsoon Fig. 4.9A, the prevailing south/south-westerly flow transports evaporation from the Arabian sea and the Bay of Bengal to the Ganges basin. Within the Ganges basin, the recycling ratios are fairly constant at around 50-60%.

4.4.4 Importance for Precipitation

The expression of moisture recycling as part of the evaporation is useful to determine which fraction of the local water sources (the evaporation) can potentially be re-used. However, it is also useful to determine basin recycling as part of the precipitation to assess how important the local recycling is compared to other parts of the water balance, such as precipitation originating from advected moisture. Figure 4.10 and 4.11 show the mean annual cycle of moisture recycling within the Ganges basin as fraction of the total precipitation and in absolute terms, respectively. In Fig. 4.10, the evaporation recycling is shown for moisture evaporating from the fraction of the basin with irrigation intensity lower than the basin median irrigation (about 8% for the Ganges (35% for the Indus)), labeled 'non-irrigated' and for moisture evaporating from the fraction of the basin with irrigation intensity higher than the median (labeled

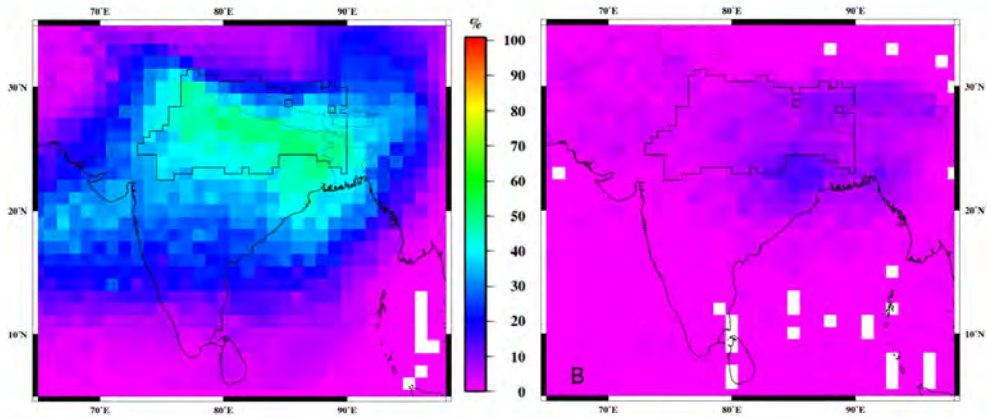


Figure 4.9: Fraction of June (A) and February (B) evaporation that precipitates in the Ganges basin (indicated with the black contour) for 1990-2009, based on ERA-interim.

'irrigated').

During the northerly winter monsoon (DJF), recycling ratios are low; the (little)

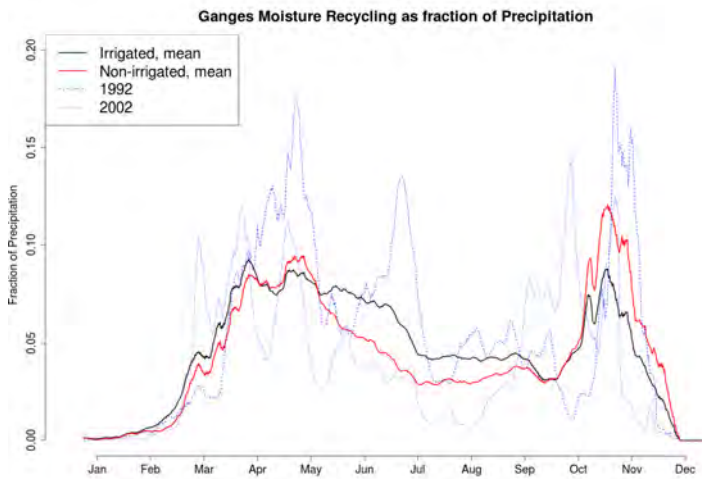


Figure 4.10: Relative importance of evaporation recycling compared to total precipitation in the Ganges basin, annual mean cycle for 1990-2009 for irrigated and non-irrigated parts of the basin and basin mean for two extreme years.

precipitation in the Ganges ($< 1\text{mm/day}$) basin is advected into the area. As seen in section 4.4.3, moisture recycling increases during MAM, and represents about 9% of the precipitation. During the peak of the summer monsoon (JJA), the fraction of

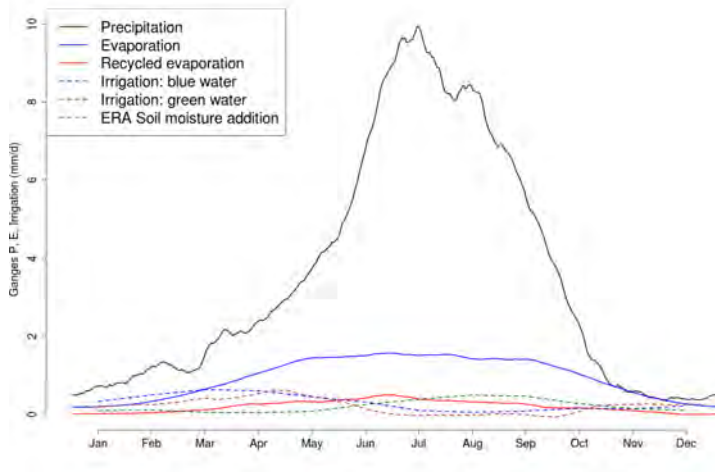


Figure 4.11: Yearly cycle of the Ganges atmospheric water budget terms (P , E , recycled E and soil moisture analysis increment) and irrigation amount (irrigation from blue and green water), for 1990-2009, based on ERA-interim and GCMW data.

recycled evaporation is still high, but a lot of moisture is advected from the Indian ocean, resulting in the monsoon rains. Due to this large influx of moisture into the basin, the fraction of precipitation that originates from within the basin reduces to about 5%. After the summer monsoon, the contribution of local moisture sources to precipitation increases again to 10%, primarily because the moisture influx and precipitation decrease. Figure 4.11 confirms that the decrease in relative importance of evaporation recycling during the monsoon months is dominated by the increase in precipitation, which increases from around 3 mm/day in May to about 8-9 mm/day in June/July. In this period, the recycled evaporation increases more modestly from about 0.3 to 0.5 mm/day.

The difference between irrigated and non-irrigated evaporation recycling in Fig. 4.10 is negligible until April. From May until September, the contribution of evaporation from irrigated areas to the total precipitation is about 2% higher than that from non-irrigated areas. During the retreating phase of the summer monsoon (October-November), recycling from non-irrigated areas has a (2%) larger contribution to total precipitation. However, an uncertainty of this analysis is that the irrigated and non-irrigated areas are not in the same locations. For every location, recycling ratios are dependent on the evaporation rate, but also on prevailing wind patterns. Therefore, throughout the year, differences in recycling ratios can occur due to wind patterns that favor moisture recycling more in irrigated than in non-irrigated areas, or vice versa.

The fraction of precipitation that is recycled within the Ganges river basin can be compared to those of other areas in the Indian subcontinent. Tables 4.1, 4.2 and 4.3 show different parts of the seasonal atmospheric water balance for the Indus river basin, the Ganges river basin and the area in India south of the Ganges and Indus basins, respectively. For the Indus basin (table 4.1), both evaporation and precipitation are lower than in the Ganges basin, especially during JJA. Moisture recycling as part of precipitation does not show a peak during MAM, but only during SON. This difference in moisture recycling in MAM between the Indus and the Ganges is due to the southwesterly winds during this time of year. This flow will export evaporation from the (north-south oriented) Indus basin, whereas it will export less evaporation from the Ganges basin, which is more east-west oriented. For the Indus basin, the annual mean evaporation is about 5.5% of precipitation.

	P	E	E_{rec}	E_{rec}/E	E_{rec}/P
DJF	1.4 (126)	0.1 (90)	0.02 (1.8)	18%	1.3%
MAM	1.63 (150)	0.53 (49)	0.07 (6.5)	12%	4%
JJA	2.74 (252)	0.96 (88)	0.2 (18)	21%	7%
SON	0.8 (73)	0.28 (25)	0.08 (7.3)	29%	10%

Table 4.1: Atmospheric water balance over the Indus river during different seasons, mean over 1990-2009. Units are in mm/d and the sum over the period is given in mm (in brackets), the relative columns are given in percentages. The first columns represent precipitation (P), evaporation (E), evaporation that recycles within the area (E_{rec}), the last two columns represent the recycling relative to the precipitation and evaporation.

	P	E	E_{rec}	E_{rec}/E	E_{rec}/P
DJF	0.75 (67)	0.26 (23)	0.014 (1.3)	5%	1.8%
MAM	2.55 (235)	1.03 (95)	0.21 (19)	20%	8%
JJA	8.02 (738)	1.50 (138)	0.52 (48)	35%	7%
SON	2.59 (236)	0.95 (86)	0.25 (23)	26%	9%

Table 4.2: Same as table 4.1, for the water balance over the Ganges river basin.

The absolute moisture recycling in the area in India south of the Indus and Ganges rivers shows a peak during JJA. However, due to limited precipitation and excess evaporation, the moisture recycling as part of precipitation is largest during MAM. For the land area in India south of the Ganges and Indus, the annual mean recycling of evaporation is 9% of precipitation.

	P (mm/d)	E (mm/d)	E_{rec} (mm/d)	E_{rec}/E	E_{rec}/P
DJF	0.33 (29.7)	0.70 (63)	0.045 (4)	6%	14%
MAM	0.51 (47)	1.08 (99)	0.13 (12)	12%	26%
JJA	4.46 (410)	1.53 (141)	0.29 (27)	19%	6%
SON	1.90 (173)	1.13 (103)	0.18 (16)	16%	9%

Table 4.3: Same as table 4.1, for the water balance over the land area in India south of the Ganges and Indus.

4.4.5 Temporal Variability of Recycling

Apart from the mean climatological recycling rates, Fig. 4.10 shows the years with minimal (2002) and maximal (1992) basin moisture recycling (averaged over both irrigated and non-irrigated areas). The inter-annual range of the importance of moisture recycling for the total precipitation is about 2% of precipitation. This inter-annual variation basin moisture recycling ($E * rr/P$, in which rr is the fraction of E that recycles) is mostly due to variations in recycling ratio (rr) and precipitation (P), which have coefficients of variation ($sd/|mean|$) of 0.15 and 0.11, respectively. The variation in evaporation (E) is smaller, the coefficient of variation is 0.02.

The annual mean (over 1990-2009) recycling ratios are 4.6% and 4.3% for the irrigated and non-irrigated part of the basin respectively. In 1992, the year with the highest recycling ratios, these were 6.5% and 5.3%, while in 2002, the year with lowest recycling ratios, these were 3.9% and 3.3%.

Figure 4.10 shows that the timescales over which the recycling ratios change is in the order of months. This suggests the recycling ratio is dominated by processes with timescales of this order, for example the large scale wind patterns and monsoon flow and not so much by processes of longer timescales, such as ocean temperatures.

4.5 Discussion

4.5.1 Reflections on Methodology

This study applies a moisture tracking method (similar to the QIBT, Dirmeyer and Brubaker (2007)) to water evaporating from the Ganges basin. The method used has the advantage that it can be used as post-processing to the atmospheric model. Therefore, it can be applied to reanalysis data. It has the advantage that the non-linear advection terms, which are neglected in bulk methods, are incorporated. However, the water cycle would be diagnosed best using tracers in atmospheric models. These are computationally expensive to run, especially for the time periods assessed in this study. It is unknown how much better an atmospheric model with tracers would describe the water cycle than the QIBT. Therefore, in this study the QIBT method

is used and the advantage of processing speed is used to calculate the entire ERA-interim dataset time period to get an impression of the climatology of recycling.

Using the reanalysis data has disadvantages. Estimates of precipitation and especially evaporation are based on sparse local measurements and satellite data and can have large errors. The errors in precipitation are larger over the oceans than over land, as more measurements are available over land. Bosilovich et al. (2011) found differences in ERA-interim precipitation (for 1990-2001) with GPCP (version 2.1) precipitation of up to 0.5 mm/day for the Ganges basin. There are less measurements of evaporation, so errors in evaporation are probably higher than the errors in precipitation. Trenberth et al. (2011) analysed the moisture and energy budgets in reanalysis data. They derived annual mean E-P using the atmospheric water budget and found slightly positive values for (2002-2008) for India in ERA-interim, while these values were negative in the MERRA reanalysis. In the current study, the annual mean of E-P was derived from the model evaporation and precipitation and it shows negative values for the majority of India's land surface for 1990-2009 from ERA-interim. In principle it is not possible for land surface to have positive E-P values (more evaporation than precipitation), unless some moisture source (for example ground water or inflow from upstream rivers) is present. As there are no large scale evaporation measurement data to verify the reanalysis evaporation, it is hard to quantify the errors.

For the methodology used in the current study, any errors in evaporation and precipitation affect the paths of the water parcel and the moisture allocation along this path. During the path of a parcel, the evaporation from the surface into the parcel is the evaporation divided by the total precipitable water (see equations 4.1 and 4.2). If more water evaporates into the parcel, the ratio of tracked water to total precipitable water decreases, consequently the distance between evaporation and precipitation location increases. As the evaporating during a time step is usually much smaller than the total precipitable water, the error in evaporation is small compared to the total precipitable water. Therefore, the paths of water tracked in this study are mostly determined by the spatial variations in precipitation, which are much larger than the spatial variations in evaporation due to the effects of orography.

Another drawback of using the reanalysis data is their violation of the water budget. As the reanalysis products are nudged towards atmospheric state variables, the moisture budgets include an analysis term (and do not close). In the method used here, the fraction of moisture precipitating out of the parcel depends on the total precipitable water. We do not separate the analysis term and the model term in the precipitable water, which might be a violation of the water balance. Over the Ganges basin, the annual sum of the analysis term of the total atmospheric column water (acquired by subtracting the previous 12-hour forecast of total atmospheric column water for the time of the analysis from the total atmospheric column water from the analysis) is -0.005 times the annual sum of total atmospheric column water. So, about

0.5% of the moisture is removed from the atmosphere annually due to the analysis term. However, for the moisture tracking method, it is more relevant to consider the analysis term per time step. For the 12-hourly time series, the average analysis term is -0.02 times the total atmospheric column water, with a standard deviation of 0.11 times this total column water. The total column water is used to determine how much of the tracked moisture precipitates at a given location and time. Therefore, these analysis terms change the footprints of evaporation (Fig. 4.6). How much the analysis terms influence basin recycling depends on the shape of the basin and time of year, but a 2% error in the footprints is probably small compared to the error made by the vertical mixing assumptions of the method.

The vertical resolution of the input data is also a cause for uncertainty. The representation of the moisture and wind profiles (especially near the surface and near steep orography) is crucial for the method used. Therefore, using input data on model levels with higher vertical resolution (either from reanalysis or GCMs) could improve the analysis. When lower vertical resolution data used in this study, the parcels will be more likely to be transported out of the lower wind speeds at the surface, compared to when higher resolution data had been used. Therefore, the water parcels will be transported faster away from the evaporation location when low vertical resolution data is used.

Finally, the representation in the reanalysis data of the water cycle in the steep mountain areas of the nearby Himalaya slopes is probably not optimal due to a lack of measurements and the representation of the mountains in the model. Moreover, the water tracking model may have trouble correctly allocating water when moisture convergence is very high.

4.5.2 Implication for Water Budget

The atmospheric paths of evaporation that have been determined measure the size of the water cycle and the fraction of moisture that recycles within an area close to the evaporation site. Obviously, these paths of evaporated water are affected by two factors: the dominant wind patterns determine the direction of transport and the precipitation patterns determine the chance that the evaporated moisture rains out again, the end point of the path. This research shows that moisture recycling within the river basin in India is determined by the annual cycle of winter and summer monsoons and ranges from 0 to 10% of precipitation. On top of this annual variation, moisture recycling is determined by the actual wind patterns, resulting in fluctuations of about 5% of precipitation on the monthly timescale (see moisture recycling for individual years in Fig. 4.10). This time scale of variation indicates that if moisture recycling is determined using budget methods, longer than monthly timescales need to be used to represent this variation.

Moreover, as wind and precipitation patterns (and relative location of orography) are different for different locations, the determination of footprints of the two focus areas (Fig. 4.6A and 4.6B) might lead to differences due to different locations. A solution to this problem is performing the same analysis on output of atmospheric models, once with explicit irrigation and once without it. This will be part of future research in which we will apply the same moisture tracking scheme to the output of five RCMs for the Indian sub-continent, for runs with and without explicit irrigation.

By determining the recycling ratio over river basins, this study links the atmospheric part of the water cycle to large scale hydrology and the land surface part of the water cycle. By doing so, recycling ratios over areas with different sizes and shapes are compared, which makes comparisons with other moisture recycling studies harder. Moreover, Fig. 4.7 shows that the relation between moisture recycling and length scale does not fit the proposed power law (eq. 4.4) very well for the Ganges basin. This is of course primarily due to the extreme orography of the Himalayas, limiting the flow northwards. However, Fig. 4.7 also shows the signature of other locations of precipitation peaks. Therefore, eq. 4.4 should be applied carefully and location of major orographic features or other features inducing precipitation maxima should be taken into account.

Furthermore, from a water availability perspective, high river basin moisture recycling rates are good for water resources within the river basin. Overall, it might be more beneficial when water is exported from a river basin to an area where the water demand is higher than from the exporting river basin. This can be determined by comparing the water footprints from this study with water demands from an integrated assessment water resources model, which is beyond the scope of the current study.

4.5.3 Role of Irrigation

Although large scale irrigation (Fig. 4.3.3) is not explicitly included in the ERA interim reanalysis, its effects are indirectly included through data assimilation. This assimilated data is under the influence of large scale irrigation through its effects in lowering temperature and increasing humidities near the earth surface. The assimilation model tries to correct near surface temperature and humidity biases by nudging the soil moisture.

To estimate the amount of moisture added or subtracted due to data assimilation, the drift of the ERA interim model with respect to the observations is determined. The analyzed soil moisture is compared to the previous 12-hour forecast valid for the same moment as the analysis. The difference between the two is the data assimilation increment. Figure 4.12 shows the average increment of the soil layer (0-288cm) moisture (in *mm/day*) over the 1990-2009 period. A comparison with Fig. 4.3.3 shows

that in the reanalysis moisture is indeed added to the soil at places where irrigation is present. Although this assimilated soil moisture addition is probably not equal to the actual irrigation amount (because the procedure assumes all the T_{2m} and q_{2m} errors are due to soil moisture only, which is unlikely), Figure 4.12 does confirm that some effects of irrigation are indirectly included.

Figure 4.11 shows the annual cycle of irrigation in the Ganges basin based on the

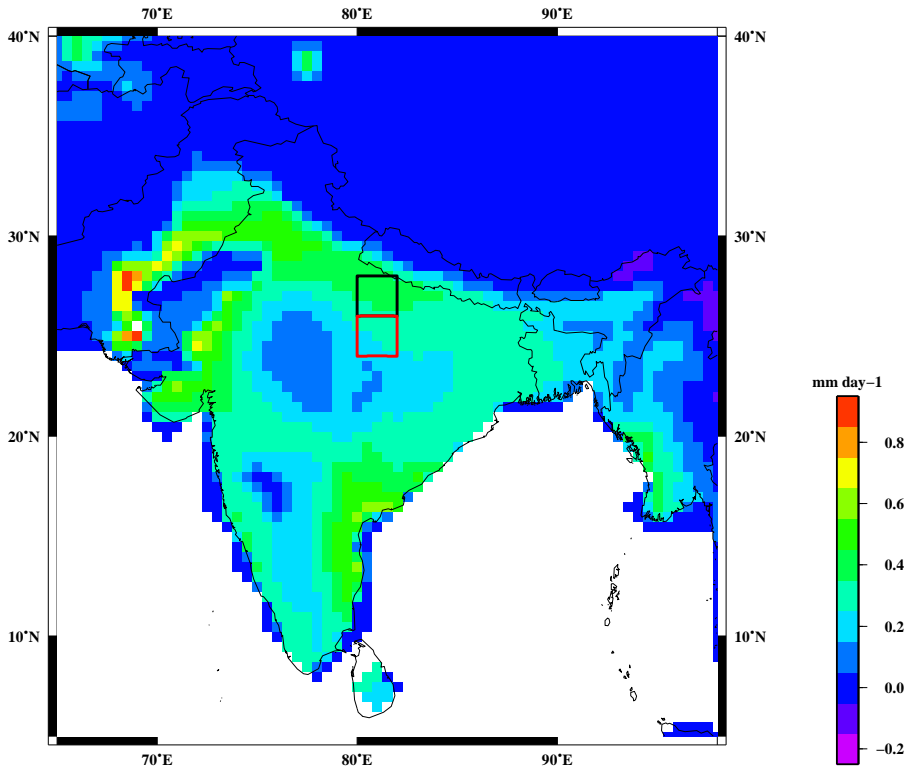


Figure 4.12: Analysis increment of the ERA interim soil moisture layers 1-4 (0-288cm depth). In the ERA interim reanalysis system, every twelve hours, the model forecast is compared to observations and the state variables of the model is changed to better reflect these observations. This change is the analysis term and the average daily value (mm/day) is plotted.

Siebert and Döll (2010) dataset, which is valid around the year 2000. The irrigation amount is divided in a green water use (use of soil water) and blue water use (use of surface water and that from aquifers). The annual mean cycle of ERA interim soil moisture analysis increment shows a similar cycle as the irrigation of blue water use

(also displayed in Fig. 4.11). Despite the indirect inclusion of irrigation effects, using the ERA-interim data is a first attempt to estimate the influence of different land uses on moisture recycling. The differences in MAM evaporation between areas A and B shown in Figure 4.5 are likely to be caused by differences in irrigation intensity in those areas shown in Figure 4.3.3, while they are unlikely to be caused by different amounts of precipitation. However, should these differences have occurred from other causes than the differences in irrigation, the first part of the current study provides information about the amount of additional evaporation that will be recycled in the Ganges river basin (the basin recycling rate of the marginal evaporation) and the second part of the study on the importance of different parts of the Ganges basin to the basin moisture recycling.

4.6 Conclusion

This work studied the atmospheric part of the water cycle for the Ganges basin in India, and how areas with different evaporation regimes contribute to this part of the water cycle. Two study areas with different hydro-meteorological regimes were studied. The monsoon dynamics dominate the fate of evaporated water, as with other aspects of the Indian climate. During the winter monsoon, any moisture evaporating from the land surface is transported southwards, away from the continent. It is essentially a loss for local water resources. During this time of the year (DJF), there is no difference between the fate of moisture evaporating from the study areas.

During the pre-summer monsoon period (MAM), the evaporation difference between the study areas was about 1 mm/day. During this time of year, the winds reverse and moisture is not transported as far away as during DJF. The fraction of evaporation that falls again as precipitation in the Ganges basin is about 0.3. However, of the additional evaporation in the study area with the highest evaporation, about 60-70% recycles within the Ganges basin.

During the summer monsoon (JJA), dominant flows are from the south and the distance the moisture travels through the atmosphere are minimal. The fraction of evaporation that recycles in the river basin is about 50-60%. When the summer monsoon retreats, the recycling ratios decrease again. Apart from the basin recycling ratios, the distance between evaporation and precipitation location is smaller for the study area with higher evaporation than for the area with lower evaporation. This could be caused by the triggering of convection by moister land surfaces and an increase in local precipitation as a consequence. By this process, the excess evaporation might be more likely to be incorporated in convective systems and precipitation.

The importance of within basin moisture recycling for precipitation shows an annual cycle as well. An annual average of about 4.5% of precipitation originates from water evaporating in the Ganges basin. During the winter monsoon, any precipitation

originates from sources outside the basin. During MAM, the contribution of recycled water to precipitation peaks at about 10%. Then, the large influx of moisture from the Indian ocean dominates the precipitation during the summer monsoon season and recycling is 5% of precipitation. After the monsoon season (Oct-Nov), local sources peak again at 10%, after which recycling reduces again.

Based on this analysis, the most irrigated parts of the Ganges basin have the largest effect on the atmospheric part of the water cycle during May to September. During this period, recycling originating from those areas contributes about 2% more precipitation than recycling from non-irrigated areas.

Although the ERA-interim dataset used does not include irrigation explicitly, the ERA-interim assimilation system adds moisture to the soil in locations and times of the year similar to actual irrigation application as documented in independent datasets. Therefore, it is hypothesized that the differences in evaporation studied might be caused by different irrigation regimes, which will be subject of future studies using explicitly modelled irrigation.

Chapter 5

Effects of Irrigation in India on the Atmospheric Water Budget

Abstract

The effect of large scale irrigation in India on the moisture budget of the atmosphere was investigated using three regional climate models and one global climate model which all performed an irrigated run and a natural run without irrigation. Using a common irrigation map, year round irrigation was represented by adding water to the soil moisture to keep it at 90% of the maximum soil moisture storage capacity, regardless of water availability.

For two focus regions, the seasonal cycle of irrigation matched that of the reference dataset, but irrigation application varied between the models by up to 0.8 mm/day. Due to the irrigation, evaporation increased in all models, but precipitation decreased due to a strong decrease in atmospheric moisture convergence.

A moisture tracking scheme was used to track individual evaporated moisture parcels through the atmosphere to determine where these lead to precipitation. Up to 35% of the evaporation moisture from the Ganges basin is recycling within the river basin. However due to a decreased moisture convergence into the river basin, the total amount of precipitation in the Ganges basin decreases.

Although a significant fraction of the evaporation moisture recycles within the river basin, the changes in large scale wind patterns due to irrigation shift the precipitation from the eastern parts of India and Nepal to the northern and western parts of India and Pakistan. In these areas where precipitation increases, the relative precipitation

increase is larger than the relative decrease in the areas where precipitation decreases. We conclude firstly, that the direct effects of irrigation on precipitation are small, and are not uniform across the models. Secondly, that a fraction of up to 35% of any marginal evaporation increase (for example due to irrigation) will recycle within the river basin. And, thirdly, that when irrigation is applied on a large scale, the dominant effect will be a change in large scale atmospheric flow that decreases precipitation in east India and increases it in west- and north India.

5.1 Introduction

To meet the growing demand for food from India's growing population, agricultural intensity and consequential irrigation have increased in India during the last century. Water has been channeled from the rivers, or pumped up from the ground to supply crops with irrigation water. Moreover, dams have been constructed to manage water supply for agriculture as well as for human consumption. The purpose of the current study is to determine the atmospheric effects of this large scale irrigation in India.

The effects of the large scale land use changes in India on the atmosphere and especially precipitation have been subject of numerous studies. Generally, the increased moisture available at the land surface is thought to result in two opposing atmospheric effects. On the one hand, the increased moisture influx into the atmosphere may increase the moist static energy of the atmosphere and subsequently the chances of convective precipitation. On the other hand, when the land surface wetness increases, the temperature contrast between the land and the sea, which drive the monsoon circulation, may decrease. When the monsoon flow decreases, less oceanic moisture is advected to the land and precipitation might reduce.

Koster et al. (2004) and Guo et al. (2006) conducted an experiment with global climate models to determine the role of the land surface in the climate. They located a hotspot of land-atmosphere coupling in India both for temperature and precipitation, although there was a significant spread among the models. Douville et al. (2001) simulated the Asian summer monsoon and found a precipitation shift from east to north India with increasing soil moisture.

Several studies specifically included irrigation into atmospheric models. Douglas et al. (2009) found for a single precipitation event that irrigation can influence the regional climate by increasing the surface moisture flux, decreasing temperature and changing regional circulations and precipitation patterns. Lohar and Pal (1995) used two-dimensional atmospheric simulations to relate a decreased precipitation between 1973-1992 in West-Bengal to an increased irrigation amount, arguing that a decreased sea-breeze can reduce precipitation. Saeed et al. (2009) found an increased precipitation in northern India due to irrigation using a regional climate model for three years,

while Niyogi et al. (2010) statistically related a decrease in precipitation in northern India to the increased irrigation amount.

Several studies suggest a decrease in monsoon flow due to a decreased land-sea contrast, Lee et al. (2009) analyzed the interannual differences in land-surface greenness (NDVI) and found that the monsoon-related precipitation (JJA) was weaker in years with more vegetation during the pre-monsoon season (MAM).

Dirmeyer et al. (2009) performed an integrated analysis of soil moisture memory, evaporation and atmospheric moisture recycling and noticed that during India's pre- and post-monsoon periods (MAM and SON), precipitation is most sensitive to soil moisture. Tuinenburg et al. (2011) used a single column atmospheric model to classify the atmospheric situations during which soil moisture has an influence on precipitation triggering using a methodology developed by Findell and Eltahir (2003a). The analysis of Tuinenburg et al. (2011) showed that during the monsoon onset and retreat seasons (MAM and SON), the atmospheric conditions allowed a positive influence of soil moisture on precipitation, while during the winter season (DJF) the atmosphere is too dry and during the summer season (JJA) too wet for an influence of the land surface.

Tuinenburg et al. (2012b) analyzed two reanalysis datasets using several land-atmosphere indicators and found a strong land-atmosphere coupling in India during the summer half year. The increase in surface wetness can lead to an increase in precipitation of 1 mm/day in north-western India, while it results in a decrease in precipitation of 0.5 mm/day in east India.

Apart from the atmospheric effects of irrigation, the hydrological effects have been studied within the EU-project WATCH, using large scale hydrological models (Haddeland et al., 2011). In a global study on the effect of irrigation and dams on river discharge, Biemans et al. (2011) found the largest effects of irrigation in Asia with a discharge reduction of up to 5%, whereas the cumulative effects of dams and irrigation showed a 10% discharge reduction.

The large scale hydrological models used by Haddeland et al. (2011) and Biemans et al. (2011) were not coupled to a GCM but driven by meteorological forcing. Thus, feedbacks between irrigation and the atmospheric water budget could not be taken into account. However, on the river basin scale, the amount of moisture that is recycled within the Ganges basin varies from 5% during DJF to 60% during JJA and can differ between areas with different evaporation regimes, such as irrigated and non-irrigated areas (Tuinenburg et al., 2012a). Therefore, the current research studies the effects of irrigation on the atmospheric water budget, using four climate models forced with natural land surface conditions and with irrigated land surface conditions. We pose the following research questions:

- What is the atmospheric response to irrigation in India?

- Is additional precipitation triggered at the irrigation location?
- How much moisture is exported from the river basin?
- Are large scale moisture flow patterns affected?

This paper is structured as follows. Section 5.2 describes the models, data and approach of the study. Section 5.3 presents the results, with subsections on the local effects in two focus regions, the fate of the evaporation from the focus regions, the Ganges river basin moisture budget and the large scale effects of irrigation. Section 5.4 presents the discussion and conclusions.

5.2 Methods

In the current study, the atmospheric effects of irrigation in India are compared using four atmospheric models (RAMS, HadCLM, ECHAM and HIRHAM) with explicit irrigation application. As a basis for irrigation, the global map of irrigated areas (Siebert et al. (2005)) is used in each. With each atmospheric model, two runs are done; one with natural conditions and one with irrigation. Both runs were performed for at least the period 1990-2000. In the natural run, the land surface moisture is allowed to evolve freely, whereas in the irrigated run, the soil moisture in the top soil layer is year round not allowed to fall below 90% of the maximum soil moisture storage capacity in irrigated areas. This approach ensures that irrigation is treated the same way in all land surface schemes.

The results of the atmospheric model simulations are compared in three ways: (1) from a local to sub-regional perspective the effects of irrigation on local variables (evaporation, (local) precipitation, etc.) are compared. (2) From a non-local perspective, the evaporation from irrigated areas is tracked through the atmosphere and the downwind 'precipitation footprint' of irrigation is determined. (3) From a regional scale, the effects on large scale circulation and monsoon flow are assessed. From the first perspective, the atmospheric effects of irrigation relevant to the local water resources are determined, while the second perspective focuses on the effects on water resources on the river basin scale. The last perspective focuses on the large scale changes in evaporation and precipitation. The moisture tracking model used in the second perspective requires three-dimensional input from the atmospheric models. This was not available for the HadRM3 model, it is therefore only executed for the other models.

This section will discuss the atmospheric models (subsection 5.2.1), the moisture tracking scheme (subsection 5.2.2), the study areas and variables compared (subsection 5.2.3) and the datasets used (subsection 5.2.4).

5.2.1 Climate Models

The four climate models used in this study are summarized in table 5.1 and described below.

Table 5.1: Summary of model characteristics.

	HIRHAM5	ECHAM	HadRM3	RAMS
Non-Hydrostatic	No	No	No	Yes
Horizontal Resolution	0.5 deg.	T63 (1.875 deg.)	0.44 deg.	44 km
Vertical Levels	19	31	19	34
Land surface scheme	rainfall-runoff scheme (Dumenil and Todini (1992))	JSBACH (Radatz et al., 2007)	MOSES (Cox et al. (1999))	LEAF2 (Walko et al. (2000))
Convection scheme	Mass flux (Tiedtke (1989), Nordeng (1994))	Mass flux (Tiedtke (1989), Nordeng (1994))	Mass flux (Gregory and Rowntree (1990))	Modified Kuo Convection scheme (Tremback (1990))
Domain	60E-100E, 4.125N-40.125N	global	53.6E-105.6E, 1.12N-37.2N	57.0E-104.5E, 3.8N-37.2N

HIRHAM5 (DMI)

The regional climate (RCM) model used in this study is HIRHAM5 (Christensen et al., 2006), which is a hydrostatic RCM developed at the Danish Meteorological Institute. It is based on the HIRLAM7 dynamics (Eerola, 2006) and the ECHAM5 physics (Roeckner et al., 2003) using the Tiedtke (1989) mass flux convection scheme, with modification after Nordeng (1994), and the Sundquist (1978) microphysics. The land surface scheme is unmodified from that used in the ECHAM5 model Roeckner et al. (2003), which employs the rainfall-runoff scheme described in the work of Dumenil and Todini (1992). Vegetation is not characterized as PFT and no tiling of different vegetation types in a grid box is modelled. Instead, grid boxes exhibit uniform vegetation with prescribed LAI dynamics. When the irrigated fractional area of a grid cell is above 20%, irrigation is applied. There is no seasonal variability in irrigation. More details on HIRHAM5 as used here are available in Lucas-Picher et al. (2011).

ECHAM/JSBACH (MPI)

In contrast to the other models used in this study, ECHAM5 (Roeckner et al., 2003) is a coarse scale global circulation model. It was applied for the time period 1978–1999

at a horizontal resolution of T63 (about 1.9°) with 31 vertical layers and a 10 minutes time step. The first 2 years are used for spin-up and disregarded in the analysis. ECHAM5 was interactively coupled to the land surface scheme JSBACH (Raddatz et al., 2007), while the ocean was substituted by a fixed SST and SIC climatology. The parametrization of the land surface is based on the LSP2 data (Hagemann, 2002). JSBACH uses a tile approach to represent different land cover types within one grid cell. For this study, a dedicated irrigated crops tile with a distinct water balance was implemented into the model, with a fractional size according to Siebert et al. (2005).

HadRM3 (Hadley Centre)

HadRM3 is a regional version of the global HadAM3 atmosphere model (Pope et al., 2000) coupled to the MOSES II land surface scheme (Essery et al., 2003), which explicitly represents subgrid heterogeneity. Boundary conditions (including SSTs) were provided by a flux adjusted global HadCM3 simulation. The irrigation implementation consists of an additional (to five other vegetation type tiles) irrigated C3 grass surface tile. For this tile, the soil moisture stress factor is set below the critical soil moisture point, so evaporation is constrained by soil moisture. Any additional water demand from unstressed evaporation is the correspondingly the irrigation demand. Irrigation is simulated year round as demanded by soil moisture.

RAMS (WUR)

RAMS (version 6.1) is forced by the ERA-interim reanalysis data from the European Centre for Medium-Range Weather Forecasts (ECMWF) every six hours, with a relaxation time at the 5 edge grid cells (around 200 km) of 5400 seconds. Monthly sea surface temperatures have been extracted from the Met Office Hadley Centre's sea ice and sea surface temperature (SST) data set, HadISST1 (Rayner et al., 2003). The land use classes have been extracted from the USGS database (Loveland et al., 2000) with a resolution of around 1 km. Irrigation is implemented using the existing irrigated crop tile in the land surface scheme. If the soil moisture drops below 90% of field capacity, moisture is added to the top soil layer for this tile every timestep.

5.2.2 Moisture Tracking Scheme

To determine the location where the added irrigation moisture ends up after being evaporated and diverted out of the area, an atmospheric moisture tracking scheme is used. The moisture tracking scheme is based on the quasi-isentropic back-trajectory scheme by Dirmeyer and Brubaker (2007) and is the same as used in Tuinenburg et al. (2012a). As in Tuinenburg et al. (2012a) it is run in a forward mode, so it determines

trajectories from evaporation to precipitation, instead of vice versa.

The scheme uses the output of any of the atmospheric models to calculate trajectories of evaporated moisture through the atmosphere. For this, 3D fields of wind speeds (u, v, w) and specific humidity (q), as well as surface fields of evaporation and precipitation are needed. For each timestep and grid cell, an evaporated moisture (parcel) from that location is tracked. This is done ten times to get a statistical sample of the moisture trajectories that captures the variability. Both the starting location within the gridcell and the starting height of the parcel are determined randomly, but the starting height is weighted by the specific humidity profile. From the starting position, the parcel is tracked by interpolating the wind speeds in space and time to the current location and time of the parcel. Discrete timesteps of about 5 minutes are used to determine the next position of the parcel.

At the start of the trajectory, the fraction of moisture evaporated from the source location equals the evaporated water divided by the total precipitable water. However, at each subsequent position of the parcel, there is an amount of evaporation entering the parcel as well as an amount of precipitation leaving the parcel. The evaporation entering the parcel reduces the fraction of tracked moisture in the parcel, so as the parcel moves further away from its starting location, the amount of original water decreases. At each location, the precipitation out of the parcel that is allocated to the evaporation in the source area is the product of the precipitation and the fraction of original water present in the parcel. This process maps the evaporation to precipitation in locations downwind.

The moisture tracking scheme is applied to all models (except HadRM), for the entire domain, with parcels released every six hours. For more details about the scheme, see Tuinenburg et al. (2012a).

5.2.3 Irrigation, Regions and Variables

The global map of irrigated areas (Siebert et al., 2005) shows heavily irrigated areas in India (see Figure 5.1). This study will compare the effects of irrigation on atmospheric variables with the focus on two regions: the eastern Ganges (EG) and western Ganges (WG) regions (outlined in Figure 5.1).

For these regions, the model runs will be compared in terms of irrigation gift, evaporation, 2-meter temperature, precipitable water, precipitation and moisture convergence.

5.2.4 Data

The global map of irrigated areas (GMIA, Siebert et al. (2005)) is used as common irrigation map by the models. The MIRCA2000 dataset Portmann et al. (2010), which is based on the GMIA, describes the seasonal cycle in the irrigation amount for the

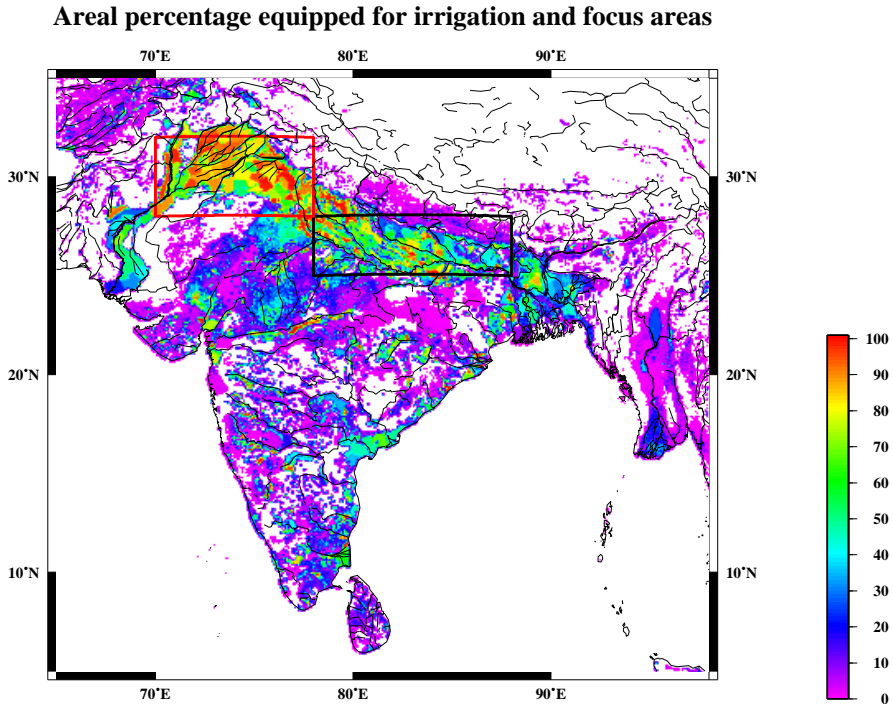


Figure 5.1: Location of eastern and western Ganges focus regions on the irrigation map (Siebert *et al.*, 2005)

situation around the year 2000. Based on this MIRCA2000 data, Siebert and Döll (2010) calculated green and blue water consumption per month using the Global Crop Water Model (GCMW). This is included as a quasi-observational reference.

Furthermore, ERA-interim is used to as boundary forcing for the RAMS and HIRHAM models, but also to compare the surface evaporation and precipitation, as well as atmospheric budgets. Surface temperatures are compared with the CRU 2.10 dataset Mitchell and Jones (2005). Precipitation is also compared to the Aphrodite (version 10) dataset Yatagai *et al.* (2009).

5.3 Results

Due to the strong annual monsoon signal, the interannual variability of the results is small. Therefore, this section presents the annual mean results over the 10 years of the simulation.

5.3.1 Irrigation Gift

The amount irrigation of irrigation that is applied in the irrigated run is not prescribed. Instead, the model soil is kept wet (at least at 90% of the maximum field capacity) and the evaporation is determined by atmospheric demand. The irrigation gift is defined as the total moisture that is added to the soil. Tables 5.2 and 5.3 show the atmospheric and surface variables from the irrigated and natural run for the east-Ganges and west-Ganges region per season, as well as some reference values from different datasets.

The first data column shows the irrigation gift, which has quite a range between

Table 5.2: *Spatial mean results (irrigation gift, evaporation (E), mean 2-meter temperature (T_{mean}), precipitation (P), moisture convergence (MC) and precipitable water (PW)) for the east Ganges focus region, per season. Units are mm/day, except for T_{mean} (K) and PW (mm). Reference values from datasets are given for irrigation, evaporation, temperature and precipitation.*

Model	Period	Irrigated						Natural				
		gift	E	T_{mean}	P	MC	PW	E	T_{mean}	P	MC	PW
ECHAM	MAM	0.55	2.02	301.0	0.84	-1.18	22.69	1.18	302.6	1.06	-0.12	22.15
	JJA	0.37	2.67	305.2	7.58	4.92	58.90	2.27	305.1	9.25	6.98	60.76
	SON	0.19	2.42	298.4	3.38	0.96	36.31	2.55	298.3	3.10	0.55	35.08
	DJF	0.22	1.21	288.7	0.41	-0.79	12.82	1.03	289.0	0.51	-0.52	11.71
HIRHAM	MAM	0.14	1.94	303.2	0.31	-1.63	24.83	1.01	305.0	0.24	-0.77	17.41
	JJA	0.12	2.47	306.7	7.77	5.30	56.56	1.75	307.1	8.76	7.00	54.96
	SON	0.08	2.67	298.5	2.58	-0.09	30.53	2.50	299.5	2.77	0.27	32.03
	DJF	0.11	1.26	290.1	0.37	-0.90	12.06	0.97	291.3	0.33	-0.64	11.67
RAMS	MAM	0.43	1.59	295.9	0.2	-1.39	23.15	0.59	296.6	0.1	-0.49	23.09
	JJA	0.41	2.51	293.1	8.42	5.91	51.21	2.26	293.5	8.71	6.45	51.19
	SON	0.33	1.26	292.6	2.02	0.76	27.05	1.08	293.0	1.68	0.60	27.04
	DJF	0.24	0.41	285.6	0.10	-0.31	12.79	0.38	285.7	0.09	-0.29	12.78
HadRM3	MAM	1.46	2.13	298.0	0.45	-1.68		0.50	300.8	0.33	-0.17	
	JJA	0.50	1.62	304.3	4.36	2.74		2.14	305.2	4.55	2.42	
	SON	0.54	2.88	292.6	0.97	-1.91		1.54	295.6	0.77	-0.77	
	DJF	0.59	1.09	280.8	0.37	-0.72		0.42	283.2	0.29	-0.13	
Dataset:		GCMW	ERA	CRU	APH							
	MAM	1.38	2.37	300.1	0.57							
	JJA	1.17	3.01	302.3	3.08							
	SON	0.93	2.73	297.7	0.84							
	DJF	0.71	0.89	289.2	0.48							

the models. The last four rows show the irrigation amounts according to the GCMW dataset (Siebert and Döll, 2010). This dataset cannot be used for comparison to the irrigation gifts in the models, because the GCMW data present actual irrigation estimates constrained by water availability, whereas the model gifts reflect maximum irrigation given the atmospheric demand. Therefore, they are only included as a ref-

Table 5.3: Same as table 5.2, but showing results for the west Ganges focus region.

Model	Period	Irrigated						Natural				
		gift	E	T_{mean}	P	MC	PW	E	T_{mean}	P	MC	PW
ECHAM	MAM	1.17	2.77	298.1	0.78	-1.99	20.19	0.79	301.2	0.45	-0.34	16.27
	JJA	1.52	3.34	308.1	0.85	-2.27	43.16	0.68	310.9	1.20	0.51	45.16
	SON	0.74	1.76	297.7	0.64	-1.49	21.90	0.64	299.8	0.61	-0.03	21.11
	DJF	0.24	0.86	285.4	0.91	0.06	10.91	0.31	287.0	0.66	0.35	9.38
HIRHAM	MAM	0.33	2.35	300.9	0.21	-2.15	24.31	0.45	304.0	0.15	-0.30	25.60
	JJA	0.34	2.81	309.3	1.22	-1.58	44.58	0.50	311.7	0.86	0.36	54.19
	SON	0.33	2.02	298.5	0.58	-1.43	22.23	0.61	301.7	0.56	-0.15	24.49
	DJF	0.33	0.90	287.5	0.58	-0.32	33.65	0.26	289.6	0.54	0.28	30.06
RAMS	MAM	0.81	1.64	296.6	1.04	-0.60	23.69	1.41	297.1	0.83	-0.58	23.67
	JJA	0.92	2.96	300.8	2.96	0	46.68	2.63	300.9	3.01	0.38	46.63
	SON	0.70	1.38	297.3	1.15	-0.23	26.38	1.10	297.8	0.92	-0.18	26.35
	DJF	0.33	0.76	287.1	1.13	0.37	15.01	0.70	287.2	1.12	0.42	15.01
HadRM3	MAM	1.01	2.30	298.4	1.53	-0.77		1.10	300.8	1.29	0.19	
	JJA	0.16	2.00	300.7	6.94	4.94		2.99	301.1	7.00	4.01	
	SON	0.07	2.36	292.7	3.19	0.83		2.58	293.7	3.12	0.55	
	DJF	0.30	1.43	282.6	0.52	-0.91		1.12	284.7	0.47	-0.65	
Dataset:		GCMW	ERA	CRU	APH							
	MAM	0.80	2.04	299.6	0.57							
	JJA	0.27	2.80	304.8	3.08							
	SON	0.17	1.78	297.9	0.84							
	DJF	0.54	0.55	287.6	0.48							

erence.

For the EG region, the model gifts all are much lower than the reference irrigation, except for the HadRM3 model, which has similar gifts during MAM and DJF, but underestimation during JJA and SON. This smaller irrigation gift compared to the GCMW data is probably due to the very moist atmosphere during the summer monsoon months (June-September) which reduces evaporative demand. This causes the model irrigation gift to be reduced, whereas this is not the case in the dataset.

For the WG region, the models gifts are closer to the GCMW data. There are some differences between the models. The HIRHAM5 model has almost no annual cycle while the others show a distinct seasonality. The ECHAM and RAMS models demand higher irrigation gifts, while the HadRM3 and HIRHAM5 models require lower gifts.

5.3.2 Local Effects of Irrigation

In the current study, the local effects of the applied irrigation are defined as the effects within the east-Ganges and west-Ganges focus regions. In the next two sections, the effects on model variables will be discussed for these two regions.

Eastern Ganges region

The effect of irrigation in the east Ganges region (first column in table 5.2) on the model variables is shown in the other columns in table 5.2. The most uniform effects of irrigation across the models are found for the surface variables. The additional moisture on the land surface provides cooling and reduces the mean surface temperature. All models show a decreased temperature, which is largest during MAM (1.6–1.8 K decrease). During the other seasons, the models differ stronger in terms of temperature decrease. Throughout all experiments conducted for this study, the irrigation always decreased the surface temperature with the sole exception of ECHAM5/JSBACH during JJA.

Another consequence of the increased soil moisture is a larger surface evaporation. However, this effect is not reproduced as uniformly by the models as the temperature response. During MAM, the increased evaporation is largest at up to 1 mm/day. During the monsoon season (JJA), there are differences across the models. While most models computed an increase (of between 0.2–0.7 mm/day) in evaporation, the HadRM3 model showed a 0.5 mm decrease in daily evaporation due to increased cloud cover and decreases incoming shortwave radiation. After the monsoon season (SON), the difference in evaporation is reduced to a small positive modulation of about 0.2 mm/day, with the exception of the ECHAM model, where this modulation becomes slightly negative.

This general increase in evaporation does not necessarily lead to higher precipitation rates within the east Ganges region. Most of the time, precipitation is lower in the irrigated model runs than in the natural model runs. In most cases, the strengthened evaporative influx from the land surface is compensated by a lower atmospheric moisture convergence. The amount of precipitable water generally increases slightly, but too little to compensate the decreased precipitation efficiency.

Western Ganges region

In the drier western Ganges region (table 5.3), the differences between the natural and irrigated runs are more pronounced than in the eastern Ganges region. The irrigation gift leads to a reduction of MAM surface temperatures that varies across the models from 1–4 K. During JJA, SON and DJF, the effect on temperature is less pronounced and varies between 0.1 and 2 K. Similar to the eastern Ganges region, irrigation always decreases the surface temperature.

Compared to eastern Ganges region, the evaporation response is much less uniform across the models and seasons. During MAM, all models show an increased evaporation ranging from 0.2–2 mm/day. However, during JJA, the HIRHAM5 and ECHAM model both increase evaporation by more than 2 mm/day, while the RAMS and HadRM3 model decrease evaporation by about 1 mm/day. During the post-monsoon

season of SON, the HadRM3 model continues to show a small negative evaporation anomaly while all other models compute an enhanced evaporation. During the winter season, all models show a small increase in evaporation.

Generally, precipitation increases in the irrigated run, compared to the natural run. In MAM, all models show an increase of about 0.1-0.3 mm/day, but the total amounts of precipitation vary distinctly. During JJA, the HIRHAM5 model shows an increase in precipitation (of 0.2 mm/day), while the other models have slight decreases. During SON and DJF, all models show a small increase of 0-0.2 mm/day.

5.3.3 Downwind Footprints of Evaporation

The moisture convergence into the eastern and western Ganges region decreases almost similarly in all models and seasons (see tables 5.2 and 5.3), meaning that more moisture is exported from the area via the atmosphere. In this section it will be investigated at which locations the exported moisture contributes to precipitation. The moisture tracking model described in section 5.2.2 is used to trace the evaporated moisture from the EG and WG regions through the atmosphere and determine where it leaves the atmosphere as precipitation. Figures 5.2 to 5.5 show the MAM footprints of the natural run (top row) and irrigated run (middle row) and their difference (bottom row). The scales show the amount of evaporation from the focus region (eastern Ganges in the right panel, western Ganges in the left panel) that precipitates at that location. The (global) areal sum of the figures is equal to the amount of evaporation in the focus region (except for the moisture that leaves the domain, or is still present in the atmosphere after 30 days of tracing. This is usually less than 10% of the evaporation). The scales also show the cumulative evaporation from the focus regions that corresponds to that particular color.

Eastern Ganges region

Under non-irrigated conditions during the monsoon onset (MAM), evaporation from the EG region is transported in north-easterly direction, towards the Himalayas. All models agree on this direction, but the exact location of the precipitation area differs slightly. The ECHAM model transports the majority of moisture into China, which is consistent with the moisture transport in the ERA-interim reanalysis (figure 5.5). The HIRHAM5 and RAMS models transport the moisture a bit more towards the east, while the RAMS model also transports a part of the moisture towards the south. The bottom row of Figures 5.2 to 5.4 show the differences between the footprints of the irrigated and natural run. The areas sums of these are equal (except for the moisture that is transported out of the domain) to the difference in evaporation in

ECHAM Footprint

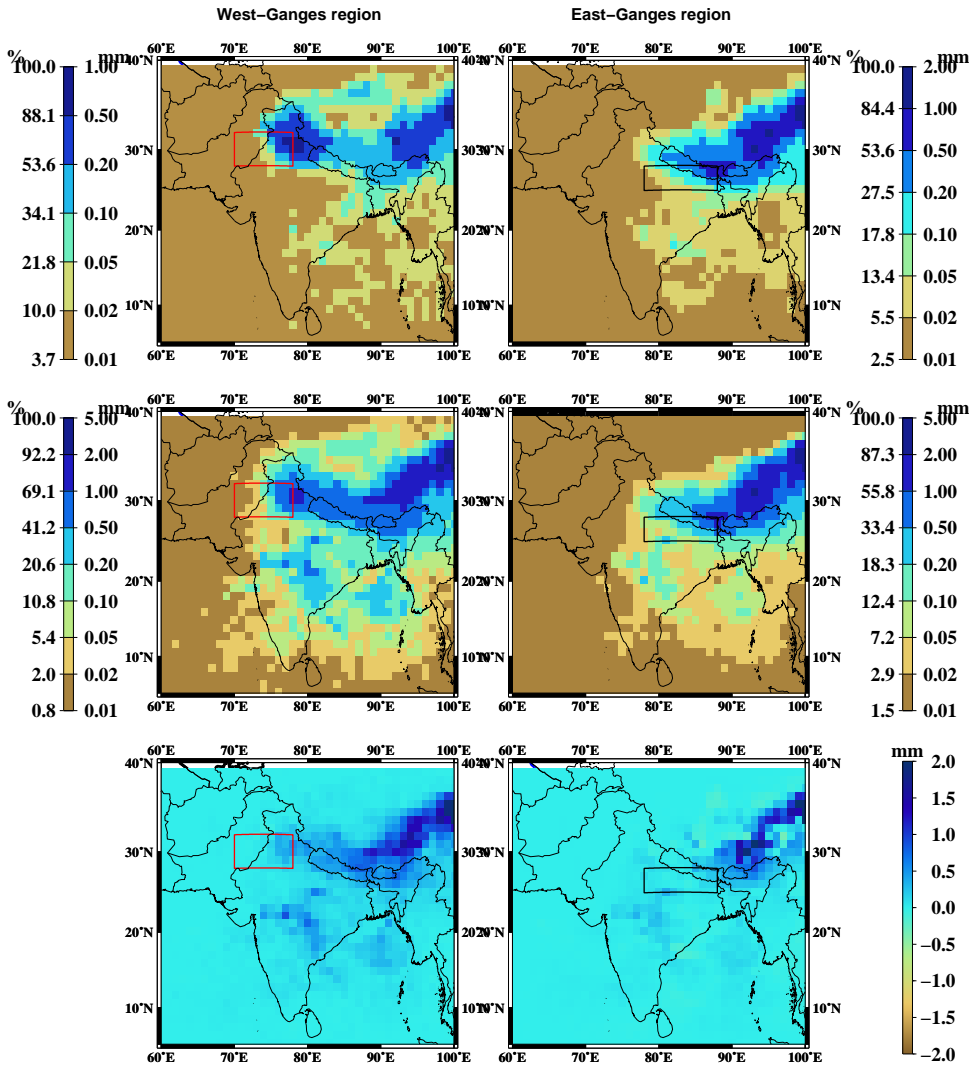


Figure 5.2: Footprints of precipitation originating from evaporation in the EG and WG regions, ECHAM model. The scale shows millimeters of precipitation as well as a cumulative fraction over the domain. (Over the domain, the precipitation adds up to the evaporation in the source region, minus the moisture that leaves the domain.). Top panel: natural run, middle panel: irrigated run, bottom panel: difference between runs.

HIRHAM Footprint

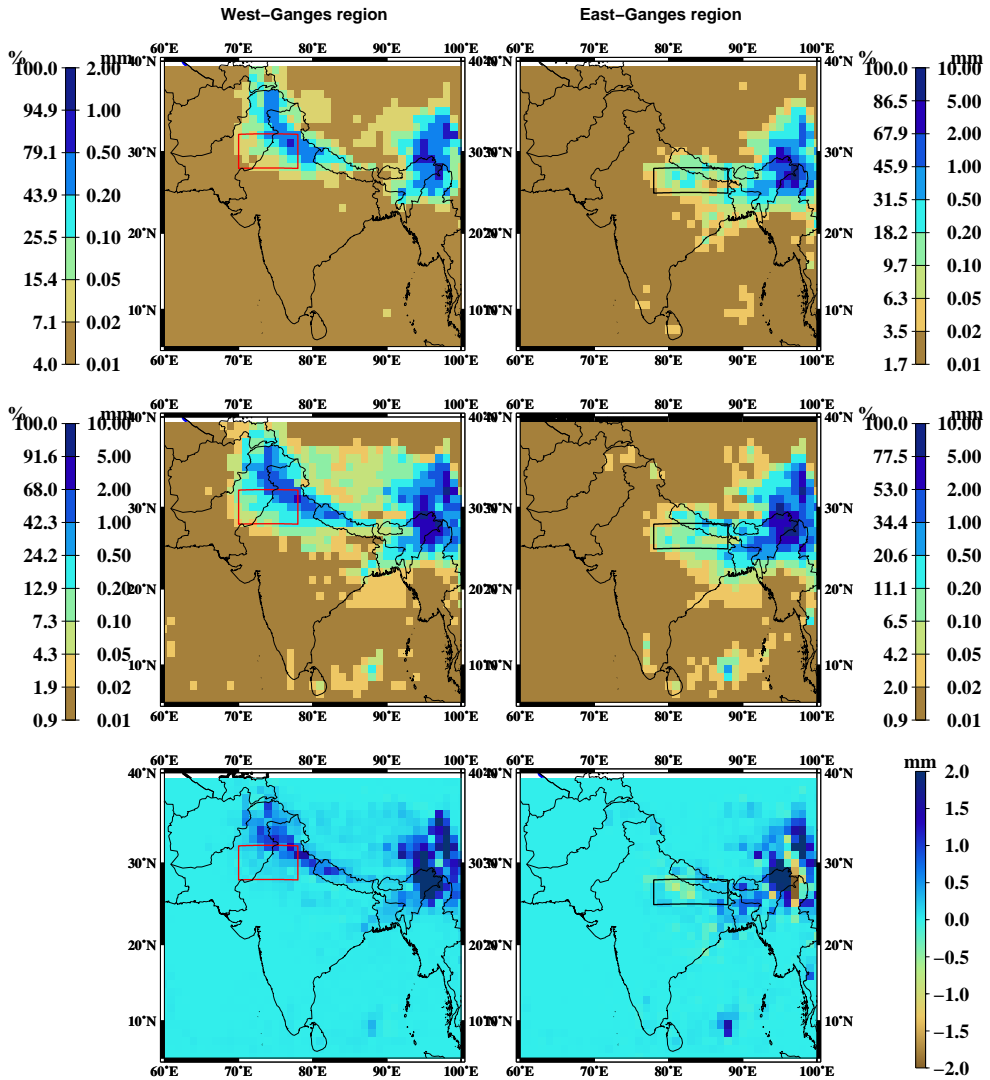


Figure 5.3: As in Figure 5.2, for HIRHAM model.

the focus regions between the irrigated and natural run. These plots reveal that for the EG region the additional evaporation from the irrigated run is transported into the far eastern provinces of India, Tibet and China. Again, the HIRHAM5 and

RAMS Footprint

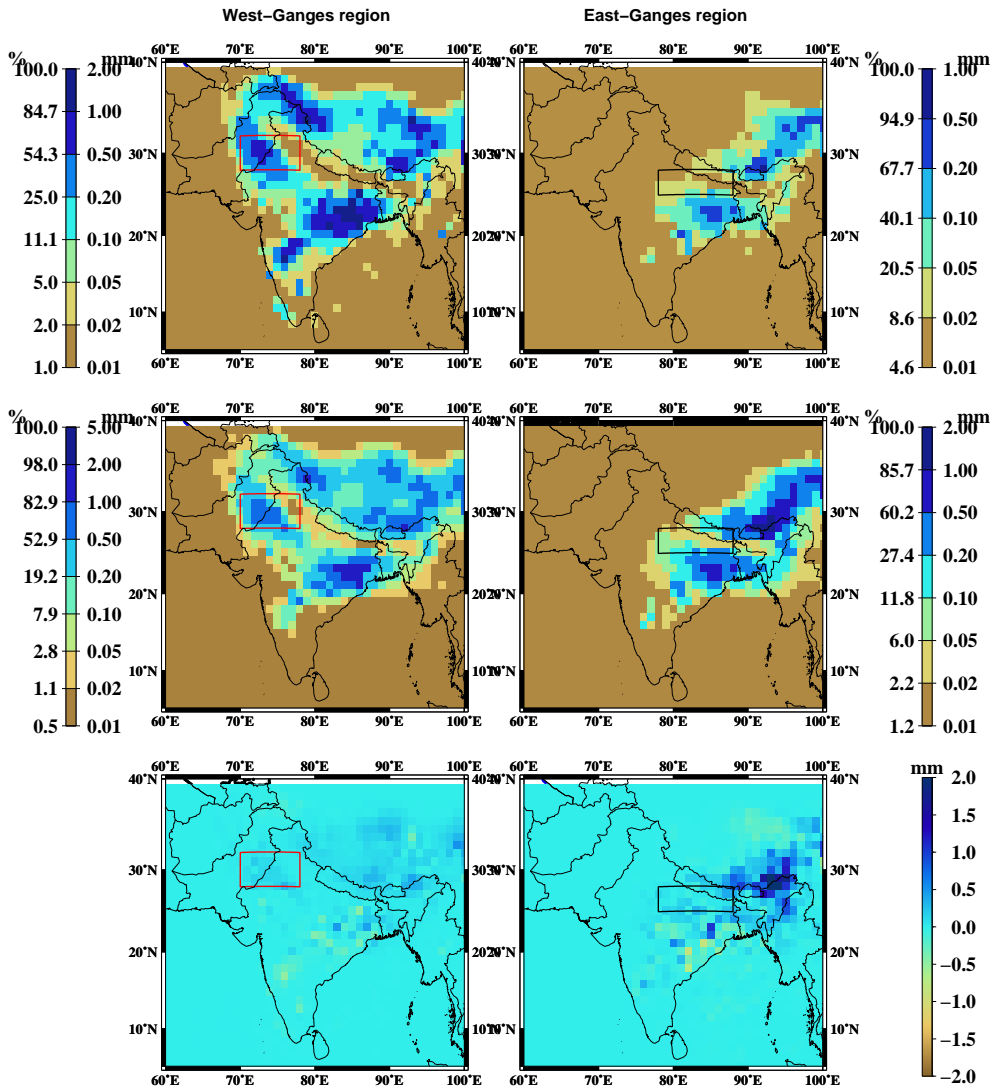


Figure 5.4: As in Figure 5.2, for RAMS model.

RAMS models transports the moisture a bit further east than the ECHAM model. Most models also show a small decrease in the evaporative footprint scattered in the

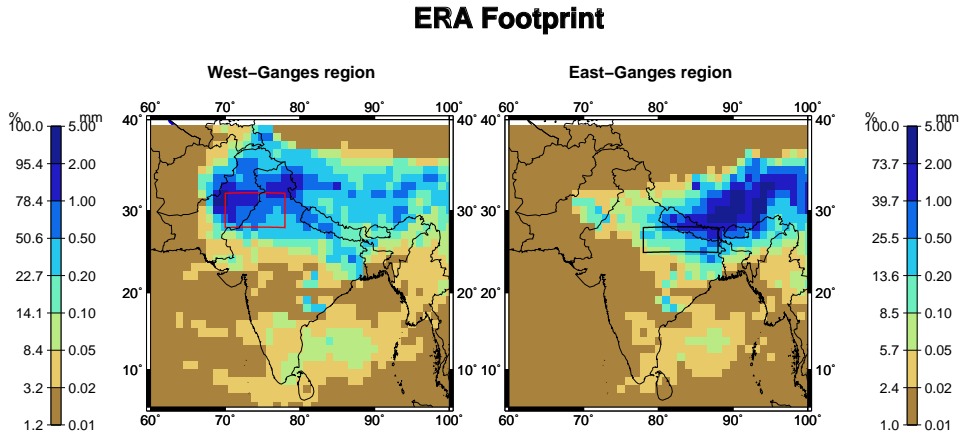


Figure 5.5: Footprints of precipitation originating from evaporation in the EG and WG regions, ERA-interim. The scale shows millimeters of precipitation as well as a cumulative fraction over the domain. (Over the domain, the precipitation adds up to the evaporation in the source region, minus the moisture that leaves the domain.).

areas north-east and south-west of the EG region. This effect is strongest for the HIRHAM5 model at the eastern boundary of the plot.

Western Ganges region

The evaporation from the WG region is transported eastward in all models, although there is lesser agreement over the exact footprints compared to the moisture transport in the EG region. The ECHAM model transports the moisture strictly to the east, while the others also show a small footprint to the west of the WG region, which corresponds to the ERA-interim footprint (figure 5.5). The HIRHAM5 model shows two precipitation regions, one close to the WG region in a band following the orography, the other in far eastern India. The ECHAM model transports the evaporation to a more continuous band following the orography. The RAMS model shows two branches, one into Tibet, towards the east and one into India towards the south-east. For the WG region, the difference between the MAM evaporation in the irrigated and naturalized runs varies across the models. The ECHAM model transports some of the additional moisture towards India, but the majority of the models direct the moisture north of the Himalayas into Tibet. The HIRHAM5 model transports the additional moisture towards the far east India and Tibet, but a significant part remains close to the WG area and is transported into Nepal, northern India and Pakistan. The

differences in WG region evaporation between the two runs in the RAMS model are negligible.

Recycling within the Ganges basin

The majority of irrigated areas in India are located on the Ganges plain (see Figure 5.1). Concerning the water budget of the Ganges basin, it is important to assess whether the evaporated moisture is transported out of the basin, or not, to get an estimate whether the basins loses water on the long term. Figures 5.6 and 5.7 show the percentage of the evaporation from the EG and WG regions respectively, that precipitates out within the Ganges basin. For MAM, this is equal to the part of the footprints in Figures 5.2 to 5.5 that falls within the Ganges basin.

For the EG region (figure 5.6), the ECHAM and RAMS models produce an annual cycle that is similar to ERA-interim, while the HIRHAM5 model overestimates the fraction of moisture that precipitates in the Ganges basin during the second half of the year. Generally, the fraction increases during the start of the year and peaks at about 35% during the summer monsoon period, with a decrease after the monsoon season to about 5%. The difference in the fraction between the irrigated and natural runs is not substantial, except in the ECHAM and RAMS model during April, May and June, where the fraction that precipitates in the Ganges basin is about 5% higher in the irrigated run than in the non-irrigated run.

For the WG region (figure 5.7), the fractions are much lower than for the EG region. The ERA-interim fraction shows an annual cycle that is near zero during the winter monsoon (DJF) and increases to about 6% during MAM, with a peak of around 9-10% during July. After this peak, the fraction drops off again to about 5% during SON.

Compared to ERA-interim, The ECHAM and RAMS models underestimated the fraction from May to August. During this period, the recycling fraction does not exceed 5%. The HIRHAM5 model does not deviate much from the fraction that is found for the ERA-interim dataset. Again, the differences between irrigated and non-irrigated runs is not very large.

5.3.4 Ganges basin moisture budget

The previous sections discussed the effects from the two focus areas, and showed that up to 40% of the evaporation precipitates in the Ganges region for both the irrigated and the natural run. Figure 5.8 shows the annual cycle of the atmospheric moisture budget for the entire Ganges basin for the ECHAM, HIRHAM5 and RAMS models.

All models show higher evaporation rates in the irrigated run than in the natural run from February until October. The amount of the evaporation that recycles within

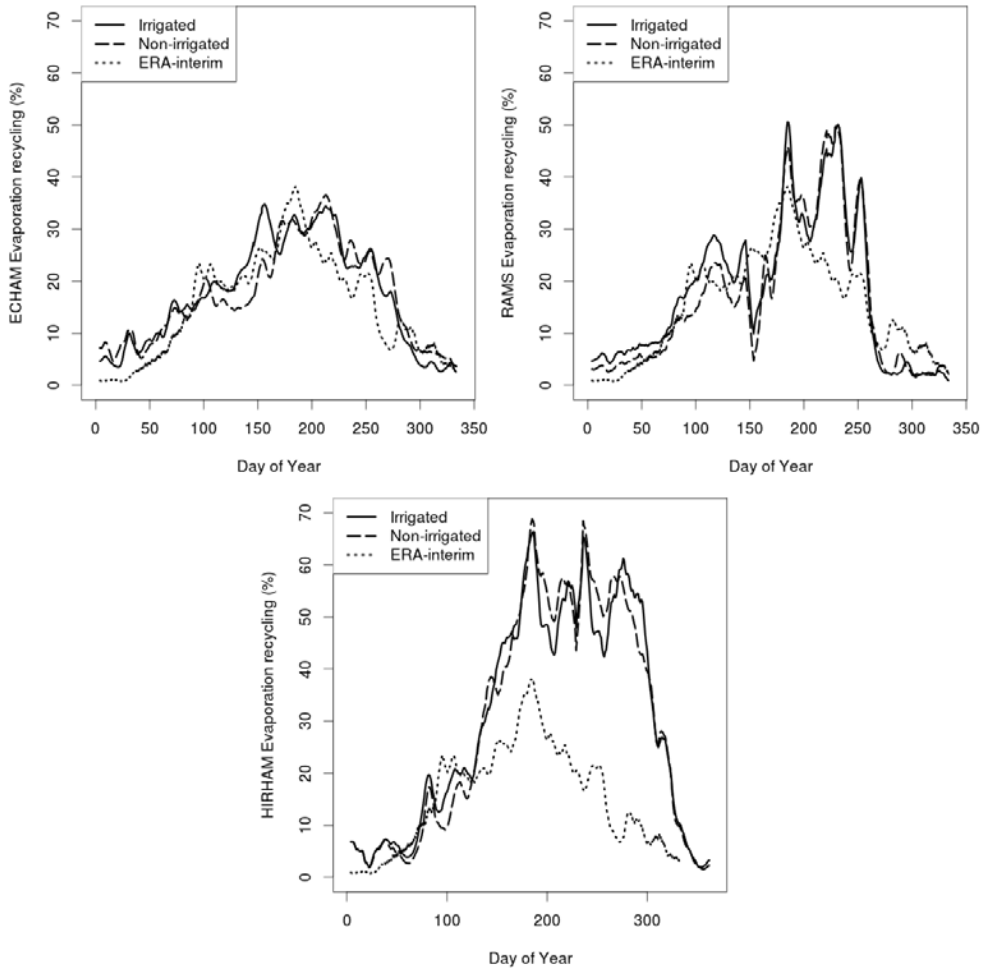


Figure 5.6: Annual cycle of the fraction of evaporation from the EG region that recycles as precipitation within the Ganges river basin, for the three models. Top left panel: ECHAM, top right: RAMS, bottom panel: HIRHAM

the Ganges basin is about equal in the irrigated and natural runs, with the exception of the 2–3 months before the monsoon onset (April, May, June), when the recycled evaporation is only marginally larger for the irrigated run.

Although the total Ganges basin precipitation of the irrigated and natural runs are quite similar, the natural runs have a higher basin precipitation in the month before the monsoon season as well as during the monsoon season for the HIRHAM5 and ECHAM models. In the RAMS model, there is no distinct difference in basin precip-

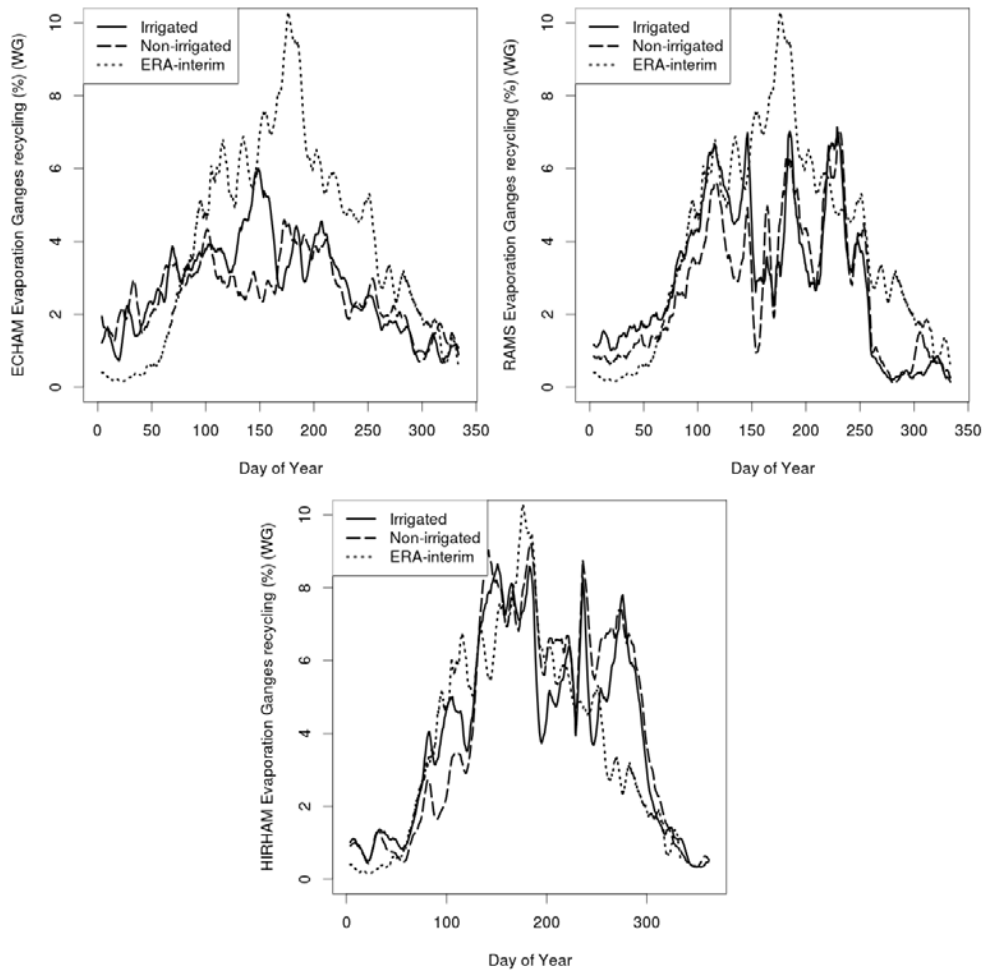


Figure 5.7: Annual cycle of the fraction of evaporation from the WG region that recycles as precipitation within the Ganges river basin, for the three models. Top left panel: ECHAM, top right: RAMS, bottom panel: HIRHAM

itation. So, despite the fact that the total basin evaporation is larger in the irrigated run during large parts of the year, and that moisture recycling rates are quite high, the total basin precipitation does not increase or sometimes decreases slightly. The increased amount of recycled evaporation cannot compensate the decreased moisture convergence into the Ganges basin.

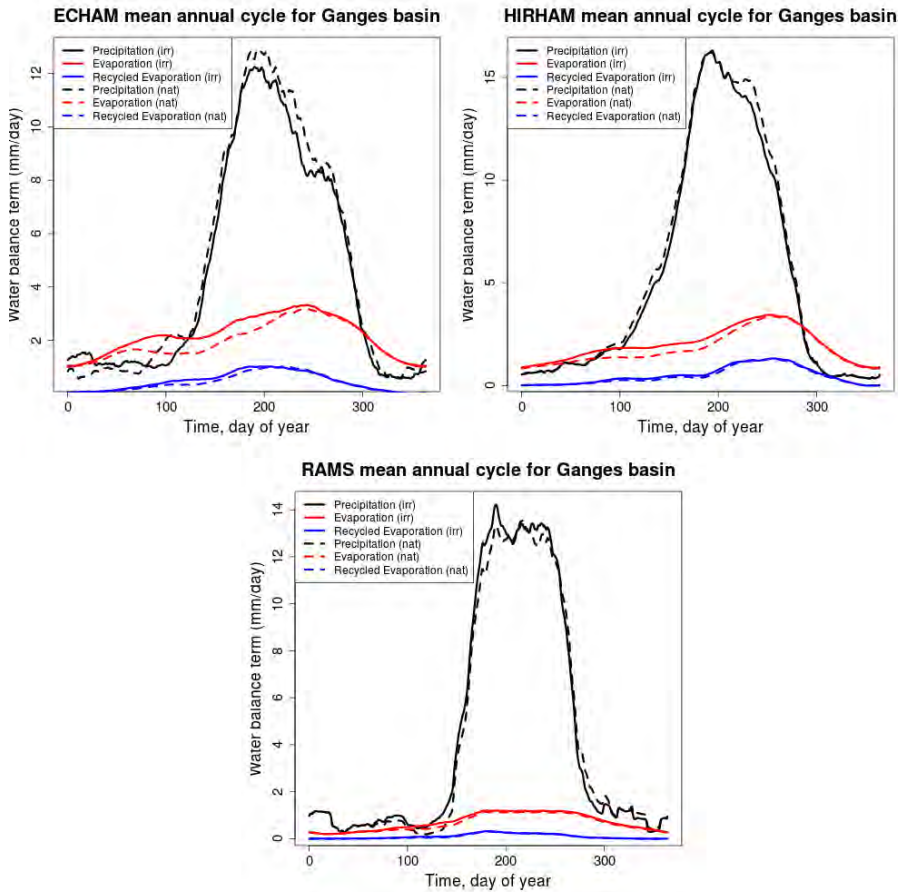


Figure 5.8: Annual cycle of Ganges basin atmospheric moisture budget (for ECHAM, HIRHAM5 and RAMS models), for irrigated and natural runs (mean over 1990-2000).

5.3.5 Regional Evaporation, Precipitation and Wind Patterns

As discussed in the previous section, the additional evaporation in the Ganges basin in the irrigated simulation does lead to a reduced Ganges basin precipitation. Figure 5.9 shows the annual mean evaporation for the entire simulated domain for the HIRHAM5, ECHAM, HadRM3 and RAMS models, for the natural and irrigated runs and their differences. The largest difference in evaporation is found in north India, in the Indus basin along the India/Pakistan border, where the evaporation can be enhanced by up to 3 mm/day. Other areas with a distinctively higher evaporation due to irrigation are the Ganges basin and the southern coastal areas, although the magnitude of the evaporation increase varies across the models. There is a decrease

in evaporation in the centre of India, away from the coastal zones. However, this decrease of about 0.2-0.3 mm/day is small compared to the increase elsewhere.

Figure 5.10 is similar to Figure 5.9, but shows the annual precipitation. The

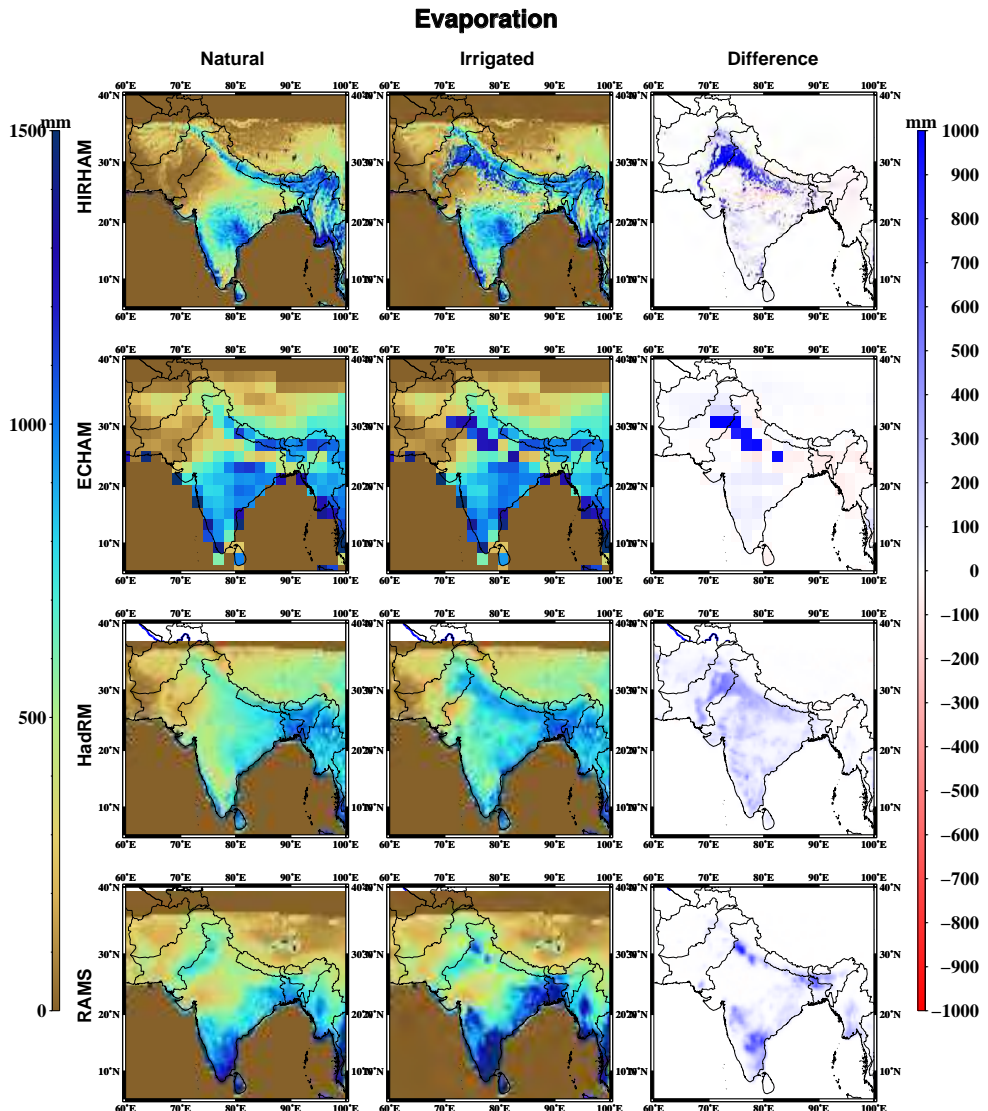


Figure 5.9: Total annual evaporation (mm) in the irrigated and non-irrigated runs, for each of the four models.

HIRHAM5, ECHAM and HadRM3 models show a shift of precipitation from the east-

ern side of India towards the north, into the Indus basin and Pakistan. In Nepal, and especially the eastern provinces of India, precipitation decreases by about 1 mm/day, whereas the increase in the north ranges from 0.5-1 mm/day. The RAMS model shows a more patchy precipitation response with unrealistically low precipitation in the Himalaya mountain range. A less pronounced precipitation difference is the decreases in the centre of India and the Ganges plain, and an increase in the western coastal areas.

The cause of this precipitation shift is a difference in atmospheric flow between the natural and irrigated runs. Figure 5.11 shows the multi model (HIRHAM5, ECHAM and RAMS) mean wind direction and speed at 850 hPa for the four seasons for both runs and their difference. While the wind patterns in the HIRHAM5 and ECHAM models are similar to each other, the RAMS model shows the same patterns, but smaller differences between natural and irrigated runs than the other models. During DJF, the wind is directed from the Ganges basin towards the Indian ocean and shows almost no difference between the natural and irrigated runs. In the pre-monsoon season (MAM), the wind direction is still dominantly from the north-west, but the wind speed is reduced in the irrigated run. Thus, their difference is a net flow from the ocean to the land.

In the natural run, the wind patterns during the monsoon season show a strong west to east flow for the southern half of India, which branches off towards the Ganges basin over the Bay of Bengal. This is still the case in the irrigated run, but the wind speeds in the Ganges basin are smaller, resulting in a reduced moisture flow from the Bay of Bengal. However, in the irrigated run, the dry atmospheric flow from continental Asia (from the north-west) towards north India is weaker and moist air from the south-east may bring some more precipitation in there. The smaller wind speeds from the ocean in the Ganges basin might explain why the basin moisture recycling increases in the irrigated runs, despite a decrease in total precipitation due to the decrease in moisture transport from the Bay of Bengal.

During the fall season (SON), the flow turns towards the south again, and the differences between the natural and irrigated runs decrease.

Figure 5.12 shows the mean annual differences between the irrigated and natural runs in evaporation and precipitation for all four models. The top panels display the absolute differences, while the lower panels display this difference relative to the natural runs. As seen in Figures 5.9 and 5.10, the absolute evaporation difference is positive almost everywhere. The relative evaporation difference is highest in the Indus river basin and in the northern Ganges river basin, where annual evaporation increases with about 50%. The additional evaporation in India's south translates only in an 10-15% increase.

The precipitation shift from the eastern Himalayas and the Ganges plain to the Indus basin and Pakistan is also clearly visible in Figure 5.12. However, the relative

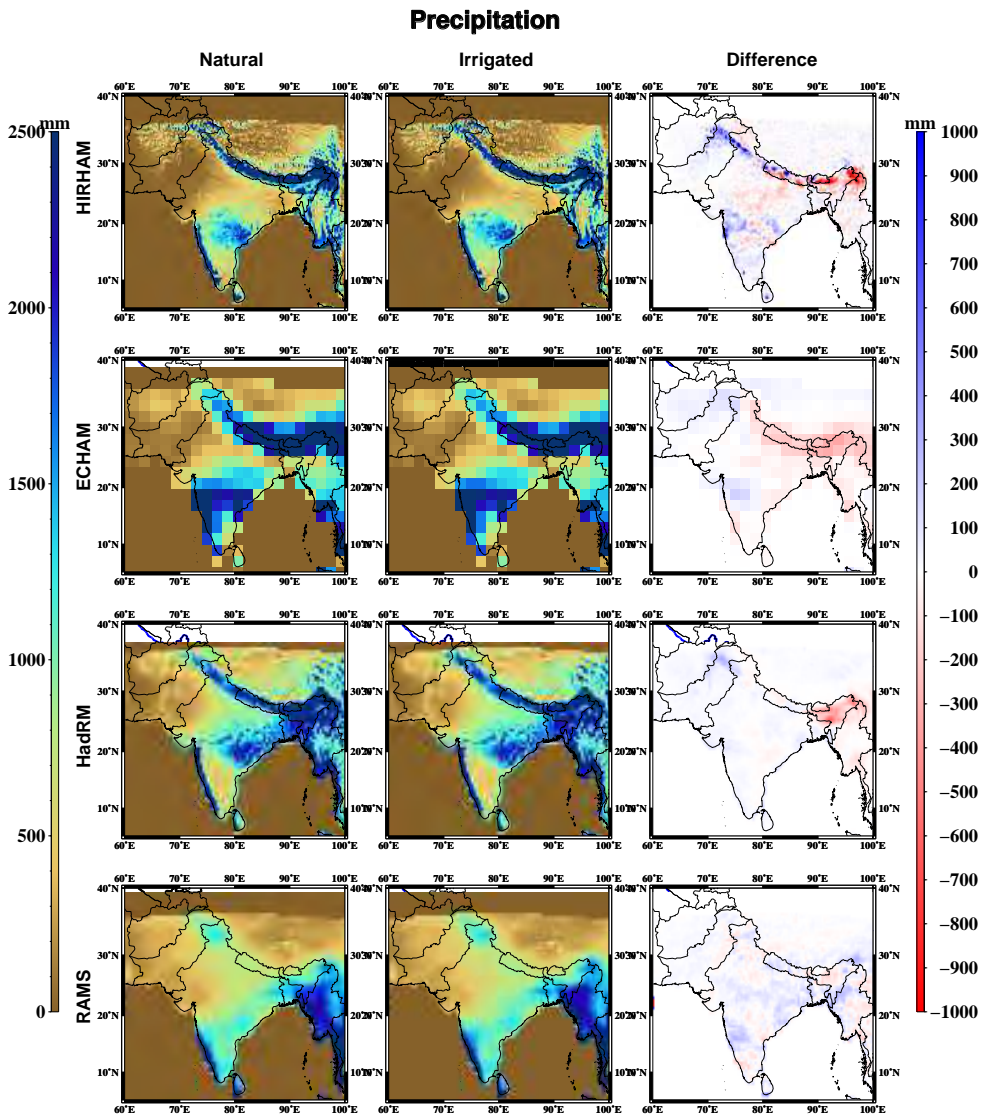


Figure 5.10: Total annual precipitation (mm) in the irrigated and non-irrigated runs, for each of the four models.

precipitation changes show quite a different picture than the absolute changes. The precipitation decreases are in areas where precipitation is already quite high, so the precipitation decrease is only about 10-15%. The precipitation increases in areas that

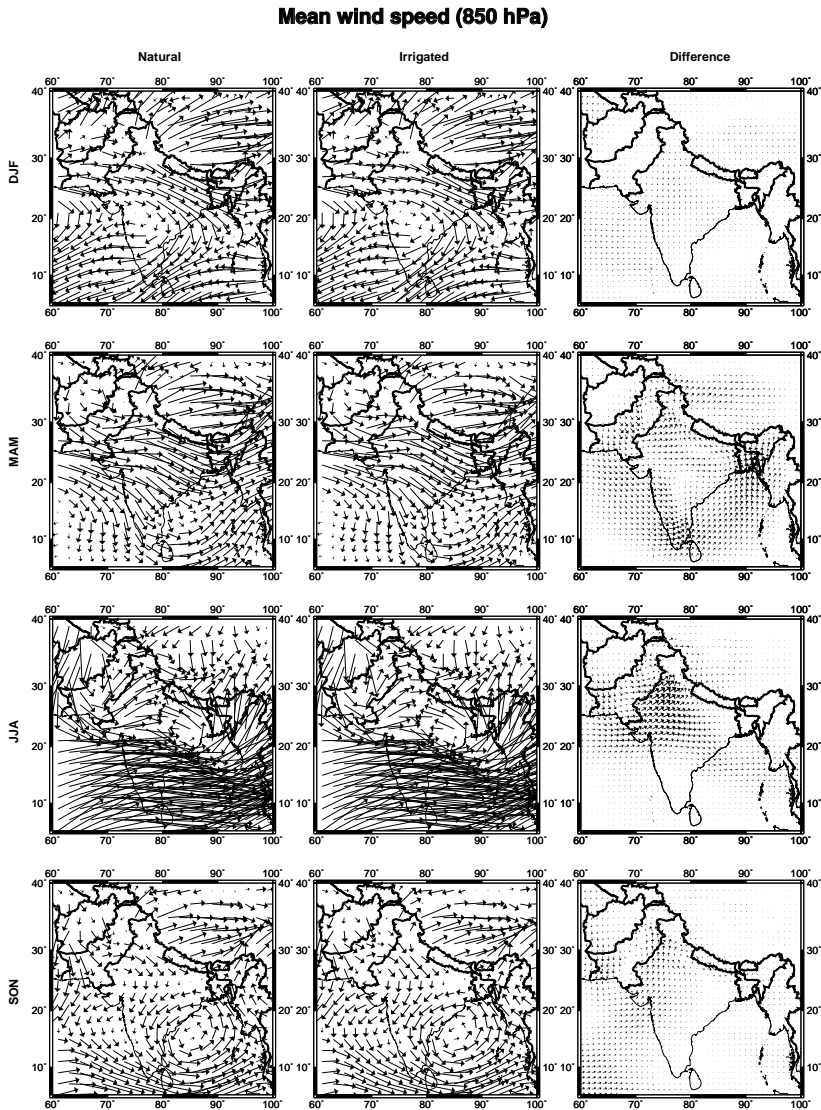


Figure 5.11: Wind direction (850 hPa) in the natural and irrigated runs and their difference per season, mean over ECHAM, RAMS and HIRHAM5 models.

are much drier, so the precipitation increases with up to 30-40% in the northern areas of the domain. In India's coastal areas, the precipitation increases with less than 10%.

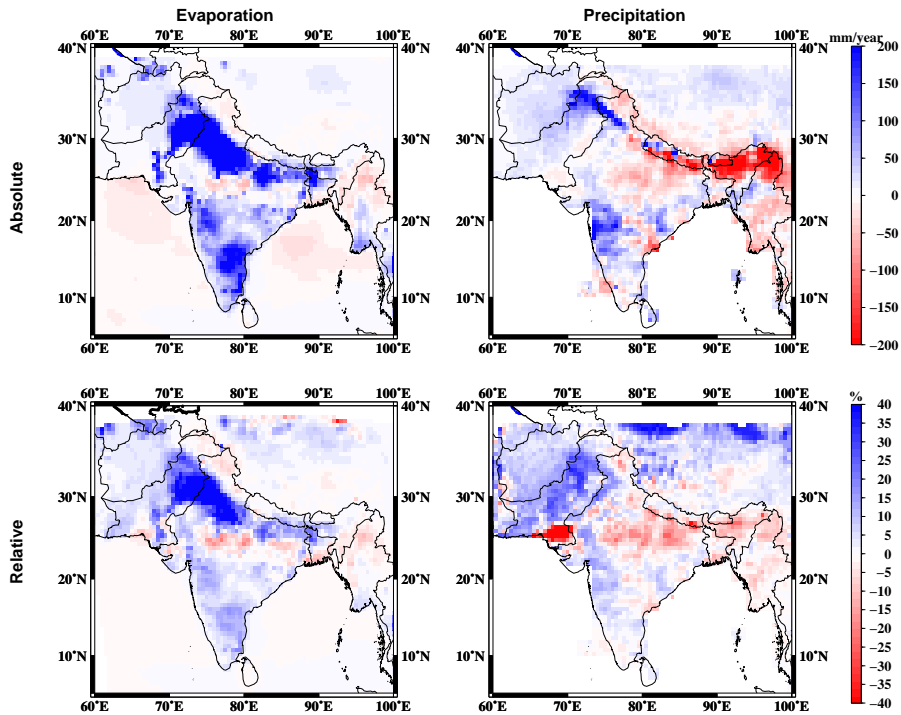


Figure 5.12: Yearly evaporation (left panels) and precipitation (right panels) difference between the irrigated and natural runs (mean over 1990-2000, and over ECHAM, HIRHAM5, HadRM3 and RAMS models). The top panels show the differences in absolute evaporation and precipitation, while the lower panels show these differences as percentage of the natural run.

5.4 Discussion and Conclusion

This study compared the effect of large scale irrigation on the atmospheric moisture budget in India using four climate models, run over ten years. Two runs were performed, one based on a natural setup in which no irrigation was applied, and another based on an irrigated setup in which moisture was applied to the top soil layer to keep the soil moisture at least at 90% of field capacity for areas prescribed by a common irrigation map.

The amount of irrigation that was required to keep the soil moisture at this level varied per model. For two regions with a high fraction of irrigated areas, the seasonal

cycle of applied moisture was following that of a observation based reference dataset, but the total differences of irrigation gift between the models varied to up to 0.8 mm/day. Thus, choosing the perspective of the atmospheric water budget (and keeping the land surface at a certain wetness), rather than the perspective of prescribing the amount of irrigation already leads to some variation among the models.

For two focus regions within the Ganges Basin, the local effects of irrigation were determined. All models agreed about the local decrease in temperature (of about 1-3 K) due to irrigation, which is similar to findings of other studies (for example Puma and Cook (2010) and Douglas et al. (2009)). Evaporation generally increased, and, perhaps counter-intuitively, usually exceeded the amount of irrigation. This may be possible due to changes in large scale flow, that could alter the atmospheric characteristics such as amount of precipitation and surface humidity and influence evaporation. Other possible causes for this evaporation increase in excess of the irrigation gift are a non-linear response of evaporation to soil moisture, changes in the ratio between bare soil evaporation and transpiration, and evaporation changes due to different moisture distribution in the soil profile. As this evaporation excess was common to all models studied here, it is unlikely to be due to model errors. The exact irrigation-evaporation response in these atmospheric models deserves more attention in future studies.

The local changes in precipitation in the two focus regions are small and not as uniform across the models as the temperature and evaporation changes. In the western Ganges focus region, the monsoon precipitation decreases and the non-monsoon precipitation increases due to irrigation. In the east Ganges focus region, precipitation decreases uniformly throughout the year due to irrigation.

The downwind precipitation effects of evaporation from the two focus regions are generally directed towards the south during SON and DJF, and towards the Himalayas as well as Tibet and eastern India during MAM and JJA. However, some of the evaporated moisture recycles within the area it evaporated from. The footprints of MAM evaporation (figures 5.2 to 5.5) are quite consistent among the models, although some models transport the moisture into a slightly different direction. Any additional moisture that is released is transported towards the eastern Himalayas.

During the winter months, all moisture is exported from the basin to the Indian ocean. During MAM, this fraction increases and it peaks during JJA, when up to 35% of the evaporation from the focus regions recycles within the Ganges basin. During SON, the fraction decreases again. The difference in moisture recycling between the natural and irrigated runs does not differ strongly, only during MAM is the recycling rate of the irrigated run a bit higher in some models. Therefore, a fraction of up to 35% of the additional moisture that is released into the atmosphere as a consequence of irrigation recycles in the Ganges basin.

Although the evaporation is higher in the irrigated run and more moisture recycles than in the natural run, the total precipitation in the Ganges basin decreases due

to a decrease in the moisture transport into the basin. The large scale changes at the land surface cause a change in atmospheric flow that shifts the precipitation from the eastern parts of India to the north-western parts and Pakistan, as well as India's southern coastal areas. The precipitation is thus shifted from wetter areas (India's east) to drier areas (India's north and Pakistan), where large relative precipitation changes occur. This loss of precipitation in the wetter areas may be of less importance than the increase in dry areas, where some crops might be grown due to the extra precipitation.

In this study, the local effects of irrigation on precipitation varied across the models. This may be due to different parametrizations of model physics, due to resolution differences, or due to forcing differences. Previous studies also show different local atmospheric responses to irrigation. Using a higher resolution model, Douglas et al. (2009) find precipitation shifts around the Ganges basin related to meso-scale circulations, which were not found in the current study. However, the decrease of sea breezes in the coastal regions in east India (Lohar and Pal, 1995) is reproduced in the current study.

An uncertainty in the moisture recycling estimates derived in this study is the treatment of evaporation and precipitation processes in the moisture recycling model. For West-Africa, van der Ent et al. (2013) show that the performance of the recycling model depends more on the evaporation assumptions than on the precipitation assumptions. The height at which evaporation is released just after it leaves the land surface can have a large effect on the moisture recycling rates. In the current study (and in Dirmeyer and Brubaker (2007) and Tuinenburg et al. (2012a), perfect mixing was assumed for evaporation. It is more realistic to release the moisture parcels just above the land surface in West-Africa (van der Ent et al., 2013). Due to different temporal and spatial resolutions of the forcing data, these conclusions cannot be directly applied to the Indian case. But, it should be noted that the evaporation release in the moisture recycling model is a consequential assumption for the current study. The effect of different assumptions regarding the evaporation release height will be a higher moisture recycling than presented in this study. The moisture recycling estimates presented here are probably the lower bounds, given the assumptions in the moisture recycling model.

The physical parameterizations and representation of the atmospheric dynamics in the models may have a large effect on the atmospheric effects of irrigation (Asharaf et al., 2012). For example, the parametrization of clouds (which varies across atmospheric models) has a direct influence on the surface radiation budget, and consequently on the evaporation. This may result in the effect that irrigation does not lead to more evaporation (and/or plant productivity), but rather to less evaporation, as less energy is available due to enhanced cloud cover. In one of present models (HadRM3) this effect was rather pronounced, but also previous work with the CAM3.3 model

already identified this possibility (Lobell et al., 2009). Pinpointing this apparent very sensitive feedback requires more attention. The large scale circulation effects of irrigation, a shift in precipitation from east to north-west India, confirms the findings of Puma and Cook (2010) and Asharaf et al. (2012). As all models in this study and several previous studies show this large scale effect of irrigation, the uncertainty in these findings is quite low and they can be considered quite robust.

We conclude that the atmospheric effects of irrigation as simulated by the four model in this study are threefold; (1) irrigation leads to lower temperatures and a higher evaporation locally, but local precipitation is not directly affected. (2) Up to 35% of any additional evaporation is recycled within the Ganges basin. Thus, of any marginal evaporation increase, up to a third of the moisture is conserved as a water resource for the basin. (3) If, however, irrigation is applied on a large scale, the large scale circulation will change and shift the moisture away from the Ganges plain towards the Indus basin and Pakistan.

Chapter 6

Synthesis

On longer timescale, the variability of the global climate and weather patterns is dominated by the variability of the oceans, which supply continental moisture and act as a large energy buffer of the climate system. On shorter timescales, the land surface state influences the climate by modulating the surface radiation balance and the vertical fluxes of moisture and energy. Examples of the influence of the land surface are urban heat island effects (an increase in temperature in cities due to the large fraction of concrete) as well as the reaction of certain chemical species in with organic compounds from forests (in effect cleaning the air).

This study focuses on the effects of the land surface on the atmospheric part of the water cycle. This is important for three reasons; the effects of (human induced) land use changes on precipitation can be used in water availability studies (for example Haddeland et al. (2011)), the land surface moisture can have an effect on the monthly to seasonal weather predictions (for example van den Hurk et al. (2012) and Koster et al. (2011)), that are useful for agricultural management, and the knowledge of the importance of the land surface processes can be used to better represent these processes in atmospheric models and reduce well known biases in these (Lobell et al., 2009). The case of India is relevant because previous studies have robustly indicated that the land surface in India is important compared to other areas globally (Koster et al. (2004), Guo et al. (2006)). This land-atmosphere coupling in India is important due to the large human caused changes in the water cycle and irrigation amount.

The effect of irrigation in India on the atmosphere has been determined from three perspectives; the local perspective, the moisture recycling perspective and the large scale perspective. Here, the results found will be presented from each perspective, as well as an integrated view across the perspectives. Based on this integrated view, the current annual cycle of irrigation patterns in India will be compared to an annual

irrigation cycle that optimizes the water availability in the Indian subcontinent. Finally, some recommendations and directions for future research are presented.

6.1 Atmospheric Effects of Irrigation

6.1.1 Local Perspective: Precipitation Triggering

From this perspective, the objectives are to determine **effects of irrigation on the local energy balance and convective precipitation** and whether **the local effect of the land surface on precipitation in India is larger than elsewhere**. Irrigation will lead to a moister land surface and a shift in the surface energy balance. The sensible heat flux will decrease and evaporation (the latent heat flux) will increase by about 0.5 mm/day (as simulated by the models in Chapter 5 (Tuinenburg et al., 2013)). The local effects of this surface change have been determined from a theoretical perspective in Chapters 2 and 3.

Based on two datasets, several diagnostics for soil-moisture precipitation coupling were determined for the summer half year (Chapter 2). Globally, there is a lot of variability in signal strength across the diagnostics and datasets. However, for all diagnostics and datasets, India stands out as one of the areas globally where the land surface has an influence on precipitation. A statistical relation between the land surface wetness and afternoon precipitation showed that in India, a moister land surface can increase the chance of afternoon precipitation with up to 20%. It could increase the amount of precipitation by up to 1 mm/day in North-West India, however the moister land surface could decrease the amount of precipitation in Eastern India with up to 0.5 mm/day. This statistical approach relates the evaporation to local afternoon precipitation. The days during which there was morning precipitation were excluded from the analysis. So, given the fact that no morning precipitation occurred, the effect of land surface wetness on afternoon precipitation is determined. This is done to eliminate the effect of large scale precipitation. However, the fact that no morning precipitation occurred is a crude way to eliminate large scale effects. Some large scale effects may have not been excluded, so this statistical approach is not purely local.

To determine the seasonal and spatial variability of the land surface influence, Chapter 3 focused on the annual cycle in India. One of the previously used diagnostics (the CTP-HI_{low} framework, which was developed for the US (Findell and Eltahir (2003a))) was scrutinized in-depth for atmospheric conditions in India. A slab model of the atmosphere (treating the atmosphere as a single column), forced with measured profiles of the atmosphere was run with a wet and dry land surface. The atmospheric conditions (analyzed in the CTP-HI_{low} framework) under which the model runs with wet and dry land surface resulted in a different precipitation were slightly drier (HI_{low}

was about 2 K higher) than for the US. Therefore, the diagnostic was adapted for the Indian situation. This means that land-atmosphere coupling diagnostics may be location (or climate) specific.

Using this adapted diagnostic, land-atmosphere coupling showed a clear seasonal cycle which varies with India's monsoon cycle. In the winter months, the atmosphere is too dry for the land surface to have an influence; no precipitation will occur regardless of land surface wetness. However, during the pre-monsoon season (especially the two month before the monsoon onset) the atmosphere becomes wetter and the land surface promotes precipitation. During the monsoon season, the atmosphere is too wet for the land surface to have an influence, precipitation will occur regardless of the land surface. However, during monsoon-break periods (up to three weeks of a reduced monsoon flow), the atmospheric conditions are such that a wet land surface will promote precipitation. Finally, during the two months after the monsoon retreat, a positive influence of the land surface is expected as well. Negative feedbacks (a wetter land surface decreasing precipitation or a drier land surface increasing precipitation) do not occur much in India.

The results confirm earlier results that soil moisture is positively related to precipitation in India and that irrigation is expected to increase precipitation due to this local coupling. However, within the research on land-atmosphere coupling, many different approaches are taken. The coupling results are either dependent on the model used, which causes very different results, or dependent on quality and the resolution of the measured data. For the land-atmosphere diagnostics, the data should resolve the daily cycle of precipitation and surface fluxes. Moreover, many diagnostics involve atmospheric lapse rates of moisture and temperature in the first few kilometers of the atmosphere. The measurements should have a high vertical resolution of the temperature and moisture profiles, as the lapse rates can be quite sensitive to this resolution.

If the approach involves measured data, the effect of soil moisture on precipitation must be isolated from the reverse effect. This is usually done using statistical techniques which may have a large influence on the result. Moreover, the influence of the land surface on precipitation may be scale dependent. On smaller scales (up to tens of kilometers), the contrast in energy and moisture fluxes between wet and dry areas may lead to precipitation over dry areas (Taylor et al. (2012)). The wet areas provide moisture to the atmosphere, while the boundary layer height may be higher over dry areas, possibly leading to precipitation there. On larger scales (hundreds of kilometers), a wetter land surface (on a spatial average) will lead to more precipitation due to an increased surface moisture flux, but this precipitation will probably still fall over drier areas within a region.

From the local perspective, we conclude that the effects of irrigation are an increased chance of convective precipitation triggering. These effects are seasonal, with the

highest effects during the two months before and after the monsoon season.

6.1.2 Moisture Recycling Perspective: Ganges Basin Recycling

The second perspective is that of the atmospheric path that a moisture particle travels. This includes the distance traveled and residence time in the atmosphere. The objectives of the research from this perspective are to determine **the direction in which additional evaporation is transported and where it leads to additional precipitation**. Moreover, it determines **how this varies seasonally and for different areas in India**.

To determine the atmospheric path of evaporation, the current study uses an atmospheric moisture tracing model that releases a large number of moisture packets and determines in which direction these go and where they return to the land surface. This model used atmospheric model output to determine the (three-dimensional) path of virtual water packets through the atmosphere. Along this path through the atmosphere, the moisture budget (with evaporation going into and precipitation out of the packet) was continuously made. This moisture budget included two moisture terms, the total moisture as well as the moisture that entered the packet at the evaporation location (the 'tagged' moisture of interest). In this way, a fraction of the precipitation along the path of the packet could be attributed to the evaporation from the location where the packet was released.

Several modelling approaches exist to determine the relation between evaporation and precipitation location of a unit of water (see Chapter 1). These approaches are either versions of a bulk budget scheme introduced by Budyko (1974), which determines the atmospheric moisture budget on an Eulerian grid, or of a Lagrangian scheme, as used to trace atmospheric chemical species, introduced by Dirmeyer and Brubaker (1999). To determine the effects of the moisture recycling model assumptions, two models using the Eulerian and Lagrangian approach are run for a case study around Lake Volta in West-Africa (van der Ent et al., 2013). For this case, a regional climate model run output which included water tracers from the Lake Volta evaporation was available. Figure 6.1 shows the fate of the Lake Volta evaporation for August 1998 as simulated by the regional climate model, the Eulerian scheme and the Lagrangian scheme.

The case study has a westward flow in the upper layers and an north-eastward flow in the lower layers. The comparison shows that the Eulerian scheme under-performs due to the strong layering of the moisture transport; the integrated vertical flux assumption is not valid. The Lagrangian scheme better simulates the patterns of the precipitation (probably due to the three ability of the parcels to be transported in

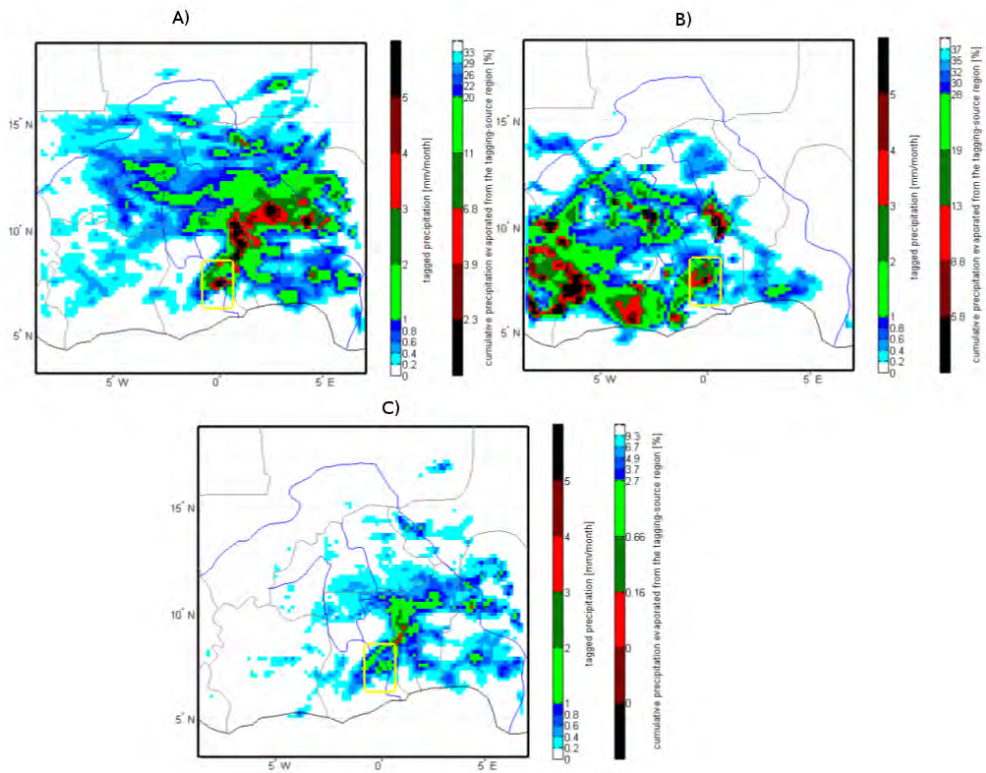


Figure 6.1: Comparison of different moisture recycling methods for Lake Volta region in West-Africa. Adapted from van der Ent et al. (2013). The panels show the precipitation traced from evaporation in the yellow box (Lake Volta) for the regional climate model with built-in tracers (panel A), the Eulerian method (WAM model (van der Ent et al. (2010)), panel B) and the Lagrangian method (Tuinenburg et al. (2011), panel C)

three dimensions), but exports too much moisture out of the basin.

Adaptation of the schemes showed improvements. Inclusion of two model layers in the Eulerian scheme improved the results significantly. For the Lagrangian scheme, the assumption of the height of the evaporation was most important. The release of the moisture from just above the surface improved the model results, the precipitation pattern and magnitude closely resembled that of the forcing RCM. However, it was noted that this improvement depends on the timestep of the forcing data. When the moisture is released from the surface, it has to mix vertically by the vertical wind speeds of the forcing data. On hourly forcing (as used in this intercomparison), the vertical wind speeds appear to reflect the (sub-timestep) turbulent moisture mixing

well. However, when forcing with larger timesteps is used, the moisture packets may stay too low when released from the surface. The assumption that all vertical layers contribute equally to precipitation was less important; a run where precipitation could only come from cloud layers improved the results only slightly.

The moisture recycling model used in this study (Chapters 4 and 5) used the assumption that directly after evaporation, moisture is distributed randomly along the vertical atmospheric moisture profile. This assumes a perfect mixing of the evaporation in the atmospheric column, which might not be realistic given the results of van der Ent et al. (2013). However, the moisture recycling intercomparison experiments over West-Africa cannot be directly compared to the Indian subcontinent given the different temporal resolution of the forcing data and the different atmospheric flow patterns.

In Chapter 4, the atmospheric moisture tracing model was applied for the Indian domain using reanalysis data. As the best estimate for the state and dynamics of the atmosphere over the last 30 years, this represents the current conditions of the annual cycle of moisture recycling. During the winter season, evaporation is transported south, towards the Indian ocean. Only a small fraction (less than 5%) of the evaporation falls again as precipitation in India. So any evaporation during the winter months is lost for India's water resources. During the spring season (MAM), the wind direction reverses as consequence of the heating contrast between land and ocean, which drives the monsoon flow. Due to this change in direction, the evaporated moisture is not transported away as far as during the winter season and the moisture recycling within the river basin increases. During the monsoon season (JJA), a large fraction (up to 60%) of evaporation recycles within the Ganges basin, the fraction of moisture that recycles within the land areas in India (Ganges and Indus basins and land areas south of those) can be up to 80%. After the monsoon season, moisture recycling decreases again, as the winds shift again towards the ocean.

The importance of recycled evaporation (versus precipitation due to moisture that is transported from adjacent areas) for precipitation again shows an annual cycle. During the winter months, a minimal amount of moisture recycles, so the contribution to precipitation is small. During MAM, recycling increases and contributes about 10% of the basin precipitation. The precipitation during the monsoon season is from sources outside the Indian continent; a large amount of moisture is transported into the basin and evaporation recycling contributes about 5% of precipitation. During October and November, when the atmospheric flow patterns change again and precipitation decreases, evaporation recycling peaks again at around 10%. After this second peak, evaporation recycling drops off rapidly.

In Chapter 5, four atmospheric models have been run without irrigation and with explicit irrigation. The output of these model runs was used as input for the atmospheric moisture tracing model to determine the influence of irrigation on moisture

recycling. The annual cycle in the fate of moisture in these model runs is similar to the one found for the reanalysis data in Chapter 4. During the winter period, the evaporated moisture is transported away from the continent towards the Indian ocean. During the pre-monsoon season (MAM), shifting wind patterns transport the evaporation towards the north-east, in the direction of the Himalayas, where it leads to precipitation. During the monsoon season, the wind patterns are from the ocean towards the land (in north-westerly direction in the Ganges basin). After the monsoon, the moisture flow reverses again.

All models simulate an increase in Ganges basin evaporation due to irrigation. The peak of this evaporation increase is during the dry pre-monsoon season, and first half of the monsoon season (April-July) when irrigation leads to an increase in evaporation of between 0.5 and 1.0 mm/day. In all models, this additional evaporation lead to a larger absolute amount of recycled evaporation within the Ganges basin. However, this absolute increase in basin recycled precipitation is small compared to the evaporation increase. The fraction of evaporation that recycles in the basin is smaller for the model runs with irrigation than for the natural runs. As the surface moisture source increases, the relative recycling rate decreases; the moisture does not lead to extra basin precipitation, but is exported from the basin. However, for two focus areas (as opposed to the total basin budget), irrigation did not affect the annual cycle in relative evaporation recycling. The decrease in the fraction of evaporation recycling due to irrigation depends on the location in the basin.

The moisture tracing model in this research assumes perfect mixing of evaporation after it leaves the land surface. This assumption will have affected the moisture recycling rates. The recycling model intercomparison by van der Ent et al. (2013) showed that the recycling rates increased substantially for the small West-African domain when the evaporated moisture is released just above the land surface. It is unclear how the results of van der Ent et al. (2013) compare to larger scale moisture recycling in the Indian subcontinent. However, in general, wind speeds increase with altitude, so moisture recycling rates will generally be higher when the evaporated moisture is released lower, because the evaporation remains longer near the release area. Therefore, the assumption of perfect mixing of evaporation used in the current study will have resulted in lower moisture recycling rates compared to assumptions of imperfect mixing. A sensitivity analysis of the moisture release height from parcels from the two areas in Figure 4.2 showed a limited effect of release height on the Ganges recycling rate. During and around the monsoon season (May-September), the release of moisture parcels near the surface increased the Ganges recycling ratio with up to 5%. During the rest of the year, the release height did not influence the Ganges basin recycling.

From the moisture recycling perspective, the effect of irrigation in the entire Ganges basin is a slight decrease in the fraction of moisture that recycles within the basin

during April-July, but due to a large increase in evaporation in that period, the absolute amount of evaporation that recycles within the Ganges basin increases slightly. However, there are differences in the effects of irrigation on moisture recycling within the basin. From a moisture recycling perspective, there are optimal locations where irrigation should be located. This will be discussed in section 6.3.

From the moisture recycling perspective, we conclude that a significant fraction (up to 60%) of evaporation recycles within the Ganges basin. Moisture recycling is largest during the monsoon season. However, during periods before and after the monsoon season, recycled evaporation is most important, when it contributes 10-15% of the total precipitation. Irrigation increases the amount of evaporation, but decreases the fraction of evaporation that recycles within the basin. Still, the absolute amount of evaporation that recycles in the Ganges basin increases.

6.1.3 Large Scale Perspective: Influence on Monsoon Flow

Apart from the local and moisture recycling effects of irrigation, the large scale **effect of irrigation on the atmospheric flow and its seasonal and spatial variability** potentially has a large influence on India's climate. An increase in the land surface humidity will decrease the land surface temperature and possibly the temperature contrast between ocean and land, which is one of the drivers of the monsoon flow. If the monsoon moisture flow is altered due to irrigation, this might have effects on the coupling strengths found in Chapters 2 and 3. The atmospheric moisture profiles may have changed, which may affect the chance of the triggering of convection. An altered monsoon flow may also affect the importance of results found for the moisture recycling perspective. If significantly more (or less) moisture is transported into the basin, the recycling of evaporation within the basin may become less (or more) important.

The atmospheric models used in Chapter 5 simulated the changes in atmospheric flow due to irrigation. During the winter season (DJF), the atmospheric flow is directed from north to south. This dry winter monsoon flow is not dependent on the land-ocean temperature contrast and irrigation has no effect on it in the simulations. During MAM, the season when the temperature contrast increases, and irrigation has an influence on the atmospheric flow. There is a net flow from the Bay of Bengal towards Bangladesh and eastern India. Also, the flow from land to ocean is decreased slightly in the Ganges basin. The large scale irrigation in the Indus basin and its consequential temperature decrease causes an increased flow to the north in Northern India and an increased flow to the south in Pakistan. During the monsoon season, the flow from the Arabian sea towards North India increases significantly. In the Ganges basin and just south of it, the monsoon flow decreases slightly. During SON, the large

scale effects of irrigation decrease, although there is still an increased flow from the Arabian sea towards North India.

Many previous model studies have demonstrated effects of irrigation on the atmospheric flow. Some meso-scale models were run on a higher spatial resolution than the models in the current study, but for shorter time periods (Saeed et al. (2009), Douglas et al. (2009)). Others were run globally and reported only annual mean irrigation effects.

Generally, climate models overestimate the surface temperature in Northern India, leading to a misrepresentation of the monsoon flow. Lucas-Picher et al. (2011) suggested that including irrigation may help the monsoon flow simulation. Although the purpose of the current study was not to validate the monsoon flows and simulated changes due to irrigation, the current study provides a first order approximation of this effect over four models.

The decrease in summer monsoon flow determined in previous studies was also found in the current study. The decrease precipitation in the coastal areas, noted by Lohar and Pal (1995) was also found. Although the precipitation increase in the band south of the Ganges basin (Douglas et al., 2009) was not reproduced in this study, the regional scale models showed mesoscale circulation precipitation features.

The large scale precipitation shift from east India to north-west India confirms the result of Puma and Cook (2010), who found such a shift for JJA. However, for south India Puma and Cook (2010) simulate a decrease in precipitation of about 1 mm/day for JJA, whereas the current study found a modest increase in south India. The monsoon flow changes in north India/Pakistan correspond to the influences of soil moisture found by Asharaf et al. (2012), who also found a shift in precipitation from east to north-west India. A shift in the monsoon flow in the southern Indian peninsula (Asharaf et al., 2012) was not found in the four atmospheric models in the current study. As noted by Asharaf et al. (2012), the local and large scale effects of irrigation determined by atmospheric models depend on the model physics and dynamics used. By using four atmospheric models, the current study aimed to provide some robustness effects of irrigation changes on large scale effects across different model set-ups. The monsoon circulation responses to irrigation are almost nowhere in India directly in the direction of the land-ocean temperature gradient, therefore the theoretical results from Zickfeld et al. (2005) may be too limited.

Irrigation has an effect on the atmospheric flow, but the shifts in wind patterns are small compared to the magnitude of the atmospheric flow. Nevertheless, these effects on wind patterns have consequences for precipitation patterns. The models in Chapter 5 simulate a decrease in precipitation of up to 1 mm/day in Eastern India and especially the mountainous areas and an increase in Southern, Western and far Northern India and Pakistan of up to 0.5 mm/day. These precipitation shifts are not only the result of large scale processes, the local and moisture recycling effects are

also included in the atmospheric models.

From the large scale perspective, we conclude that the effects of large scale irrigation are a shift in precipitation from East-India to West and North-India. This shift occurs during May-September.

6.2 Effects on Hydrological Cycle

The three perspectives described in this study show different effects of irrigation on precipitation. The Ganges basin precipitation, that was assumed to be the same for the hydrological model runs shown in Figure 1.4 may be affected in different ways.

This research has shown that irrigation has two opposing effects. The importance of these effects depends on the size of the irrigated area. These effects are indicated in Figure 6.2, which shows the scales of the processes in this research and their effects. Irrigation of a marginally small area (from ten to hundred kilometers) will lead to an increase in precipitation triggering, increasing the Ganges total precipitation. Moreover, the additional evaporation will not be lost for the Ganges basin entirely, a fraction of the evaporation will contribute to the precipitation. On this scale of irrigation, the positive effects from the local and moisture recycling perspectives are more important than the negative effects from the large scale perspective and the effect of irrigation on Ganges precipitation is positive.

However, irrigation on large scales such as simulated by the atmospheric models in Chapter 5 (larger than hundreds of kilometers) will lead to shifts in atmospheric flow and precipitation. The positive effects of precipitation triggering and moisture recycling are still present, but the negative effect of the shift in monsoon patterns dominates the Ganges precipitation, which will decrease.

For the hydrological models in Haddeland et al. (2011) and Hagemann et al. (2012), the effects of a changed land surface on precipitation is small. The atmospheric models, which simulated two extreme cases of no irrigation and full irrigation, simulated a small decrease in precipitation for the Ganges basin. Moreover, the variability in the simulated effect of irrigation on Ganges basin precipitation across the models was small compared to the variability in evaporation and discharge across the hydrological models. It is therefore recommended to decrease the uncertainty in and variability across the large scale hydrological models in simulating the effects of land use changes, before including the atmospheric feedbacks of land use change in these models.

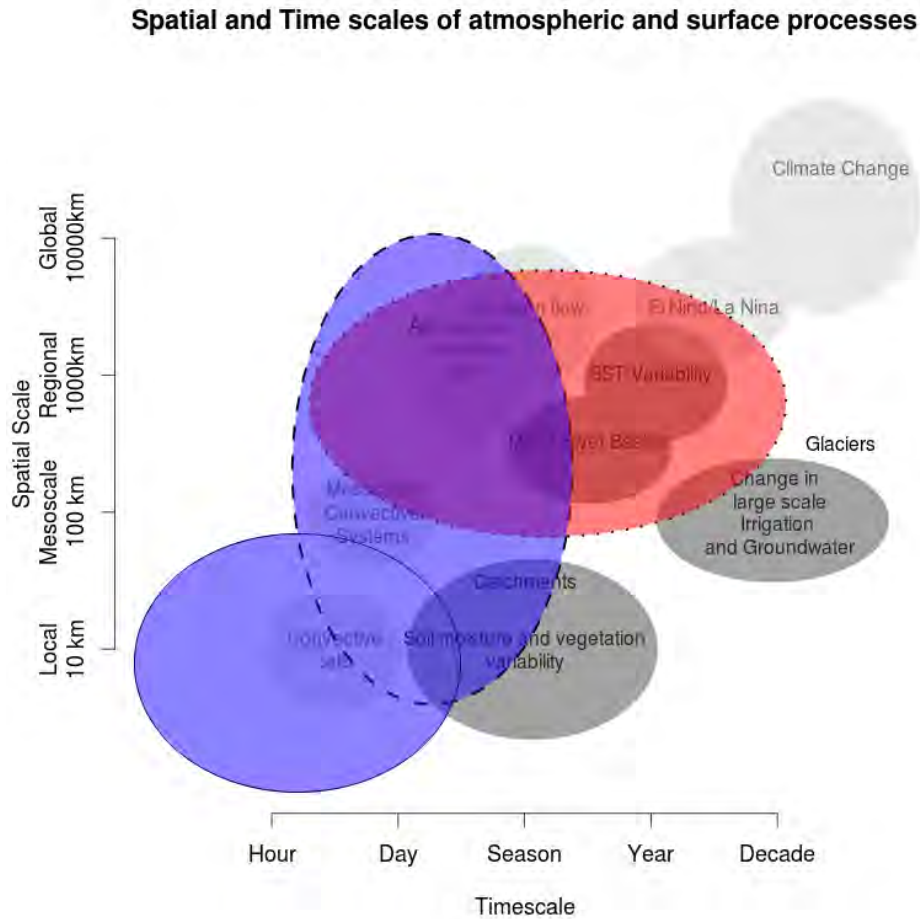


Figure 6.2: The length and time scales of the processes and perspectives in this research. The local and moisture recycling perspectives (colored blue) have a positive contribution to the Ganges precipitation, while the large scale perspective (colored red) have a negative contribution to this precipitation.

6.3 Ideal Irrigation

This research has focused on the atmospheric effects of the current irrigation patterns. However, it is interesting to reverse the question and to determine the ideal location for irrigation in India, with the focus on minimizing the effect of irrigation on India's water resources. The objective of this ideal irrigation is to maximize precipitation

triggering and moisture recycling within the Indian subcontinent to minimize the water resources losses for the subcontinent as a whole.

The theoretical (modelling) approaches used in this study to determine the atmospheric effects of the current irrigation patterns can also be applied to different irrigation patterns (except for the atmospheric models in Chapter 5). The atmospheric effects of different irrigation patterns can be determined and irrigation patterns that optimize India's water efficiency from an atmospheric moisture budget perspective can thus be determined. Obviously, the atmospheric moisture budget is not the only aspect that determines the location of irrigation. Moisture availability, soil types, distance to labor and food markets, are among the aspects that influence the location of irrigation as well.

Here, the effect of a marginal increase of irrigation (an increase that is so small that the large scale atmospheric flow patterns are not influenced) in a location on India's water resources are defined as the combined effects from the local and moisture recycling perspective. A small increase in irrigation can lead to an increase or decrease in local precipitation (local perspective) and a fraction of the additional evaporation may recycle within India's land surface. The ideal irrigation index is the sum of these effects:

$$III = AFS + E_{additional} * India_{recycling} \quad (6.1)$$

in which III is the ideal irrigation index, AFS is the amplification feedback strength; the increase in local precipitation due to a moister land surface (Chapter 2 and Findell et al. (2011)), $E_{additional}$ is the additional evaporation due to irrigation and $India_{recycling}$ is the fraction of the evaporation that recycles within the Indian subcontinent (Ganges and Indus river basins and land areas south of those basins). For the AFS, the values found in Chapter 2 are used. The evaporation recycling is determined from the evaporation recycling fractions found in Chapter 4. The amount of additional evaporation due to irrigation is taken from the model mean additional evaporation from Chapter 5. It varies seasonally and is assumed to be 2 mm (MAM), 1 mm (JJA), 1 mm (SON) and 0.5 mm (DJF).

This ideal irrigation index corresponds to effect of irrigation on the water resources in India, with units of millimeters per day. However, a positive value does not mean that more moisture is available in India, as the amount water needed for irrigation will practically always be higher than the ideal irrigation index. Moreover, the effect of irrigation is a local decrease in water resources (due to irrigation), whereas the increases in water resources will be located elsewhere in India. Note that this index does not explicitly include the effects on large scale circulation, so it is only valid for irrigation on length scales of up to around 100 km.

The left column in Figure 6.3 shows the irrigation water use from streams, reservoirs and rivers (blue water, mm/day) around the year 2000. The columns show the four seasons. The right column shows the ideal irrigation (mm/day) index for those four

seasons. Although both columns are in mm/day, the left column shows an actual amount of irrigation, whereas the right column shows an effect of irrigation on the river basin precipitation. The amount of irrigation that has to be applied for that effect is almost always higher than the actual effect. Therefore, only the spatial patterns of the columns in Figure 6.3 can be compared directly.

During MAM and JJA, there is a difference in the ideal irrigation index between East and West India. In West, and especially North-West India, irrigation may trigger precipitation and a large fraction of evaporation returns to the Indian peninsula as precipitation. In the coastal areas of East India, less precipitation may be triggered due to irrigation. Moreover, only a small fraction of the evaporation from those areas returns to the Indian peninsula, so the ideal irrigation index is negative. During SON and especially DJF, the effects of irrigation on the precipitation of the Indian peninsula are small.

A comparison with the actual irrigation amount shows that if the atmospheric moisture budget were the only aspect to consider, irrigation activity in the Ganges basin should be shifted to areas in the upper Ganges basin, away from the coastal areas where the river enters the ocean. In the Indus basin, the irrigation activity should be shifted towards the lower areas of the basin, near the coast.

6.4 Outlook and Recommendations

This research has analyzed the effect of irrigation on the atmosphere from three perspectives. Each of these perspectives approached the problem with different scientific data, models and tools. The data, models and tools are continuously improved. New measurements with new interpretations become available, processes in models are improved and faster, more accurate tools become available. This section provides an outlook onto how the technologies that will become available can be used to analyze the effect of irrigation on the atmosphere in more detail.

6.4.1 Local Land-Atmosphere Coupling and spatial variability

Previous studies of the local land-atmosphere coupling has produced a wide range coupling strengths, coupling strength diagnostics and global hotspots. The coupling strengths varied strongly across the diagnostics, data sets used to derive the diagnostic and approach taken. The current research has shown this for two indicators and two datasets (Chapter 2). Furthermore, it has shown that indicators may be regional (climate) specific (Chapter 3).

It is therefore recommended to first define a common definition of land-atmosphere coupling strength, which should explicitly include the chain of land surface-precipitation processes (soil moisture-evaporation-boundary layer transport and dynamics-cloud

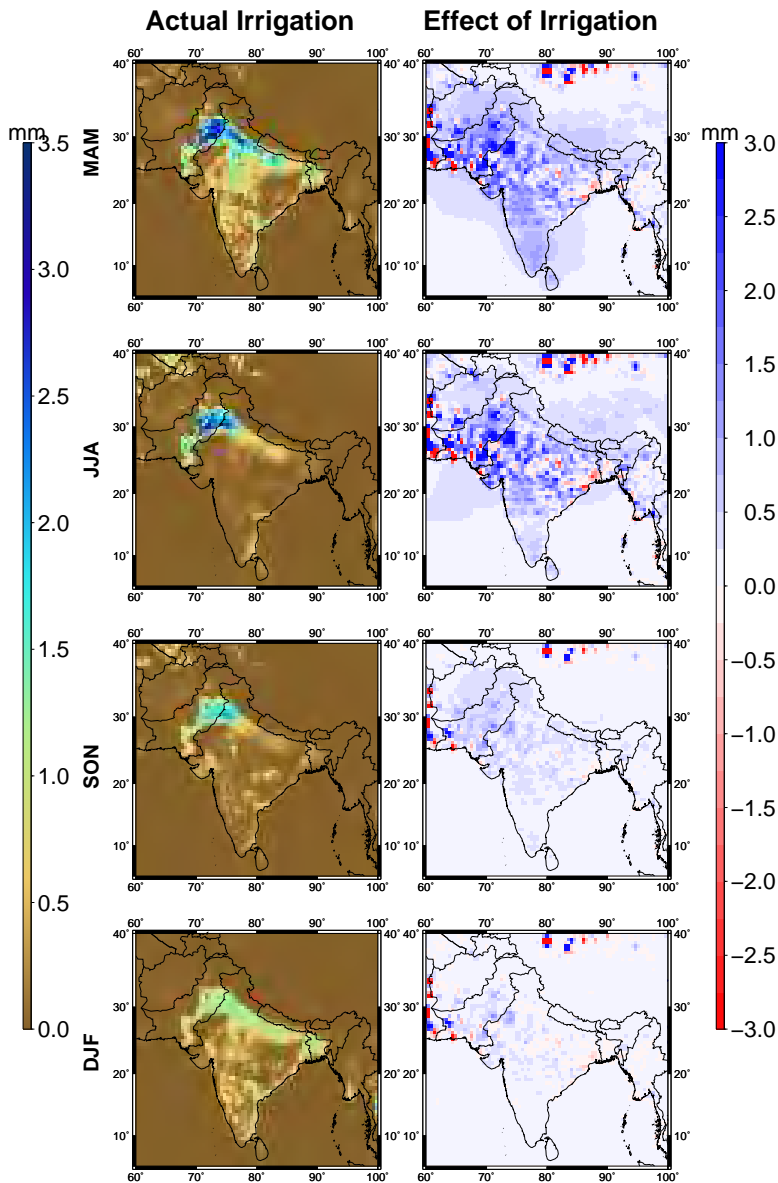


Figure 6.3: Seasonal comparison of actual irrigation and an estimate of the effect of irrigation based on results from the current study. Left column: Amount of blue water (water from streams, rivers and reservoirs) irrigation applied (mm/day, Portmann et al. (2010)). Right column: Ideal irrigation index (mm/day); estimated effect of marginal irrigation on precipitation in the Indian peninsula (Ganges and Indus river, as well as land areas south of those basins), based on moisture recycling estimates from Chapter 4 and precipitation enhancement estimates (AFS) from Chapter 2.

formation-precipitation) and temporal and spatial scales. Given recent results from Taylor et al. (2012), it should be determined whether precipitation is influenced by surface moisture or by variability of surface moisture (dry and wet patches), and how this depends on the spatial scale. After this, a benchmark study should be set up using a high quality dataset as input for land-atmosphere coupling diagnostics. In this dataset, the daily cycle of surface fluxes should be well resolved and the resolution in the atmospheric vertical should be high enough to resolve the moisture and temperature lapse rates above the boundary layer. This should be done for several locations with different land uses and climates. (Currently, the GEWEX-GLASS LoCo working group (Santanello et al. (2011)) is setting up such a study for the ARM Southern Great Plains site in the US.) Finally, the spatial variability of surface wetness should be considered. On scales under hundred kilometers, the effects of dry and wet patches on local circulation, boundary layer dynamics and precipitation triggering should be studied. The results of these studies could be applied to better understand the local influence of irrigation and possibly to determine optimal irrigation layouts.

6.4.2 Constraining Moisture Recycling Models with Water Isotope Measurements

The atmospheric moisture tracing model that is used in the moisture recycling perspective determines the atmospheric moisture budget from different forcing datasets. However, several approaches exist to determine this budget. Each of these approaches consists of a number of assumptions regarding horizontal moisture transport and vertical mixing, evaporation and precipitation processes. van der Ent et al. (2013) determined the effect of these assumptions for a case in West-Africa. However, these assumptions are related to the resolution of the forcing dataset.

It is therefore recommended to repeat the work by van der Ent et al. (2013). Using the output of a global atmospheric model with explicit moisture tracing, the approaches of determining the atmospheric moisture budget should be compared, with special attention to the vertical mixing between the output timesteps. Such a study would improve the knowledge about moisture recycling models and could be used to determine the uncertainty in the moisture recycling in India.

An other approach to improve the moisture recycling models is to constrain them with stable isotope measurements. Naturally, water occurs in a number of isotopes which have a slight mass difference. Due to this mass difference, the isotope ratio is different in water vapor that has just evaporated from the ocean than in the ocean water itself. After each evaporation and precipitation process, the isotope ratio changes. Therefore, precipitation can be analyzed for its isotopic constitution. The isotope ratio determines whether the water has just evaporated over the ocean or that it is more likely to have evaporated over land, and trends in this ratio can yield informa-

tion about land use changes (for example Henderson-Sellers et al. (2002), Pfahl and Wernli (2008) and Brown et al. (2008)). This information should be compared to the moisture recycling model output to determine how well it predicts this ratio under the given assumptions in the recycling model.

6.4.3 Influence of Marginal irrigation

This study shows that there are two contrasting atmospheric effects of irrigation (in the Ganges basin); an increase in precipitation due to local triggering and moisture recycling and a decrease in precipitation due to a change in large scale wind patterns. The importance of these effects depends on the scale of the irrigation. On a smaller scale, the first effects are expected to be more important. On larger scales, the second effect is expected to be more important. However, the current study has not determined at which scales the net effects shift signs.

It is recommended to determine the relation between irrigation extent and the relative importance of the effects determined in this study. Regional atmospheric models could be used to repeat the experiment described in Chapter 5 with varying amounts and different locations of irrigation. The ideal irrigation index (section 6.3) could be used as a starting point.

6.4.4 Inclusion of irrigation in atmospheric models

This study included explicit irrigation in four atmospheric models (Chapter 5). Uniformly across the models, the surface temperature decreased. This decrease has also been observed in other studies that performed such an experiment (for example Puma and Cook (2010) and Lobell et al. (2009)). The cooling effect of irrigation is largely due to a shift in the surface energy flux partitioning from sensible to latent heat. However, a secondary effect may be a cooling due to a decrease in incoming shortwave radiation caused by clouds that are formed due to the irrigation. Explicit inclusion of irrigation may reduce the positive temperature bias present in irrigated areas in many GCMs (Lobell et al., 2009).

Other types of atmospheric models may be improved by including irrigation. Chapter 4 showed that in the ERA-interim reanalysis model (Dee et al., 2011), the moisture assimilation into the soil layers corresponds to the irrigation application in India, both spatially and temporally. This suggests that the indirect effects of irrigation (higher specific humidity and lower temperature in the lower atmosphere) are included in the atmospheric measurements that force the reanalysis model. Despite the fact that the surface fluxes are not the primary goal of atmospheric reanalysis, applying moisture to the soil as irrigation rather than pure assimilation would make the reanalysis product more physically based. The advantage would be that the remaining moisture

assimilation would be due to model errors or lack of data, so the shortcomings of the reanalysis would be more visible and easier to improve. Furthermore, the large scale hydrology community would benefit from more physically based surface fluxes as the variability of current global estimations of evaporation is very large.

6.4.5 Effect of irrigation on Himalaya glaciers

The atmospheric models in Chapter 5 showed a precipitation shift from the Eastern Himalayas to the Western Himalayas. Several studies have noted that the glacier extent in the Eastern Himalayas decreased during the 20th century, whereas the extent in the Western Himalayas increased (Immerzeel et al. (2010), Hewitt (2005)). It is recommended to investigate the relation between the irrigation increase during the 20th century and the glacier dynamics during this period.

The recommended approach to determine this influence would be to first determine the source of the moisture that precipitates on the Himalaya glaciers. Figure 6.4 shows this evaporation source of Himalaya precipitation, which was determined by running the moisture tracing model from this study in backward mode.

The glaciers receive their precipitation from moisture that evaporated either nearby on the Ganges plain, or from the Arabian sea, or from continental Asia, depending on the season. Harding et al. (2012) show that a significant fraction of this precipitation originates from evaporation from irrigated areas. A next step would be to repeat the analysis of Figure 6.4 for the atmospheric models used in Chapter 5.

To determine the glacier dynamics effect of a different Himalaya precipitation due to irrigation, the precipitation from the atmospheric models should be used as input for a local glacier dynamics model to test the effect of the timing of the precipitation differences on the glaciers. This glacier dynamics model should also be run with input from 20th century climate runs to test the influence of climatic changes versus irrigation changes.

6.4.6 Interaction of irrigation with monsoon variability

A last recommendation is to study the effects of irrigation on monsoon variability in more detail. This study has focus on the mean annual cycles (over ten years) of the effects of irrigation. However, it would be quite interesting to determine the irrigation effects during a year with a weak summer monsoon. Are the positive (local and moisture recycling) effects found in this study relevant during weak monsoon year, or is the monsoon flow further weakened due to irrigation? Similarly, what is the role of irrigation during strong monsoon years? These questions are relevant from a water management perspective, because the extreme years are often more relevant than the mean.

Evaporation sources of Himalaya precipitation, ERA–interim

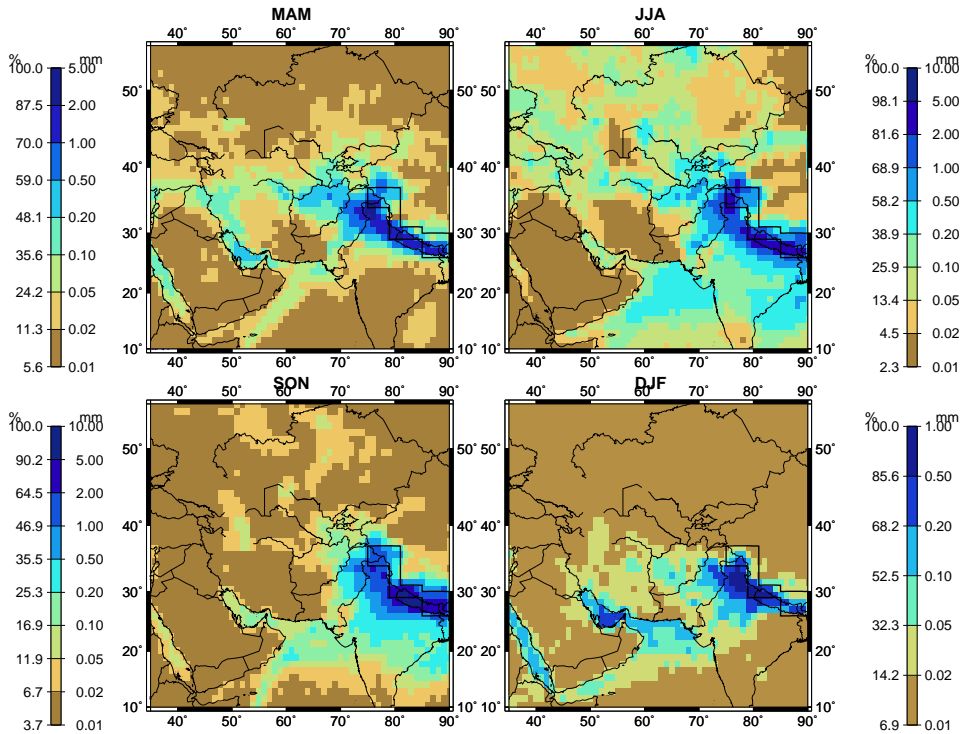


Figure 6.4: Evaporation sources for Himalaya precipitation, based on ERA-interim Dee et al. (2011), per season (adapted from Harding et al. (2012)).

Moreover, the irrigation effects during monsoon break periods can be significant. During monsoon break periods, the large scale monsoon flow shuts down for a period of up to three weeks. During these periods, the local effects of irrigation found in this study may be important.

These questions of the role of irrigation in monsoon variability can be answered partially by analyzing the model runs from the atmospheric models used in this study. However, these were only run over ten years, which is a small sample to study extreme years. Therefore, the model runs could be repeated over a longer period to acquire a better sample of extreme years. Alternatively, on the edges of the atmospheric models, the monsoon flow could be forced to be similar to the flow during extreme years.

Bibliography

- Alfieri, L., Claps, P., D'Odorico, P., Laio, F. and Over, T.M., 2008. An analysis of the soil moisture feedback on convective and stratiform precipitation. *Journal of Hydrometeorology*, 9(2): 280–291.
- Angevine, W.M., Grimsdell, A.W., Hartten, L.M. and Delany, A.C., 1998. The flatland boundary layer experiments. *Bulletin of the American Meteorological Society*, 79(3): 419–431.
- Asharaf, S., Dobler, A. and Ahrens, B., 2012. Soil moisture–precipitation feedback processes in the indian summer monsoon season. *Journal of Hydrometeorology*, 13(5).
- Barry, R.G. and Chorley, R.J., 2003. *Atmosphere, weather, and climate*. 8th edn., Routledge, London :, 421 p. pp.
- Bates, B.C., Kundzewicz, Z., Wu, S. and (Editors), J.P., 2008. *Climate Change and Water. Technical Paper of the Intergovernmental Panel on Climate Change*. Tech. rep., IPCC Secretariat, Geneva.
- Betts, A.K., 2004. Understanding hydrometeorology using global models. *Bulletin of the American Meteorological Society*, 85(11): 1673–1688.
- Betts, A.K., Ball, J.H., Beljaars, A.C.M., Miller, M.J. and Viterbo, P.A., 1996. The land surface–atmosphere interaction: A review based on observational and global modeling perspectives. *Journal of Geophysical Research D: Atmospheres*, 101(D3): 7209–7225.
- Betts, A., Köhler, M. and Zhang, Y., 2009. Comparison of river basin hydrometeorology in era-interim and era-40 reanalyses with observations. *Journal of Geophysical Research D: Atmospheres*, 114: D02101, doi:10.1029/2008JD010761.

- Biemans, H., 2012. Water constraints on future food production. *PhD Thesis, Wageningen University*: 168 pp.
- Biemans, H., Haddeland, I., Kabat, P., Ludwig, F., Hutjes, R.W.A., Heinke, J., Von Bloh, W. and Gerten, D., 2011. Impact of reservoirs on river discharge and irrigation water supply during the 20th century. *Water Resources Research*, 47(3).
- Bisselink, B. and Dolman, A.J., 2008. Precipitation recycling: Moisture sources over europe using era-40 data. *Journal of Hydrometeorology*, 9(5): 1073–1083.
- Boé, J., 2012. Modulation of soil moisture-precipitation interactions over france by large scale circulation. *Climate Dynamics*: 1–18.
- Bosilovich, M.G. and Schubert, S.D., 2002. Water vapor tracers as diagnostics of the regional hydrologic cycle. *Journal of Hydrometeorology*, 3(2): 149–165.
- Bosilovich, M., Robertson, F. and Chen, J., 2011. Global energy and water budgets in merra. *Journal of Climate*.
- Brown, D., Worden, J. and Noone, D., 2008. Comparison of atmospheric hydrology over convective continental regions using water vapor isotope measurements from space. *Journal of Geophysical Research D: Atmospheres*, 113(15).
- Brubaker, K.L. and Entekhabi, D., 1996. Analysis of feedback mechanisms in land-atmosphere interaction. *Water Resources Research*, 32(5): 1343–1357.
- Brubaker, K.L., Entekhabi, D. and Eagleson, P.S., 1993. Estimation of continental precipitation recycling. *Journal of Climate*, 6(6): 1077–1089.
- Budyko, M.I., 1974. *Climate and Life*. Academic Press, 508 pp.
- Burde, G.I. and Zangvil, A., 2001a. The estimation of regional precipitation recycling. part i: Review of recycling models. *Journal of Climate*, 14(12): 2497–2508.
- Burde, G.I. and Zangvil, A., 2001b. The estimation of regional precipitation recycling. part ii: A new recycling model. *Journal of Climate*, 14(12): 2509–2527.
- Christensen, O.B., Drews, M., Christensen, J.H., Dethloff, K., Ketelsen, K., Hebestadt, I. and Rinke, A., 2006. *The HIRHAM regional climate model, version 5*. Tech. rep., DMI Tech. Rep.
- CIA, 2009. *The world factbook 2009*. Central Intelligence Agency, Washington D.C.
- Claussen, M., Cox, P., Zeng, X., Viterbo, P., Beljaars, A., Betts, R., Bolle, H.J., Chase, T. and Koster, R., 2004. The global climate. In: P.K. et al. (Ed.), *Vegetation, Water, Humans and the Climate*, Springer, Berlin, pp. 33–57.

- Cox, P.M., Betts, R.A., Bunton, C.B., Essery, R.L.H., Rowntree, P.R. and Smith, J., 1999. The impact of new land surface physics on the gcm simulation of climate and climate sensitivity. *Climate Dynamics*, 15(3): 183–203.
- De Ridder, K., 1997. Land surface processes and the potential for convective precipitation. *Journal of Geophysical Research D: Atmospheres*, 102(25): 30085–30090.
- Dee, D.P., Uppala, S.M., Simmons, A.J., Berrisford, P., Poli, P., Kobayashi, S., Andrae, U., Balmaseda, M.A., Balsamo, G., Bauer, P., Bechtold, P., Beljaars, A.C.M., van de Berg, L., Bidlot, J., Bormann, N., Delsol, C., Dragani, R., Fuentes, M., Geer, A.J., Haimberger, L., Healy, S.B., Hersbach, H., Hlm, E.V., Isaksen, I., Kllberg, P., Khlr, M., Matricardi, M., McNally, A.P., Monge-Sanz, B.M., Morcrette, J., Park, B., Peubey, C., de Rosnay, P., Tavolato, C., Thpaut, J. and Vitart, F., 2011. The era-interim reanalysis: Configuration and performance of the data assimilation system. *Quarterly Journal of the Royal Meteorological Society*, 137(656): 553–597.
- Dirmeyer, P.A., 2011. A history and review of the global soil wetness project (gswp). *Journal of Hydrometeorology*, 12(5): 729–749.
- Dirmeyer, P.A. and Brubaker, K.L., 1999. Contrasting evaporative moisture sources during the drought of 1988 and the flood of 1993. *Journal of Geophysical Research D: Atmospheres*, 104(D16): 19383–19397.
- Dirmeyer, P.A. and Brubaker, K.L., 2007. Characterization of the global hydrologic cycle from a back-trajectory analysis of atmospheric water vapor. *Journal of Hydrometeorology*, 8(1): 20–37.
- Dirmeyer, P.A., Schlosser, C.A. and Brubaker, K.L., 2009. Precipitation, recycling, and land memory: An integrated analysis. *Journal of Hydrometeorology*, 10(1): 278–288.
- Döll, P., 2002. Impact of climate change and variability on irrigation requirements: A global perspective. *Climatic Change*, 54(3): 269–293.
- Douglas, E.M., Beltrn-Przekurat, A., Niyogi, D., Pielke Sr., R.A. and Vrmsmarty, C.J., 2009. The impact of agricultural intensification and irrigation on land-atmosphere interactions and indian monsoon precipitation - a mesoscale modeling perspective. *Global and Planetary Change*, 67(1-2): 117–128.
- Douville, H., Chauvin, F. and Broqua, H., 2001. Influence of soil moisture on the asian and african monsoons. part i: Mean monsoon and daily precipitation. *Journal of Climate*, 14(11): 2381–2403.

- Dumenil, L. and Todini, E., 1992. A rainfall-runoff scheme for use in the hamburg climate model. *Advances in theoretical hydrology*: 129–157.
- Eerola, K., 2006. *About the Performance of HIRLAM version 7.0*. Tech. rep., HIRLAM Newsletter.
- Ek, M. and Holtslag, A., 2004. Influence of soil moisture on boundary layer cloud development. *Journal of Hydrometeorology*, 5: 86–99.
- Eltahir, E.A.B., 1998. A soil moisture-rainfall feedback mechanism 1. theory and observations. *Water Resources Research*, 34(4): 765–776.
- Essery, R.L.H., Best, M.J., Betts, R.A., Cox, P.M. and Taylor, C.M., 2003. Explicit representation of subgrid heterogeneity in a gcm land surface scheme. *Journal of Hydrometeorology*, 4(3): 530–543.
- Ferguson, C.R. and Wood, E.F., 2011. Observed land-atmosphere coupling from satellite remote sensing and reanalysis. *Journal of Hydrometeorology*, 12(6): 1221–1254.
- Findell, K.L., 2001. Atmospheric controls on soil moisture-boundary layer interactions. *PhD Thesis, Massachusetts Institute of Technology*: 172 pp.
- Findell, K.L. and Eltahir, E.A.B., 1997. An analysis of the soil moisture-rainfall feedback, based on direct observations from illinois. *Water Resources Research*, 33(4): 725–735.
- Findell, K.L. and Eltahir, E.A.B., 2003a. Atmospheric controls on soil moisture-boundary layer interactions. part i: Framework development. *Journal of Hydrometeorology*, 4(3): 552–569.
- Findell, K.L. and Eltahir, E.A.B., 2003b. Atmospheric controls on soil moisture-boundary layer interactions. part ii: Feedbacks within the continental united states. *Journal of Hydrometeorology*, 4(3): 570–583.
- Findell, K.L., Gentine, P., Lintner, B.R. and Kerr, C., 2011. Probability of afternoon precipitation in eastern united states and mexico enhanced by high evaporation. *Nature Geoscience*, 4(7): 434–439.
- Foley, J.A., Ramankutty, N., Brauman, K.A., Cassidy, E.S., Gerber, J.S., Johnston, M., Mueller, N.D., O’Connell, C., Ray, D.K., West, P.C., Balzer, C., Bennett, E.M., Carpenter, S.R., Hill, J., Monfreda, C., Polasky, S., Rockstrm, J., Sheehan, J., Siebert, S., Tilman, D. and Zaks, D.P.M., 2011. Solutions for a cultivated planet. *Nature*, 478(7369): 337–342.

- Goessling, H.F. and Reick, C.H., 2011. What do moisture recycling estimates tell us? exploring the extreme case of non-evaporating continents. *Hydrology and Earth System Sciences*, 15(10): 3217–3235.
- Gregory, D. and Rowntree, P.R., 1990. A mass flux convection scheme with representation of cloud ensemble characteristics and stability-dependent closure. *Monthly Weather Review*, 118(7): 1483–1506.
- Guimberteau, M., Laval, K., Perrier, A. and Polcher, J., 2012. Global effect of irrigation and its impact on the onset of the indian summer monsoon. *Climate Dynamics*, 39(6): 1329–1348.
- Guo, Z., Dirmeyer, P.A., Koster, R.D., Bonan, G., Chan, E., Cox, P., Gordon, C.T., Kanae, S., Kowalczyk, E., Lawrence, D., Liu, P., Lu, C., Malyshev, S., McAvaney, B., McGregor, J.L., Mitchell, K., Mocko, D., Oki, T., Oleson, K.W., Pitman, A., Sud, Y.C., Taylor, C.M., Verseghy, D., Vasic, R., Xue, Y. and Yamada, T., 2006. Glace: The global land-atmosphere coupling experiment. part ii: Analysis. *Journal of Hydrometeorology*, 7(4): 611–625.
- Haddeland, I., Clark, D.B., Franssen, W., Ludwig, F., Vo, F., Arnell, N.W., Bertrand, N., Best, M., Folwell, S., Gerten, D., Gomes, S., Gosling, S.N., Hagemann, S., Hanasaki, N., Harding, R., Heinke, J., Kabat, P., Koirala, S., Oki, T., Polcher, J., Stacke, T., Viterbo, P., Weedon, G.P. and Yeh, P., 2011. Multimodel estimate of the global terrestrial water balance: Setup and first results. *Journal of Hydrometeorology*, 12(5): 869–884.
- Hagemann, S., 2002. *An improved land surface parameter dataset for global and regional climate models*. MPI-Report 336, Max Planck Institute for Meteorology, Hamburg, Germany.
- Hagemann, S., Chen, C., Clark, D.B., Folwell, S., Gosling, S.N., Haddeland, I., Hanasaki, N., Heinke, J., Ludwig, F., Voß, F. and Wiltshire, A.J., 2012. Climate change impact on available water resources obtained using multiple global climate and hydrology models. *Earth System Dynamics Discussions*, 3(2): 1321–1345, doi: 10.5194/esdd-3-1321-2012.
- Harding, R., Best, M., Blyth, E., Hagemann, S., kabat, P., Tallaksen, L.M., Warnaars, T., Wiberg, D., Weedon, G.P., van Lanen, H., Ludwig, F. and Haddeland, I., 2011. Watch: Current knowledge of the terrestrial global water cycle. *Journal of Hydrometeorology*, 12(6): 1149–1156.
- Harding, R., Blyth, E., Tuinenburg, O. and Wiltshire, A., 2012. Land atmosphere feedbacks and their role in the water resources of the ganges basin. *Science of the Total Environment*, Accepted.

- Held, I.M. and Soden, B.J., 2006. Robust responses of the hydrological cycle to global warming. *Journal of Climate*, 19(21): 5686–5699.
- Henderson-Sellers, A., McGuffie, K. and Zhang, H., 2002. Stable isotopes as validation tools for global climate model predictions of the impact of amazonian deforestation. *Journal of Climate*, 15(18): 2664–2677.
- Hewitt, K., 2005. The karakoram anomaly? glacier expansion and the 'elevation effect,' karakoram himalaya. *Mountain Research and Development*, 25(4): 332–340.
- Hohenegger, C., Brockhaus, P., Bretherton, C.S. and Schr, C., 2009. The soil moisture-precipitation feedback in simulations with explicit and parameterized convection. *Journal of Climate*, 22(19): 5003–5020.
- Immerzeel, W.W., van Beek, L.P.H. and Bierkens, M.F.P., 2010. Climate change will affect the asian water towers. *Science*, 328(5984): 1382–1385.
- Joyce, R.J., Janowiak, J.E., Arkin, P.A. and Xie, P., 2004. Cmorph: A method that produces global precipitation estimates from passive microwave and infrared data at high spatial and temporal resolution. *Journal of Hydrometeorology*, 5(3): 487–503.
- Juang, J., Katul, G.G., Porporato, A., Stoy, P.C., Siqueira, M.S., Detto, M., Kim, H. and Oren, R., 2007. Eco-hydrological controls on summertime convective rainfall triggers. *Global Change Biology*, 13(4): 887–896.
- Kalnay, E., Kanamitsu, M., Kistler, R., Collins, W., Deaven, D., Gandin, L., Iredell, M., Saha, S., White, G., Woollen, J., Zhu, Y., Chelliah, M., Ebisuzaki, W., Higgins, W., Janowiak, J., Mo, K.C., Ropelewski, C., Wang, J., Leetmaa, A., Reynolds, R., Jenne, R. and Joseph, D., 1996. The ncep/ncar 40-year reanalysis project. *Bulletin of the American Meteorological Society*, 77(3): 437–471.
- Kanamitsu, M., Ebisuzaki, W., Woollen, J., Yang, S., Hnilo, J.J., Fiorino, M. and Potter, G.L., 2002. Ncep-doe amip-ii reanalysis (r-2). *Bulletin of the American Meteorological Society*, 83(11): 1631–1643+1559.
- Kim, C.P. and Entekhabi, D., 1998a. Feedbacks in the land-surface and mixed-layer energy budgets. *Boundary-Layer Meteorology*, 88(1): 1–21.
- Kim, C.P. and Entekhabi, D., 1998b. Impact of soil heterogeneity in a mixed-layer model of the planetary boundary layer. *Hydrological Sciences Journal*, 43(4): 633–658.
- Kohler, M., Kalthoff, N. and Kottmeier, C., 2010. The impact of soil moisture modifications on cbl characteristics in west africa: A case-study from the amma campaign. *Quarterly Journal of the Royal Meteorological Society*, 136(SUPPL. 1): 442–455.

- Koster, R., 1986. Global sources of local precipitation as determined by the nasa/giss gcm. *Geophysical Research Letters*, 13(2): 121–124.
- Koster, R.D., Dirmeyer, P.A., Guo, Z., Bonan, G., Chan, E., Cox, P., Gordon, C.T., Kanae, S., Kowalczyk, E., Lawrence, D., Liu, P., Lu, C., Malyshev, S., McAvaney, B., Mitchell, K., Mocko, D., Oki, T., Oleson, K., Pitman, A., Sud, Y.C., Taylor, C.M., Verseghy, D., Vasic, R., Xue, Y. and Yamada, T., 2004. Regions of strong coupling between soil moisture and precipitation. *Science*, 305(5687): 1138–1140.
- Koster, R.D., Mahanama, S.P.P., Yamada, T.J., Balsamo, G., Berg, A.A., Boisserie, M., Dirmeyer, P.A., Doblas-Reyes, F.J., Drewitt, G., Gordon, C.T., Guo, Z., Jeong, J., Lee, W., Li, Z., Luo, L., Malyshev, S., Merryfield, W.J., Seneviratne, S.I., Stanelle, T., van den Hurk, B.J.J.M., Vitart, F. and Wood, E.F., 2011. The second phase of the global land-atmosphere coupling experiment: Soil moisture contributions to subseasonal forecast skill. *Journal of Hydrometeorology*, 12(5): 805–822.
- Koster, R.D., Guo, Z., Dirmeyer, P.A., Bonan, G., Chan, E., Cox, P., Davies, H., Gordon, C., Kanae, S., Kowalczyk, E., Lawrence, D., Liu, P., Lu, C.H., Malyshev, S., McAvaney, B., Mitchell, K., Mocko, D., Oki, T., Oleson, K.W., Pitman, A., Sud, Y., Taylor, C.M., Verseghy, D., Vasic, R., Xue, Y. and Yamada, T., 2006. Glace: The global land-atmosphere coupling experiment. part i: Overview. *Journal of hydrometeorology*, 7: 590–610.
- Lawrence, D.M. and Slingo, J.M., 2005. Weak land-atmosphere coupling strength in hadam3: The role of soil moisture variability. *Journal of Hydrometeorology*, 6(5): 670–680.
- Lee, E., Chase, T.N., Rajagopalan, B., Barry, R.G., Biggs, T.W. and Lawrence, P.J., 2009. Effects of irrigation and vegetation activity on early indian summer monsoon variability. *International Journal of Climatology*, 29(4): 573–581.
- Lee, E., Sacks, W.J., Chase, T.N. and Foley, J.A., 2011. Simulated impacts of irrigation on the atmospheric circulation over asia. *Journal of Geophysical Research D: Atmospheres*, 116(8).
- Lobell, D., Bala, G., Mirin, A., Phillips, T., Maxwell, R. and Rotman, D., 2009. Regional differences in the influence of irrigation on climate. *Journal of Climate*, 22(8): 2248–2255.
- Lohar, D. and Pal, B., 1995. The effect of irrigation on premonsoon season precipitation over south west bengal, india. *Journal of Climate*, 8(10): 2567–2570.
- Lucas-Picher, P., Christensen, J.H., Saeed, F., Kumar, P., Asharaf, S., Ahrens, B., Wiltshire, A.J., Jacob, D. and Hagemann, S., 2011. Can regional climate models represent the indian monsoon? *Journal of Hydrometeorology*, 12(5).

- Lytinska, Z., Parfiniewicz, J. and Pinkowski, H., 1976. The prediction of air mass thunderstorms and hails. *Proc. WMO Symp. on the Interpretation of Broad-Scale NWP Products for Local Forecasting Purposes, Warsaw, Poland, WMO*: 128–130.
- Mahanama, S.P.P. and Koster, R.D., 2005. Agcm biases in evaporation regime: Impacts on soil moisture memory and land-atmosphere feedback. *Journal of Hydrometeorology*, 6(5): 656–669.
- Meehl, G.A., 1994a. Coupled land-ocean-atmosphere processes and south asian monsoon variability. *Science*, 266(5183): 263–267.
- Meehl, G.A., 1994b. Influence of the land surface in the asian summer monsoon: external conditions versus internal feedbacks. *Journal of Climate*, 7(7): 1033–1049.
- Mitchell, T.D. and Jones, P.D., 2005. An improved method of constructing a database of monthly climate observations and associated high-resolution grids. *International Journal of Climatology*, 25(6): 693–712.
- Niyogi, D., Kishtawal, C., Tripathi, S. and Govindaraju, R.S., 2010. Observational evidence that agricultural intensification and land use change may be reducing the indian summer monsoon rainfall. *Water Resources Research*, 46(3).
- Nordeng, T., 1994. *Extended versions of the convective parameterization scheme at ECMWF and their impact on the mean and transient activity of the model in the tropics, Technical memorandum*. Tech. Rep. 206, 4, European Centre for Medium Range Weather Forecasts, Reading, U.K.
- Numaguti, A., 1999. Origin and recycling processes of precipitating water over the eurasian continent: Experiments using an atmospheric general circulation model. *Journal of Geophysical Research D: Atmospheres*, 104(D2): 1957–1972.
- O’Hare, G., 1997. The indian monsoon part 2: The rains. *Geography*, 82(4): 335–352.
- Orlowsky, B. and Seneviratne, S.I., 2010. Statistical analyses of land-atmosphere feedbacks and their possible pitfalls. *Journal of Climate*, 23(14): 3918–3932.
- Pfahl, S. and Wernli, H., 2008. Air parcel trajectory analysis of stable isotopes in water vapor in the eastern mediterranean. *Journal of Geophysical Research D: Atmospheres*, 113(20).
- Pope, V.D., Gallani, M.L., Rowntree, P.R. and Stratton, R.A., 2000. The impact of new physical parametrizations in the hadley centre climate model: Hadam3. *Climate Dynamics*, 16(2-3): 123–146.

- Portmann, F., Siebert, S. and Döll, P., 2010. Mirca2000–global monthly irrigated and rainfed crop areas around the year 2000: A new high-resolution data set for agricultural and hydrological modeling. *Global Biogeochemical Cycles*, 24(1): GB1011.
- Puma, M.J. and Cook, B.I., 2010. Effects of irrigation on global climate during the 20th century. *Journal of Geophysical Research D: Atmospheres*, 115(16).
- Raddatz, T.J., Reick, C.H., Knorr, W., Kattge, J., Roeckner, E., Schnur, R., Schnitzler, K.G., Wetzell, P. and Jungclaus, J., 2007. Will the tropical land biosphere dominate the climate-carbon cycle feedback during the twenty-first century? *Clim. Dyn.*, 29(6): 565–574, doi:10.1007/s00382-007-0247-8.
- Rienecker, M.M., Suarez, M.J., Gelaro, R., Todling, R., Bacmeister, J., Liu, E., Bosilovich, M.G., Schubert, S.D., Takacs, L., Kim, G., Bloom, S., Chen, J., Collins, D., Conaty, A., Da Silva, A., Gu, W., Joiner, J., Koster, R.D., Lucchesi, R., Molod, A., Owens, T., Pawson, S., Pegion, P., Redder, C.R., Reichle, R., Robertson, F.R., Ruddick, A.G., Sienkiewicz, M. and Woollen, J., 2011. Merra: Nasa’s modern-era retrospective analysis for research and applications. *Journal of Climate*, 24(14): 3624–3648.
- Roeckner, E., Bäuml, G., Bonaventura, L., Brokopf, R., Esch, M., Giorgetta, M., Hagemann, S., Kirchner, I., Kornbluh, L., Manzini, E., Rhodin, A., Schlese, U., Schulzweida, U. and Tompkins, A., 2003. *The atmospheric general circulation model ECHAM5. Part I: Model description*. Rep. 349, Max Planck Institute for Meteorology, Hamburg.
- Saeed, F., Hagemann, S. and Jacob, D., 2009. Impact of irrigation on the south asian summer monsoon. *Geophysical Research Letters*, 36(20).
- Santanello, J.A., Peters-Lidard, C.D. and Kumar, S.V., 2011a. Diagnosing the sensitivity of local land-atmosphere coupling via the soil moisture-boundary layer interaction. *Journal of Hydrometeorology*, 12(5): 766–786.
- Santanello, J.A., Ferguson, C., Ek, M., Dirmeyer, P., Tuinenburg, O., Jacobs, C., van Heerwaarden, C., Findell, K., Gentile, P. and Lintner, B., 2011b. *Local Land-Atmosphere Coupling (LoCo) Research: Status and Results*. Tech. rep., GEWEX News Letter 21, no. 4.
- Schär, C., Lüthi, D., Beyerle, U. and Heise, E., 1999. The soil-precipitation feedback: A process study with a regional climate model. *Journal of Climate*, 12(2-3): 722–741.
- Seneviratne, S.I., Corti, T., Davin, E.L., Hirschi, M., Jaeger, E.B., Lehner, I., Orlowsky, B. and Teuling, A.J., 2010. Investigating soil moisture-climate interactions in a changing climate: A review. *Earth-Science Reviews*, 99(3-4): 125–161.

- Siebert, S. and Döll, P., 2010. Quantifying blue and green virtual water contents in global crop production as well as potential production losses without irrigation. *Journal of Hydrology*, 384(3-4): 198–217.
- Siebert, S., Döll, P., Hoogeveen, J., Faures, J., Frenken, K. and Feick, S., 2005. Development and validation of the global map of irrigation areas. *Hydrology and Earth System Sciences*, 9(5): 535–547.
- Siqueira, M., Katul, G. and Porporato, A., 2009. Soil moisture feedbacks on convection triggers: The role of soil-plant hydrodynamics. *Journal of Hydrometeorology*, 10(1): 96–112.
- Sundquist, H., 1978. A parameterization scheme for non-convective condensation including prediction of cloud water content. *Quart. J. Roy. Meteor. Soc.*, 104: 677–690.
- Taylor, C.M., Gounou, A., Guichard, F., Harris, P.P., Ellis, R.J., Couvreux, F. and De Kauwe, M., 2011. Frequency of sahelian storm initiation enhanced over mesoscale soil-moisture patterns. *Nature Geoscience*, 4(7): 430–433.
- Taylor, C.M., de Jeu, R.A.M., Guichard, F., Harris, P.P. and Dorigo, W.A., 2012. Afternoon rain more likely over drier soils. *Nature*, 378.
- Teuling, A.J., Hirschi, M., Ohmura, A., Wild, M., Reichstein, M., Ciais, P., Buchmann, N., Ammann, C., Montagnani, L., Richardson, A.D., Wohlfahrt, G. and Seneviratne, S.I., 2009. A regional perspective on trends in continental evaporation. *Geophysical Research Letters*, 36(2).
- Tiedtke, M., 1989. A comprehensive mass flux scheme for cumulus parameterization in large-scale models. *Monthly Weather Review*, 117(8): 1779–1800.
- Tremback, C., 1990. *Numerical simulation of a mesoscale convective complex: model development and numerical results*. Ph.D. thesis, Colorado State University, Department of Atmospheric Science, Fort Collins, CO 80523.
- Trenberth, K.E., 1999. Atmospheric moisture recycling: Role of advection and local evaporation. *Journal of Climate*, 12(5 II): 1368–1381.
- Trenberth, K.E., Fasullo, J.T. and Mackaro, J., 2011. Atmospheric moisture transports from ocean to land and global energy flows in reanalyses. *Journal of Climate*, 24: 4907–4924.
- Tuinenburg, O.A., Hutjes, R.W.A., Jacobs, C.M.J. and Kabat, P., 2011. Diagnosis of local land-atmosphere feedbacks in india. *Journal of Climate*, 24(1): 251–266.

- Tuinenburg, O.A., Hutjes, R.W.A. and Kabat, P., 2012a. The fate of evaporated water from the ganges basin. *Journal of Geophysical Research*, 117(D01107): 1–17.
- Tuinenburg, O.A., Jacobs, C., Santanello, J., Ek, M., Elbers, J., Kabat, P. and Hutjes, R., 2012b. Land-atmosphere indicators from reanalysis datasets. *Journal of Hydrometeorology*, Submitted.
- Tuinenburg, O.A., Stacke, T., Wiltshire, A., Lucas-Picher, P. and Hutjes, R., 2013. Effects of irrigation in india on the atmospheric water budget. *Journal of Hydrometeorology*, Submitted.
- Uppala, S.M., Kallberg, P.W., Simmons, A.J., Andrae, U., da Costa Bechtold, V., Fiorino, M., Gibson, J.K., Haseler, J., Hernandez, A., Kelly, G.A., Li, X., Onogi, K., Saarinen, S., Sokka, N., Allan, R.P., Andersson, E., Arpe, K., Balmaseda, M.A., Beljaars, A.C.M., van de Berg, L., Bidlot, J., Bormann, N., Caires, S., Chevallier, F., Dethof, A., Dragosavac, M., Fisher, M., Fuentes, M., Hagemann, S., Hlm, E., Hoskins, B.J., Isaksen, L., Janssen, P.A.E.M., Jenne, R., McNally, A.P., Mahfouf, J., Morcrette, J., Rayner, N.A., Saunders, R.W., Simon, P., Sterl, A., Trenberth, K.E., Untch, A., Vasiljevic, D., Viterbo, P. and Woollen, J., 2005. The era-40 re-analysis. *Quarterly Journal of the Royal Meteorological Society*, 131(612): 2961–3012.
- van den Hurk, B., Doblas-Reyes, F., Balsamo, G., Koster, R.D., Seneviratne, S.I. and Camargo Jr., H., 2012. Soil moisture effects on seasonal temperature and precipitation forecast scores in europe. *Climate Dynamics*, 38(1-2): 349–362.
- van den Hurk, B.J.J.M. and van Meijgaard, E., 2010. Diagnosing land-atmosphere interaction from a regional climate model simulation over west africa. *Journal of Hydrometeorology*, 11(2): 467–481.
- van der Ent, R.J., Savenije, H.H.G., Schaefli, B. and Steele-Dunne, S.C., 2010. Origin and fate of atmospheric moisture over continents. *Water Resources Research*, 46(9).
- van der Ent, R., Tuinenburg, O., Knoche, H., Kunstmann, H. and Savenije, H., 2013. Should you use a simple or complex model for moisture recycling and atmospheric water tracing? *Hydrology and Earth System Sciences*, To besubmitted.
- van Heerwaarden, C.C., de Arellano, J.V., Moene, A.F. and Holtslag, A.A.M., 2009. Interactions between dry-air entrainment, surface evaporation and convective boundary-layer development. *Quarterly Journal of the Royal Meteorological Society*, 135(642): 1277–1291.
- Wada, Y., van Beek, L.P.H., Sperna Weiland, F.C., Chao, B.F., Wu, Y. and Bierkens, M.F.P., 2012. Past and future contribution of global groundwater depletion to sea-level rise. *Geophysical Research Letters*, 39(9).

- Wada, Y., van Beek, L.P.H., van Kempen, C.M., Reckman, J.W.T.M., Vasak, S. and Bierkens, M.F.P., 2010. Global depletion of groundwater resources. *Geophysical Research Letters*, 37(20).
- Walko, R.L., Band, L.E., Baron, J., Kittel, T.G., Lammers, R., Lee, T.J., Ojima, D., Sr., R.A.P., Taylor, C., Tague, C., Tremback, C.J. and Vidale, P.L., 2000. Coupled atmosphere-biophysics-hydrology models for environmental modeling. *Journal of applied meteorology*, 39: 931–944.
- Wang, B. and Fan, Z., 1999. Choice of south asian summer monsoon indices. *Bulletin of the American Meteorological Society*, 80(4): 629–638.
- Wang, K. and Dickinson, R.E., 2012. A review of global terrestrial evapotranspiration: Observation, modeling, climatology, and climatic variability. *Reviews of Geophysics*, 50(2).
- Webster, P.J., Magan a, V.O., Palmer, T.N., Shukla, J., Tomas, R.A., Yanai, M. and Yasunari, T., 1998. Monsoons: processes, predictability, and the prospects for prediction. *Journal of Geophysical Research C: Oceans*, 103(C7): 14451–14510.
- Weedon, G.P., Gomes, S., Viterbo, P., Shuttleworth, W.J., Blyth, E., Sterle, H., Adam, J.C., Bellouin, N., Boucher, O. and Best, M., 2011. Creation of the watch forcing data and its use to assess global and regional reference crop evaporation over land during the twentieth century. *Journal of Hydrometeorology*, 12(5): 823–848.
- Wei, J., Dickinson, R.E. and Chen, H., 2008. A negative soil moisture-precipitation relationship and its causes. *Journal of Hydrometeorology*, 9(6): 1364–1376.
- Yatagai, A., Arakawa, O., Kamiguchi, K., Kawamoto, H., Nodzu, M.I. and Hamada, A., 2009. A 44-year daily gridded precipitation dataset for asia based on a dense network of rain gauges. *SOLA*, 5: 137–140.
- Yoshimura, K., Oki, T., Ohte, N. and Kanae, S., 2004. Colored moisture analysis estimates of variations in 1998 asian monsoon water sources. *Journal of the Meteorological Society of Japan*, 82(5): 1315–1329.
- Zhang, L., Dirmeyer, P.A., Wei, J., Guo, Z. and Lu, C., 2011. Land-atmosphere coupling strength in the global forecast system. *Journal of Hydrometeorology*, 12(1): 147–156.
- Zickfeld, K., Knopf, B., Petoukhov, V. and Schellnhuber, H.J., 2005. Is the indian summer monsoon stable against global change? *Geophysical Research Letters*, 32(15).

Summary

During the 20th century, an increasing population increased the demand for food. As a consequence, agricultural activity has expanded and become more intense. A part of this intensification is the use of irrigation systems to water crops. Due to this irrigation, dams and channeling systems, water can be made available for agriculture in places or during seasons with limited precipitation.

In monsoon climates, such as India, the majority of the precipitation falls in one season. During the rest of the year, water that is stored in dammed reservoirs can be made available to spread the water availability more evenly over the year. Previous studies with large scale hydrological models have shown that as a consequence of human influences (such as dams and irrigation systems), the river flow decreases during the wet monsoon months, but the evaporation of water into the atmosphere increases during the dry months. However, these large scale hydrological models did not take into account the atmospheric effects of a changed land surface.

This PhD research studies these atmospheric effects of large scale irrigation in India. Three perspectives are taken to determine the influence of irrigation: (1) the local effects of a moister land-surface on the triggering of precipitation (i.e. does the change in land surface wetness lead to a different amount of precipitation?), (2) the atmospheric fate of evaporation due to irrigation (i.e. where does the evaporation lead to (down-wind) precipitation?), and (3) the effects of a moister land-surface on the large scale (monsoon) moisture transport patterns (i.e. do the monsoon flows change significantly due to large scale irrigation?)

In the first part (the first perspective), several land-atmosphere diagnostics are tested globally. The goal of these diagnostics is to determine the influence of the land surface on precipitation, based on surface and atmospheric conditions. Of these diagnostics, the CTP-HI_{low} framework (Convective Triggering Potential and Humidity Index of the LOWER atmosphere) of Findell and Eltahir (2003a) performed well globally and

over the Indian region. The summertime atmospheric conditions were diagnosed using this framework and the presence of a land-atmosphere coupling hot-spot in the Indian peninsula, proposed by previous studies (Koster et al. (2004)), is confirmed. Secondly, the local perspective is taken in the Indian subcontinent. The CTP- HI_{low} framework is tested in India, using an atmospheric slab model (a simple, one-dimensional model of the atmosphere) combined with atmospheric soundings (balloon measurements of temperature and moisture of an atmospheric profile of up to 30 km). This model is run twice; once with a wet land surface and once with a dry land surface. The results of these model runs can have two outcomes; the land surface does not have an influence on precipitation or it does have an influence. The CTP- HI_{low} framework proves to be useful to classify the potential influence of the land surface. When the atmosphere is very wet (low values of HI_{low}), precipitation will occur regardless of the land surface, when the atmosphere is very dry (high HI_{low} values) no precipitation will occur, regardless of the land surface. However, for intermediate HI_{low} values, the effect of the land surface depends on the stability or the amount of convective energy (CTP) in the atmosphere. The stability of the atmosphere is related to how fast a particle will ascend in the atmosphere, which depends mostly on the temperature profile. For positive, but low convective potentials ($0 < CTP < 200$ J/kg), a wet land surface will produce more precipitation than a dry land surface. However, for high amounts of convective potential ($CTP > 200$ J/kg), a dry land surface will produce more precipitation. For India, a small adaptation of the framework improved the performance in predicting the influence of the land surface on precipitation triggering. For India, the effect of the land surface on precipitation is seasonal. During the periods two months before the monsoon onset and after the monsoon retreat, precipitation triggering was found to be sensitive to land surface wetness. During those periods, a wet land surface is expected to increase precipitation. The atmospheric conditions under which a wet land surface is expected to decrease precipitation do not occur frequently in India. During the dry winter season, the atmosphere is too dry for the land surface to have an influence on precipitation. During the monsoon period, the atmosphere is too wet for the land surface to have an influence on precipitation, it will occur regardless of the land surface conditions.

In the third part of the study, the moisture recycling perspective was taken and the atmospheric moisture budget of the Ganges basin is studied. A three-dimensional moisture tracing model is used to release moisture parcels from the Ganges basin, similarly to a class of school children releasing helium-filled balloons with their address on it. These parcels were transported along the wind patterns. During the trajectory of the parcel through the atmosphere, some moisture will precipitate out of it and contribute to the precipitation at that location. For each location, many parcels were released for every time step of 6 hours. Similar to the balloons of the school children that are hopefully sent back to them, the fate of the released moisture

was accounted.

The fraction of the evaporated moisture that subsequently falls as precipitation (recycles) within the Ganges basin shows a strong seasonality. During the winter months, practically all evaporation parcels were transported towards the Indian ocean and were lost for the Ganges basin. During the pre-monsoon months, the recycled fraction increased and was between 30-40%. During the monsoon months, the recycling peaks at up to 60%, after which it drops off again. The importance of recycled evaporation to the total precipitation peaks during the pre-monsoon and post-monsoon periods, when it contributes up to 15% of the precipitation.

In the last part of the study, the effects from the local and moisture recycling perspectives are compared to those from the large scale perspective. Four atmospheric models were run with and without irrigation to test the large scale effects of irrigation on the Ganges basin atmospheric water budget and the influence on large scale atmospheric moisture transport. The local effects on precipitation were minimal and not uniform across the models. The Ganges river basin evaporation increased, as well as the amount of evaporation recycled within the river basin. However, the large scale wind patterns showed a uniform change across the models. Due to an increased flow in the direction of north-west India, the precipitation in east-India decreased while it increased in north-west India and Pakistan. Therefore, the Ganges basin precipitation decreased slightly.

The conclusion of the work is that from the local perspective and the moisture recycling perspective, irrigation will lead to more precipitation in India. A wetter land surface will trigger some additional precipitation (especially just before and after the monsoon season) and a significant fraction of the evaporation will return to the same river basin as precipitation. However, from the large scale perspective, large scale irrigation will shift the wind patterns due to changes in the land-sea temperature contrast; precipitation will decrease slightly in the Ganges basin and be shifted towards the Indus basin and north-west India.

The effects of irrigation on precipitation is small compared to the hydrological response of human influences simulated by the large scale hydrological models. Moreover, the spread in response across these hydrological models is large compared to the simulated effects of irrigation by the atmospheric models. Therefore, it is recommended to improve the large scale hydrological models and reduce their uncertainty before including the feedbacks of land use changes on their precipitation input.

Samenvatting

In de twintigste eeuw is de vraag naar voedsel sterk toegenomen, met name door de enorme bevolkingsgroei. Als gevolg van deze toename is de landbouwareaal uitgebreid en is de landbouw intensiever geworden. Deze intensivering is deels bereikt door een toename in het gebruik van irrigatiesystemen om gewassen te voorzien van water. Hierdoor kunnen gewassen groeien op locaties waar dat anders niet zou kunnen, of gedurende periodes dat dit anders niet zou kunnen.

In Moessongebieden, zoals India, is de neerslag sterk seizoensgebonden, bijna alle neerslag valt in een paar maanden. Om de waterbeschikbaarheid gedurende de rest van het jaar op peil te houden kan de neerslag uit de moessonperiode worden opgeslagen achter dammen en in reservoirs. Gedurende de droge periodes kan dit opgeslagen water getransporteerd worden naar de gebieden waar het nodig is. Eerdere studies die gebruik maakten van grootschalige hydrologische modellen hebben aangetoond dat het menselijke ingrijpen (door middel van dammen en reservoirs) in de hydrologische cyclus een verminderde rivierafvoer gedurende de moesson maanden en een toegenomen verdamping gedurende de droge maanden tot gevolg heeft. Echter, de effecten van een veranderend landoppervlak (door grootschalige irrigatie) op de atmosfeer worden genegeerd in deze modellen.

In dit promotieonderzoek worden deze atmosferische effecten van grootschalige irrigatie in India vanuit drie perspectieven benaderd: (1) de lokale effecten van een natter landoppervlak op het ontstaan van neerslag (valt er meer of minder neerslag als gevolg van de natheid van de bodem?), (2) het benedenwindse effect van verdamping vanuit geïrrigeerde gebieden (waar komt de verdamping weer neer als neerslag?) en (3) de effecten van een natter landoppervlak op de grootschalige (moesson) circulatie (worden de moesson sterkte en stromingspatronen veranderd door grootschalige irrigatie?).

In het eerste deel (het lokale perspectief) worden er op mondiale schaal verscheidene indicatoren getest die bepalen of het landoppervlakte een rol speelt bij het ontstaan van

neerslag. Deze indicatoren worden bepaald op basis van de oppervlakte-eigenschappen van het land, maar ook op basis van de atmosferische toestand (zoals de vochtigheid en temperatuur). Op verschillende plekken op de aarde wordt de rol van het landoppervlakte bij het ontstaan van neerslag anders beoordeeld door de verschillende indicatoren en deze sterkte is ook afhankelijk van de gebruikte data. Echter, voor India laten de indicatoren zien dat er tijdens het zomer halfjaar (April tot en met September) een invloed is van het landoppervlak in de neerslagvorming. In India zal een natter oppervlak niet alleen de hoeveelheid neerslag doen toenemen, maar ook de kans op neerslag.

Vervolgens is binnen het lokale perspectief naar India gekeken. Eén van de indicatoren uit het eerste deel, is uitgebreider getest en enigszins aangepast voor India. Hierbij is een simpel één-dimensionaal model van de atmosfeer gebruikt dat alleen het (hoogte)profiel van de temperatuur en vochthoeveelheden simuleert. Voor het bepalen van de beginsituatie van het model is gebruik gemaakt van sonde-metingen van de atmosfeer (metingen waarbij er een weerballon gebruikt wordt om de temperatuurs- en vochtprofielen van de eerste 30 km van de atmosfeer te bepalen). Met dit simpele model is één maal een droge bodem en één maal een natte bodem gesimuleerd om te bepalen of de bodemvochtigheid een invloed op neerslag heeft. De resultaten lieten zien dat gedurende de droge periode (November tot Februari), de atmosfeer zo droog is dat er geen neerslag ontstaat, onafhankelijk van de bodem. Gedurende de moessontijd (Juni tot Augustus) is de atmosfeer zo vochtig dat er neerslag ontstaat, onafhankelijk van de bodem. Echter, in de twee maanden voorafgaand aan de moessontijd en de twee maanden na de moessontijd zal een nattere bodem (en dus irrigatie) tot meer neerslag leiden.

In het tweede deel van deze studie is overgestapt naar het perspectief van de benedenwindse effecten van irrigatie. Het vochtbudget van de atmosfeer is bepaald door middel van een drie-dimensionaal model dat vochtdeeltjes volgt door de atmosfeer. Dit model liet de verdamping van vocht van de irrigatiegebieden in India als virtuele deeltjes de atmosfeer in en volgde ze tot ze weer naar het aardoppervlak terugkwamen als neerslag. Deze procedure is vergelijkbaar met een klas kinderen die heliumballonnen loslaten om te kijken hoe ver ze komen en in welke richting ze gaan. Net als de ballonnen worden de vochtdeeltjes meegenomen door de wind. Een verschil met de ballonnen is echter dat er op ieder moment in de baan van het deeltje neerslag uit kan vallen of verdamping van de bodem in kan komen.

Het deel van de verdamping vanuit het rivierstroomgebied van de Ganges dat binnen datzelfde stroomgebied terugkomt als neerslag varieert sterk met de seizoenen. Gedurende de winter wordt alle verdamping naar de Indische oceaan in het zuiden getransporteerd en slechts een klein deel valt als neerslag in het Ganges stroomgebied. In de maanden voor het moessonseizoen is het deel van de verdamping dat terugkomt in het stroomgebied tussen de 30 en 40%, om in het moessonseizoen te

pieken met 60%, waarna het weer afneemt. Het aandeel van de verdamping binnen het rivierstroomgebied van de Ganges in de neerslag binnen datzelfde stroomgebied is maximaal vlak voor en vlak na het moessonseizoen, wanneer deze verdamping tot 15% van de neerslag levert.

In het laatste deel van de studie zijn de effecten van het lokale perspectief en de benedenwindse perspectief vergeleken met de effecten op een grootschalig perspectief. Hiervoor zijn vier klimaatmodellen twee keer gedraaid, één keer mét en één keer zonder irrigatie. De lokale effecten van irrigatie waren klein en deze effecten verschilden tussen de modellen. Er was meer verdamping in het Ganges stroomgebied en deze verdamping leidde tot meer neerslag in het Ganges stroomgebied. Er trad echter in alle modellen een verandering op in de grootschalige stromingspatronen. Door een vochtigere stroming in de richting van noord-west India onstond er een neerslag verschuiving van oost India naar noord-west India. Ondanks een toename van neerslag vanuit de lokale verdamping nam de totale hoeveelheid neerslag in het Ganges stroomgebied een klein beetje af.

De conclusie van dit onderzoek is dat vanuit het lokale perspectief en het perspectief van de benedenwindse effecten, irrigatie zal leiden tot meer neerslag. Een vochtiger land oppervlak zal lokaal leiden tot het ontstaan van neerslag (vlak voor het begin van de moesson en vlak na het terugtrekken hiervan). Een vrij groot deel van de verdamping in het Ganges stroomgebied komt weer terug als neerslag in hetzelfde stroomgebied, een deel van het irrigatiewater kan dus in theorie worden hergebruikt. Echter, de grootschalige effecten van irrigatie zullen leiden tot minder neerslag in het Ganges stroomgebied doordat de moessonstroming (die gestuurd wordt door het temperatuurverschil tussen land en zee) iets verschuift. Deze grootschalige effecten leiden tot een kleine afname in neerslag in het Ganges stroomgebied en een toename in noord-west India en het Indus stroomgebied.

De atmosferische effecten van irrigatie die in dit onderzoek naar voren zijn gekomen zijn klein in vergelijking met de hydrologische effecten van menselijk ingrijpen, zoals gesimuleerd met behulp van een aantal grootschalige hydrologische modellen. Bovendien lopen de resultaten van deze hydrologische modellen nogal uiteen, zeker in vergelijking met de eensgezindheid van de grootschalige atmosferische modellen in dit proefschrift. De aanbeveling vanuit dit onderzoek is dan ook om eerst de grootschalige hydrologische modellen te verbeteren en hun onzekerheid te verkleinen, voordat de effecten van landgebruiksverandering op de neerslag wordt meegenomen in de hydrologische modellen.

Dankwoord

Het boekje dat voor u ligt is het resultaat van mijn onderzoekswerk van de afgelopen jaren. Het doen van een promotieonderzoek heb ik ervaren als een proces met veel vrijheden. Deze vrijheden zijn onder andere het kiezen uit de vele onderzoeksrichtingen en methodes, maar ook het indelen en plannen van het onderzoek naar eigen inzicht. Deze vrijheden brengen echter wel de verantwoordelijkheid voor een goede afronding met zich mee. Tijdens mijn promotieperiode zijn er vele mensen geweest die mij op mijn verantwoordelijkheden of vrijheden (of beide) attenteerden.

Als eersten wil ik mijn begeleiders Pavel Kabat en Ronald Hutjes bedanken voor de fijne samenwerking. Jullie hebben beide de juiste vragen gesteld en me zo nu en dan herinnerd aan het onderzoeksdoel. Gelukkig hebben jullie het me ook op zijn tijd zelf uit laten zoeken.

Cor Jacobs, jij hebt altijd erg minutieus naar mijn werk gekeken en dat is het eindproduct zeer ten goede gekomen. Daarnaast heeft het mij gedetailleerder naar mijn werk laten kijken. Bedankt!

During this research, I have worked together with a number of people, which resulted in some nice papers. Joe Santanello, I appreciate our collaboration on 'local coupling', thanks for your many thoughts and suggestions. Eleanor Blyth, Andy Wiltshire and Richard Harding, thanks for pulling off our overview paper, that went very smooth. Philippe Lucas-Picher, Andy Wiltshire and Tobias Stacke, thanks for your cooperation in the model-intercomparison and your patience with my PhD schedule.

Ruud van der Ent, ik waardeer het zeer dat we in alle openheid 'onze' twee methodes konden vergelijken en daar een mooi paper van gemaakt hebben.

Hester en Michelle, wat fijn dat we samen naar Wageningen konden reizen en lekker hebben kunnen praten over onderzoeks- en office-politics. File is leuker met jullie!

Eddy, bedankt voor onze samenwerking, jouw enthousiasme en de biertjes in India.

De schrijfweken van ESS-CC heb ik ervaren als heerlijke weken met hard werken,

leuke discussies en nieuwe culinaire inzichten. Iedereen die mee was; bedankt!

Mijn kamergenoten gedurende de afgelopen jaren, Ruud, Robbert, Saskia, Iwan, Marleen, Olaf en Petra, bedankt voor het voeren van discussies over computer-scripts, het plotten van resultaten en andere belangrijke zaken in het leven.

Herbert en Wietse, jullie hebben mij ingewijd in RAMS en de data processing daarvan. Dat is aardig gelukt, maar ik ben bang dat het niet mijn favoriete stuk software gaat worden. . .

Het was fijn om af en toe na een dag werken een potje te kunnen tafeltennissen bij SVE. Professor Mark en Doctor Erik, ik zie uit naar het oordeel van jullie schaduwleescommissie.

Het was heel prettig om een complex onderzoeksonderwerp tijdens etentjes, weekenden weg en vakanties uit te leggen aan vrienden. Pieter, Hester, Joost, Karlijn, Mark, Annamarië, Arnoud, Susan, Wouter, Janneke, Bram, Rebecca, Annemiek, Menno, Hans en Orna, bedankt voor het aanhoren van verhalen over bijvoorbeeld meteorologische data of onderzoeksplannen en ook heel erg bedankt voor het laten weten wanneer het wel genoeg was.

Mark en Arnoud, ik vind het een eer dat jullie mijn paranimfen zijn.

Ik ben blij dat ik Stichting Kip op Zondag heb kunnen overtuigen van het belang van irrigatie in India op de Nederlandse kipconsumptie. Leuk dat het ieder jaar weer op rijm gezet is. Piet, Marion, Sander, Jantien, Josefen, Joep, Janna, Roeland, Anne en Thijn, bedankt voor de oppasuurtsjes en andere gezelligheid.

Mijn ouders Wil en Henk en zus Geerte, ik ben blij dat jullie mij altijd gesteund hebben in het leven, ook als ik het verder zoek dan noodzakelijk. Ondanks het feit dat papa er niet meer is heb ik tijdens dit promotieonderzoek dikwijls zijn advies ter harte genomen om vooral de dingen te doen die je leuk vindt en daar op te focussen. Mijn lieve schatten Hanne en Silke, wat is het een genot om de grotemensenwereld af en toe in te ruilen voor duplo, knutselen, soepstengels en fruihapjes.

Lieve Annemieke, het is een feest om met jou te zijn! Wat fijn dat ik bij jou mijn frustraties over triviale onderwerpen kwijt kon, nog fijner dat je me dan op de echt belangrijke dingen wees. Ik realiseer me dat jij, vooral de laatste periode, menig avondje alleen hebt moeten slijten. Maar, het is af! Tijd voor een nieuw hoofdstuk, l'aventure commence!

Publications

- Tuinenburg, O.A., Hutjes, R.W.A., Jacobs, C.M.J. and Kabat, P., 2011. Diagnosis of local land-atmosphere feedbacks in india. *Journal of Climate*, 24(1): 251–266.
- Tuinenburg, O.A., Hutjes, R.W.A. and Kabat, P., 2012a. The fate of evaporated water from the ganges basin. *Journal of Geophysical Research*, 117(D01107): 1–17.
- Tuinenburg, O.A., Jacobs, C., Santanello, J., Ek, M., Elbers, J., Kabat, P. and Hutjes, R., 2012b. Land-atmosphere indicators from reanalysis datasets. *Journal of Hydrometeorology*, Submitted.
- Tuinenburg, O.A., Stacke, T., Wiltshire, A., Lucas-Picher, P. and Hutjes, R., 2013. Effects of irrigation in india on the atmospheric water budget. *Journal of Hydrometeorology*, Submitted.
- Santanello, J.A., Ferguson, C., Ek, M., Dirmeyer, P., Tuinenburg, O., Jacobs, C., van Heerwaarden, C., Findell, K., Gentine, P. and Lintner, B., 2011. *Local Land-Atmosphere Coupling (LoCo) Research: Status and Results*. Tech. rep., GEWEX News Letter 21, no. 4.
- Harding, R., Blyth, E., Tuinenburg, O. and Wiltshire, A., 2012. Land atmosphere feedbacks and their role in the water resources of the ganges basin. *Science of the Total Environment*, Accepted.
- van der Ent, R., Tuinenburg, O., Knoche, H., Kunstmann, H. and Savenije, H., 2013. Should you use a simple or complex model for moisture recycling and atmospheric water tracing? *Hydrology and Earth System Sciences*, To be submitted.

Curriculum Vitae

- 1981 Born in 's Graveland, The Netherlands.
- 1992-1998 Secondary school, Hondsrugcollege, Emmen.
- 1998-2005 M.Sc. Environmental Science, Utrecht University
– Interaction between vegetation and hydrology
Advisors: Dr. Ir. Max Rietkerk and Dr. Stefan Dekker
- 2005-2006 Aveiro University, Portugal
– Study of the hydrology after forest fires in northern Portugal.
- 2006-2008 Desert Research Foundation of Namibia
– Study of groundwater recharge in ephemeral rivers
– Feasibility study of hybrid energy systems in Southern Africa.
- 2008-2013 Ph.D. research at Wageningen University
– Atmospheric effects of large scale irrigation in India.
The research is carried out at the Earth System Science and Climate Change group under the supervision of Dr. Ronald Hutjes and Prof. Dr. Pavel Kabat.



Netherlands Research School for the
Socio-Economic and Natural Sciences of the Environment

C E R T I F I C A T E

The Netherlands Research School for the
Socio-Economic and Natural Sciences of the Environment
(SENSE), declares that

Obbe Arjan Tuinenburg

born on 17 March 1981 in 's Graveland, the Netherlands

has successfully fulfilled all requirements of the
Educational Programme of SENSE.

Wageningen, 15 April 2013

the Chairman of the SENSE board

Prof. dr. Rik Leemans

the SENSE Director of Education

Dr. Ad van Dommelen

The SENSE Research School has been accredited by the Royal Netherlands Academy of Arts and Sciences (KNAW)



K O N I N K L I J K E N E D E R L A N D S E
A K A D E M I E V A N W E T E N S C H A P P E N



The SENSE Research School declares that **Mr. Obbe Tuinenburg** has successfully fulfilled all requirements of the Educational PhD Programme of SENSE with a work load of 42 ECTS, including the following activities:

SENSE PhD Courses

- o Environmental Research in Context
- o Research Context Activity: Organizing Writing Week (October 2009) and monthly PhD meetings (April 2011-July 2012) for ESS-CALM group

Other PhD and Advanced MSc Courses

- o PRACE Summer School on High Performance Computing
- o Mesoscale Meteorological Modelling
- o Clouds and Climate
- o PhD Scientific Writing
- o Mobilising your – scientific – network

Oral Presentations

- o The Indian summer monsoon - Does irrigation matter? SENSE Symposium, 26 January 2009, Wageningen
- o *Local Land-Atmosphere Feedbacks in India*. EU-WATCH project meeting, 3 November 2010, Amsterdam
- o Hydrology in the Air: Influence of Irrigation on the Atmospheric part of the Water Cycle. American Meteorological Society meeting, 24-28 January 2011, Seattle, United States
- o *Land-Atmosphere Feedbacks in India*. NASA Terrestrial Water Cycle Symposium, 20 January 2011, Washington DC, United States
- o *Diagnosing Local Coupling Indicators from Reanalyses*. GEWEX PAN-GASS Conferences, GEWEX-LoCo workgroup, September 2012, Boulder, United States

SENSE Coordinator PhD Education

Drs. Serge Stalpers

Cover design by Nelleke Gerlsma, based on a painting by Stijn Rietman ("Woman in irrigated field near Lac Andraikiba, Antsirabe, Madagascar", original photo: Annemieke van Wesemael).

The research in this thesis was undertaken as part of the European Union (FP6) funded Integrated Project WATCH (contract 036946).

Financial support from Wageningen University for printing this thesis is gratefully acknowledged.